PAVOL JOZEF ŠAFÁRIK UNIVERSITY IN KOŠICE

NFA 2025

The 9th International Conference on

NOVEL MATERIALS

Fundamentals and Applications 2025

12 -15th October 2025

Tatranská Lomnica, **High Tatras**

Metrohm

Chemistry A European Journal

Chemistry Europe

NATO OTAN

innovlab startup centre of

SBaA SLOVENSKÁ BATÉRIOVÁ ALIANCIA

T··Systems·

InoHub Energy

BIOTATRY

Funded by the European Union NextGenerationEU

RECOVERY AND RESILIENCE PLAN

MINISTERSTVO ŠKOLSTVA, VEDY, VÝSKUMU A ŠPORTU SLOVENSKEJ REPUBLIKY

SLOVAK RESEARCH AND DEVELOPMENT AGENCY

ÚSTAV CHEMICKÝCH VIED

https://nfa.science.upjs.sk

Pavol Jozef Šafárik University in Košice
Faculty of Science

BOOK OF ABSTRACTS

The 9th International Conference on Novel Materials Fundamentals and Applications

October 12-15, 2025

Organized by:

Department of Physical Chemistry
Faculty of Science
Pavol Jozef Šafárik University in Košice
&
Slovak Chemical Society
Bratislava

Košice 2025

The 9th International Conference on Novel Materials Fundamentals and Applications
Book of Abstracts

Edited by:
Mgr. Soňa Király
Institute of Chemistry, Faculty of Science, Pavol Jozef Šafárik University in Košice, Moyzesova 11, 040 01 Košice, Slovakia, sona.kiraly@upjs.sk

Reviewed by:
RNDr. Ondrej Petruš, PhD.
Slovak Academy of Sciences, *Watsonova 47, 04001 Košice, Slovakia, opetrus@saske.sk*

Ing. Miroslav Kohan, PhD.
Department of Biomedical engineering and Mesasurement, Faculty of Mechanical engineering, Technical University in Košice, Letná 1/9, 04200 Košice, Slovakia, mirosav.kohan@tuke.sk

Organized by:
Pavol Jozef Šafárik University in Košice
Slovak Chemical Society
Slovak Battery Alliance

Available at: www.unibook.upjs.sk
Publication date: 15.10. 2025

ISBN 978-80-574-0444-6 (e-publication)

LIST OF CONTENTS

LIST OF AUTHORS

5

6

Preface

On behalf of the Organizing Committee of the 9th International Conference on *Novel Materials Fundamentals and Applications (NFA 2025)*, we are pleased to present these proceedings. The conference will be held on 12–15 October 2025 at the Grandhotel Praha**** in Tatranská Lomnica, situated in the High Tatras, Slovakia. The event is jointly organized by Pavol Jozef Šafárik University in Košice in cooperation with the Slovak Academy of Sciences and Slovak Battery Alliance.

NFA 2025 offers an international forum for researchers working in the broad field of advanced materials to present their most recent achievements, exchange scientific ideas, and discuss emerging trends. The primary objective of the meeting is to foster interdisciplinary dialogue and stimulate collaboration across the international research community.

These proceedings include the full papers of both oral and poster contributions presented at the conference. We trust that this collection will provide readers with a representative overview of the progress in materials research and highlight the diversity and significance of the topics discussed during NFA 2025.

We gratefully acknowledge the efforts of all contributing authors, whose work has ensured the scientific quality of the conference, and we extend our appreciation to the reviewers for their careful evaluation of the manuscripts. Our thanks also go to the organizing team for their commitment and dedication in preparing this event. We also wish to acknowledge the various national and international projects and funding schemes that supported the research presented at this conference, without which many of the results could not have been achieved.

We wish all participants an inspiring and fruitful scientific gathering in the High Tatras and hope that NFA 2025 will serve as a valuable opportunity for advancing knowledge and building new collaborations in the field of novel materials.

Ivana Šišoláková

Lectures

9th International Conference on Novel Materials Fundamentals and Applications
High Tatras, 12.10.-15.10.2025

The Rise of the Nanocellulose Chip: Electronic Design and Automation Toolchains

E. Bencurova[a,*], M. Jung[b], T. Dandekar[a,c]
[a] Julius Maximilian University of Würzburg, Department of Bioinformatics, Würzburg, Germany,
[b] Julius Maximilian University of Würzburg, Institut of Computer Science, Würzburg, Germany, [c] European Molecular Biology Laboratory, Heidelberg, Germany
* elena.bencurova@uni-wuerzburg.de

Introduction

The current trend in the semiconductor industry faces notable challenges, such as enormous production of e-waste, and the use of toxic chemicals in production. Conventional chip manufacturing and recycling methods create significant environmental issues, prompting the need to explore new computing approaches, novel materials, and improved chip designs. In response, carbon-based materials are being studied for more energy-efficient computing systems, with nanocellulose (NC) emerging as a highly promising alternative (*Figure 1*).

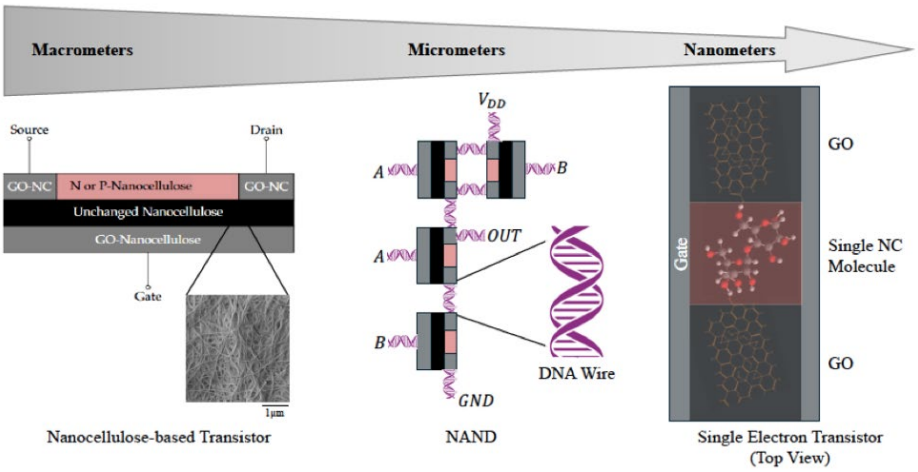

Figure 1 Miniaturisation process of transistors, shifting from macroscale to nanoscale designs [1]. At the macroscale, traditional transistors feature three layers: a source made of non-doped nanocellulose (insulator), unaltered nanocellulose (semiconductor), and graphene oxide-treated nanocellulose (GO-Nanocellulose), with metal electrodes acting as the gate. In the microscale, miniaturised transistors are connected by DNA wires (e.g., GND, V^{DD}), enabling molecular-scale signal transfer. At the nanoscale, single-electron transistors are an example of our emerging technology, comprising nanocellulose "islands" and graphene oxide (GO) components that allow only one electron to pass at a time through quantum effects such as Coulomb blockade.

Cellulose is the most abundant natural polymer on Earth, a linear biopolymer composed of several β(1→4) linked D-glucose units. Its renewability, biocompatibility, and biodegradability offer distinct advantages over synthetic materials typically used in electronic devices (*Figure 2*). NC is a versatile material that can be engineered to display suitable electronic and semiconducting properties. It provides ideal support for ink-printed transistors and eco-friendly paper electronics [2, 3]. This work aims to investigate how chips entirely based on nanocellulose, including those with semiconductor properties and transistors, might be fabricated using Electronic Design Automation (EDA) toolchains.

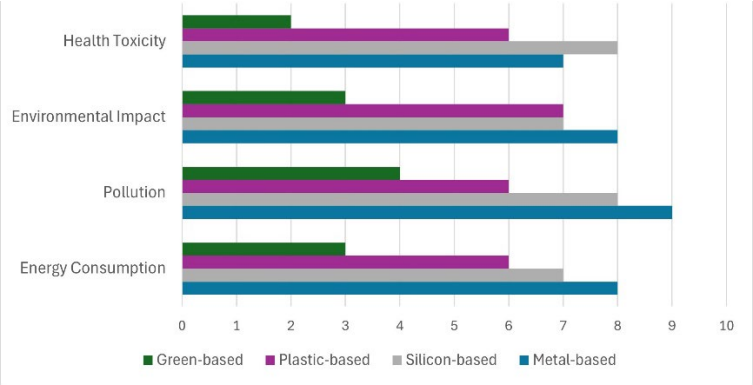

Figure 2 Comparative environmental impact of metal, silicon, plastic, and green electronics. Data were collected from the literature; categories on the x-axis represent impact areas, and the y-axis shows the normalised impact levels on a scale from 1 to 10 [1].

The Envisioned Nanocellulose-Based Transistor

We propose a transistor made exclusively from nanocellulose-derived materials, as illustrated in *Figure 1*, left picture:

-Dielectric Layer: Untreated nanocellulose can function as the dielectric layer between the gate electrode and the organic semiconductor;

-Semiconductive Channel: P-type or N-type nanocellulose, based on the findings from previous research [4, 5], forms the semiconductive channel;

-Conducting Parts (Electrodes): The electrodes (gate, source, and drain) are composed of nanocellulose highly doped with graphene oxide (GO) to achieve low-resistance contacts.

This proposed design signifies a major step towards environmentally friendly chips that could enable miniaturisation comparable to traditional electronics. Additionally, nanocellulose can be functionalised by incorporating various conductive materials to attain the desired electrical properties for semiconductor technology. Graphene and Graphene Oxide (GO): Graphene is the most commonly used material to enhance NC conductivity; highly conductive materials can be obtained using a "one-pot approach" with graphene oxide loading, maintaining thermal stability and mechanical strength [5]. The interaction between graphene and NC can be physical or chemical, via TEMPO oxidation, which introduces carboxylate groups to improve dispersion and form covalent bonds with graphene oxide, enhancing stability and conductivity [6]. Beyond graphene, carbon nanotubes, (nano)-carbon black, and nanodiamond are also utilised to improve conductivity [7]. Additionally, polymers such as polyaniline (PANI) and polypyrrole (PPy) can significantly enhance NC's electrical performance and mechanical properties, making them suitable for flexible electronics, sensors, and supercapacitors [8, 9]. These materials not only boost electrical characteristics but also contribute to the structural integrity and functionality of NC composites, positioning NC as a key material for flexible electronics and high-performance applications.

Electronic Design Automation (EDA) for Nanocellulose-Based Technology

To facilitate the manufacturing of complex digital circuits, such as microprocessors, from nanocellulose, we also propose a conceptual framework for an Electronic Design Automation (EDA) tool chain. This is essential for expanding application possibilities and addressing e-waste, as biodegradable microprocessors could enable transient wireless smart sensor systems (e.g., for health monitoring or agriculture) that do not require retrieval for disposal. The suggested workflow for designing and fabricating nanocellulose-based complex digital circuits (*Figure 3*) involves four main steps: fabrication, process design kit, standard cell library, and cell library-based digital design.

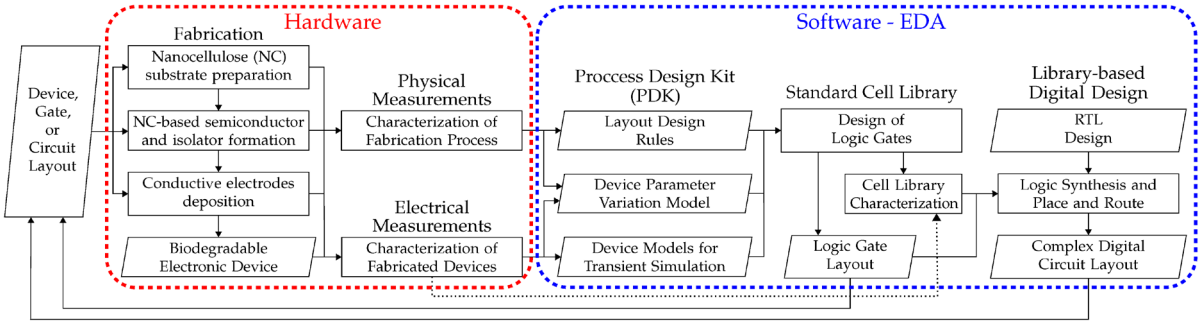

Figure 3 Processing flow for the design and fabrication of digital circuits based on nanocellulose-based transistors [1].

The first step is to create a single transistor using a nanocellulose-based process, drawing on methods for producing nanocellulose conductors and semiconductors. The Process Design Kit (PDK) is the most basic level of abstraction, defining the physical design rules based on the precision limits of the fabrication process (e.g., minimum width, length, and spacing of electrodes). The PDK also includes device models for software simulation and expected variation models for parameters such as dielectric thickness and channel width. A comprehensive PDK is essential to address issues like limited transistor density and performance variations. At the logic gate level, multiple transistors are connected to perform basic logic operations (e.g., NOT, AND, OR, NAND gates), forming the standard cell library. These universal gates are vital for implementing any logic computation. Currently, a significant gap exists in developing a PDK and standard cell library based on fully biodegradable devices.
The highest level of design involves creating complex modules such as microprocessors by interconnecting logic gates specified in the cell library. This cell library-based digital design process includes hardware synthesis tools that convert high-level descriptions (e.g., Verilog, VHDL) into sequences of logic gates, while Place and Route (PNR) tools position these gates and establish wiring to reduce non-idealities. The final output is a fabrication layout (GDS format). This integrated RTL-to-GDS flow, once established, can streamline the design of large-scale organic circuits, promoting the development of sustainable electronics [1].
Despite its promising properties, integrating NC into chip technology poses several challenges: the hydrophilic nature of nanocellulose, thermal degradation, precise shaping, and a high level of biodegradability (the risk of fungal degradation). However, versatile treatments can be applied to overcome these obstacles.
In summary, it is feasible to construct a high-performance, fully nanocellulose-based chip, with all dielectric, conductive, and semiconductive layers. This development offers a fully biodegradable alternative to conventional electronics, eliminating toxic materials. While further development, including optimisation of the NC transistor and parameterisation of chip design steps, will require time, the fundamental potential is clear, supported by solid experimental data demonstrating the assembly of these components into functional transistors. The outlined design automation steps, combined with advances in material science and chip fabrication, provide a clear pathway for future innovations in environmentally friendly and sustainable electronic devices.

References

[1] E. Bencurova, A. Chinazzo, B. Kar, M. Jung, and T. Dandekar, "How Far Is the Nanocellulose Chip and Its Production in Reach? A Literature Survey," *Nanomaterials,* vol. 14, no. 18, pp. 1536, 2024, doi: 10.3390/nano14181536.
[2] T. Hassinen, A. Alastalo, K. Eiroma, T. – M. Tenhunen, V. Kunnari, T. Kaljunen, U. Forsström and T. Tammelin, "All-printed transistors on nano cellulose substrate," *MRS Advances,* vol. 1, pp. 645-650, 2016, doi: 10.1557/adv.2015.31.
[3] Z. Rafiee, A. Elhadad, and S. Choi, "Revolutionizing papertronics: advanced green, tunable, and flexible components and circuits," *Advanced Sustainable Systems,* vol. 8, no. 6, p. 2400049, 2024, doi: 10.1002/adsu.202400049.
[4] M. S. Vasheghani Farahani, M. Nikzad, and M. Ghorbani, "Fabrication of Fe-doped ZnO/nanocellulose nanocomposite as an efficient photocatalyst for degradation of methylene blue under visible light," *Cellulose,* vol. 29, no. 13, pp. 7277-7299, 2022, doi: 10.21203/rs.3.rs-1049927/v1.
[5] J. Yu, Z. Zhu, H. Zhang, Y. Qiu, D. Yin, Y. Cheng, & S. Wang, "Stepwise carbonization of nanocellulose to N-doped carbons with structural transformation and enhanced peroxymonosulfate activation," *Chemical Engineering Journal,* vol. 407, p. 127185, 2021, doi: 10.1016/j.cej.2020.127185.

9th International Conference on Novel Materials Fundamentals and Applications
High Tatras, 12.10.-15.10.2025

Nanoporous Silica Pathways Toward Targeted Antithrombotic Treatment

E. Benova[a,*], N. Kiraly[a], M. Sulekova[b], V. Zelenak[a]
[a] Institute of Chemistry, Faculty of Science, P.J. Šafárik University, Moyzesova 11, 04001 Košice, Slovakia
[b] University of Veterinary Medicine and Pharmacy in Košice, Komenského 73, 041 81, Košice, Slovakia
* eva.benova@upjs.sk

Introduction

Thrombotic disorders continue to be a significant global health issue, with millions of cases occurring each year worldwide. Standard treatments involve the systemic delivery of antithrombotic medications, such as anticoagulants, antiplatelet agents, and thrombolytic agents. Although these drugs are clinically effective, they have notable disadvantages, including short biological half-lives, frequent dosing requirements, and a higher risk of serious side effects like bleeding or blood pressure fluctuations. Additionally, poor site selectivity results in systemic exposure to the drugs rather than targeted treatment at the thrombus location [1], [2].

Nanoparticle-based drug delivery presents opportunities to address these limitations. Mesoporous silica nanoparticles (MSNs) are particularly appealing due to their high surface area, adjustable pore size, and surface functionalization ability, which together enable efficient drug loading and sustained release. When combined with magnetic iron oxide cores in Fe_3O_4@SiO_2 core–shell structures, these carriers exhibit enhanced responsiveness to external magnetic fields, thereby creating pathways for targeted drug accumulation at thrombotic sites [3].

Apixaban, a direct factor Xa inhibitor with well-established oral efficacy, was chosen as a model antithrombotic drug. While its clinical use is limited by systemic bleeding risks and restricted targeting ability, encapsulation within nanoporous silica matrices may extend release, enhance safety, and reduce overall dosage by delivering it locally to clot regions [4].

The novelty of this work lies in testing drug release in the direct presence of blood clots and monitoring fibrin morphology by SEM, in combination with the development of magnetically targetable Fe_3O_4@SiO_2 nanocarriers. This work presents ongoing research into two nanoparticle platforms: (i) spherical mesoporous silica (SMS-60) nanoparticles functionalized with organic ligands for apixaban encapsulation, and (ii) magnetic core–shell Fe_3O_4@SiO_2 nanoparticles designed to integrate sustained release with external targeting capability.

Materials and Methods

Spherical mesoporous silica (SMS-60) nanoparticles were synthesized and subsequently functionalized with thiol, chloropropyl, and amino ligands to tune surface interactions. Apixaban loading was performed via wet impregnation using methanol solutions, ensuring penetration into 3–5 nm pores. Nanoparticles were characterized by: N_2 adsorption–desorption (surface area 320-600 m^2/g, pore size 3-5 nm, pore volume 0.1-0.6 cm^3/g), transmission electron microscopy (morphology, particle size distribution), thermal gravimetry (presence of organic ligand, drug loading content), and infrared spectroscopy (functional groups, drug–matrix interactions).

In vitro release experiments were carried out in simulated gastric (pH 2) and physiological (pH 7.4) media. Release profiles were recorded over 168 h, followed by stabilization at plateau levels after 72 hours. To simulate clinical dosing, repeated administration was modelled by introducing additional apixaban-loaded nanoparticles after 72 h, and monitoring resumed release. To simulate therapeutic conditions, apixaban solutions (0.1, 0.25 and 0.5 mg/mL) were introduced to model blood clots, with morphological changes in the fibrin network evaluated by SEM. Ongoing experiments involve replacing pure apixaban solutions with apixaban-loaded SMS-60 nanoparticles under the same conditions.

Parallel work is focused on Fe_3O_4@SiO_2 magnetic core–shell nanoparticles. These are synthesized by coprecipitation of Fe_3O_4 cores, followed by TEOS hydrolysis and subsequent porous silica shell formation with CTAB or PEG surfactants. Magnetic characterization by SQUID magnetometry confirmed their superparamagnetic behaviour and responsiveness to external fields, verifying that they may be suitable for targeted delivery in biomedical applications. Drug loading and release experiments are being extended to this system, with release monitored by HPLC to ensure drug quantification.

Results and Preliminary Findings

SMS-60 nanoparticles were successfully synthesized, functionalized, and impregnated with apixaban. N_2 sorption confirmed porosity (3–5 nm pore range) and high specific surface area, while TEM revealed uniform spherical morphology. FTIR analysis confirmed surface functionalization and indicated drug–matrix interactions. TGA analysis indicated effective drug loading. Drug release studies demonstrated a continuous and sustained profile across both acidic and physiological pH. More than 85 % of apixaban (from 60 to 180 mg of apixaban per g of carrier) depending on the sample and pH conditions) was released over 72 h, followed by a plateau. Such sustained release profiles indicate strong potential for controlled dosing. Notably, repeated administration of fresh drug-loaded nanoparticles restarted the release cycle, highlighting the feasibility of controlled, long-term dosing strategies.

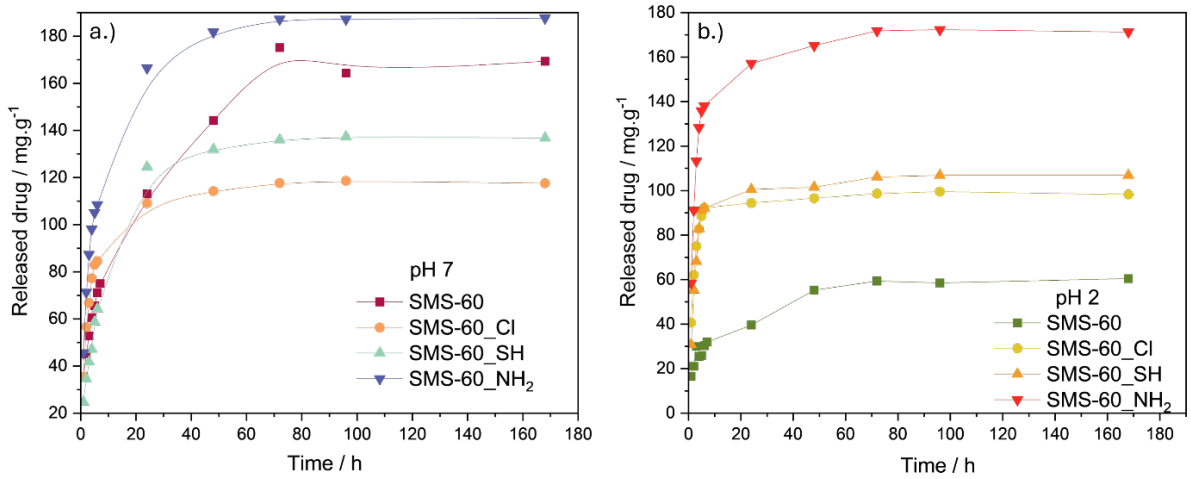

Figure 1 Cumulative apixaban release from SMS-60 nanoparticles under *a.*) physiological (pH 7) and *b.*) gastric fluid (pH 2) conditions over 168 h.

Incubation of clots with apixaban solutions revealed concentration-dependent effects. Early (3 h), minimal morphological changes were observed. However, after 24 and 48 h, SEM imaging revealed disruption of the fibrin mesh, including thinning of fibres and increased pore sizes within the network. These structural changes suggest that apixaban exposure alters clot morphology in vitro. Current experiments focus on clot incubation with apixaban-loaded SMS-60 nanoparticles. Full datasets are in progress.

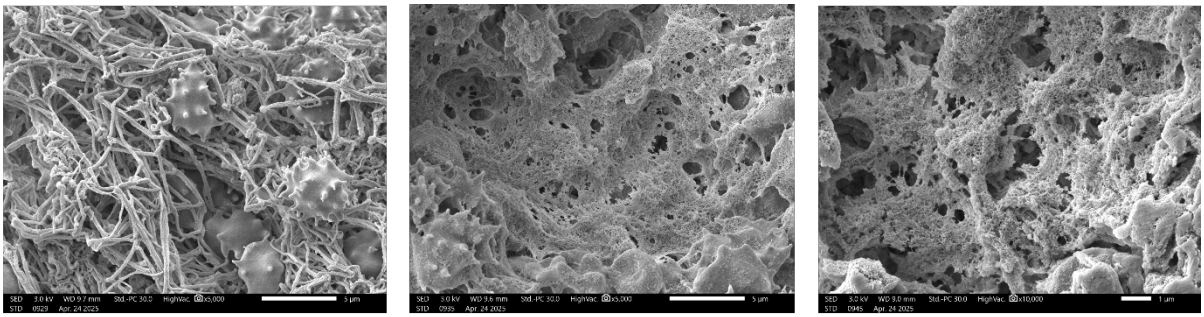

Figure 2 SEM images of blood clots: *a.*) untreated control, *b.*) after 24 h incubation with apixaban (0.25 mg/mL), *c.*) after 24 h incubation with apixaban (0.5 mg/mL), showing disruption of fibrin network.

The development of Fe_3O_4@SiO_2 nanoparticles is underway, with early structural characterization confirming successful core–shell morphology. SQUID magnetometry measurements (ZFC/FC at 100 Oe, 5 K and 300 K) revealed superparamagnetism at physiological temperature (*Figure 3*), confirming responsiveness to external magnetic fields and suitability for biomedical targeting. This verification underscores their potential to be guided externally to thrombotic sites, where the porous silica shell can sustain localized drug release. Such carriers thus address two major clinical challenges simultaneously: minimizing systemic side effects and achieving site-specific drug action. Apixaban impregnation is currently underway, with release studies planned via HPLC.

Conclusion and Outlook

This research highlights the potential of nanoporous silica platforms for advanced antithrombotic drug delivery. Mesoporous silica nanoparticles enable efficient apixaban loading and sustained release, while clot-interaction studies suggest feasible drug penetration into fibrin networks. The integration of magnetic cores into Fe_3O_4@SiO_2 architectures further introduces the possibility of spatially controlled delivery via external magnetic fields.

The novelty of this approach lies in combining controlled, sustained drug release with targeted clot localisation—two factors that may significantly improve therapeutic efficacy while minimizing systemic side effects. Future work will focus on optimizing drug loading into magnetic core–shell carriers, evaluating clot penetration under magnetic guidance, and quantifying drug release kinetics in physiologically relevant conditions. By advancing these directions, nanoporous silica pathways may provide a foundation for safer and more effective strategies in thrombosis management, ultimately reducing bleeding risks while enhancing therapeutic precision.

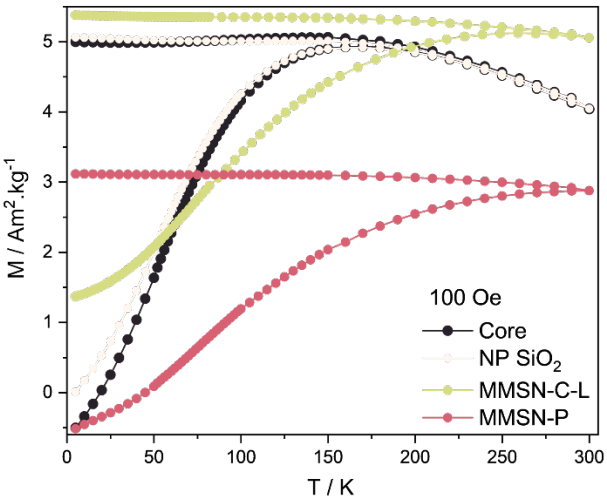

Figure 3 ZFC/FC magnetisation curves of Fe_3O_4@SiO_2 nanoparticles at 100 Oe, showing blocking at low T and superparamagnetism at 300 K.

Acknowledgements
This work was supported by the EU NextGenerationEU through the Recovery and Resilience Plan for Slovakia, project No. 09I03-03-V04-00722.

References
[1] M. Alquwaizani, L. Buckley, C. Adams, and J. Fanikos, 'Anticoagulants: A Review of the Pharmacology, Dosing, and Complications', *Curr. Emerg. Hosp. Med. Rep.*, vol. 1, no. 2, pp. 83–97, 2013, doi: 10.1007/s40138-013-0014-6.
[2] S. Hassanpour, H.-J. Kim, A. Saadati, P. Tebon, C. Xue, F. W. van den Dolder, J. Thakor, B. Baradaran, J. Mosafer, A. Baghbanzadeh, N. R. de Barros, M. Hashemzaei, K. J. Lee, J. Lee, S. Zhang, W. Sun, H.-J. Cho, S. Ahadian and A. Khademhosseini, 'Thrombolytic agents: Nanocarriers in controlled release', *Small Weinh. Bergstr. Ger.*, vol. 16, no. 40, p. e2001647, Oct. 2020, doi: 10.1002/smll.202001647.
[3] F. da S. Bruckmann, F. B. Nunes, T. da R. Salles, C. Franco, F. C. Cadoná, and C. R. Bohn Rhoden, 'Biological Applications of Silica-Based Nanoparticles', *Magnetochemistry*, vol. 8, no. 10, Art. no. 10, Oct. 2022, doi: 10.3390/magnetochemistry8100131.
[4] M. Fralick, M. Colacci, S. Schneeweiss, K. F. Huybrechts, K. J. Lin, and J. J. Gagne, 'Effectiveness and Safety of Apixaban Compared With Rivaroxaban for Patients With Atrial Fibrillation in Routine Practice: A Cohort Study', *Ann. Intern. Med.*, vol. 172, no. 7, pp. 463–473, Apr. 2020, doi: 10.7326/M19-2522.

9th International Conference on Novel Materials Fundamentals and Applications
High Tatras, 12.10.-15.10.2025

Evaluation of the Activity of $Mo_xNi_yAl_z$ -Based Alloy for the Hydrogen Evolution Reaction on Different Substrates

R. Bodnarova[a,*], D. Volavka[a], V. Komanicky[a]
[a] Institute of Physics, Faculty of Science, P. J. Safarik University, Park Angelinum 9, 040 01, Kosice, Slovak Republic
* renata.bodnarova@upjs.sk

Today's society faces critical challenges such as the energy crisis and the associated environmental pollution. Using green hydrogen (H_2), produced by water electrolysis, represents an ecological source of energy [1], [2]. The growing global demand for hydrogen production is leading to intensive research into catalytic materials for the hydrogen evolution reaction (HER) [3]. Alkaline water electrolysis is a promising method of hydrogen production [4]. As is well known, the best catalysts for HER are materials containing Pt. The researchers aim to prepare materials that will be catalytically active without platinum group metals (PGM). Currently, research uses more cost-effective elements that are more abundant on Earth [3], such as nickel (Ni) and its alloys. Mo-Ni-Al alloy shows promising results for hydrogen evolution in alkaline electrolyzers. The preparation of catalysts in the form of thin films provides the advantage of stabilizing phases that do not occur in bulk materials under normal conditions. This technology makes it possible to more precisely control the structure and composition of materials, which improves their catalytic and electrochemical properties [5], [6].

Based on our previous research [5], [6], we focused on the development of Mo-Ni-Al thin-film catalysts. Using magnetron sputtering, we prepared a series of Mo-Ni-Al samples with a composite ratio of 80:5:15 at a temperature of 800°C. A series of samples was deposited on various substrates, including carbon-based materials (GC, HOPG, and C) and nickel-based substrates (Ni, NiFe foil, NiTa foil, and Ni fiber). The HER electrocatalytic performance of the samples was investigated in 1 M NaOH electrolyte. A series of reference samples composed of Ni on the same substrates was deposited on the same substrates. A comparative analysis of the HER activity (*Figure 1*) between the Ni samples and the $Mo_{80}Ni_5Al_{15}$(800°C) alloys enabled the identification of the influence of alloying and substrate selection on catalytic performance.

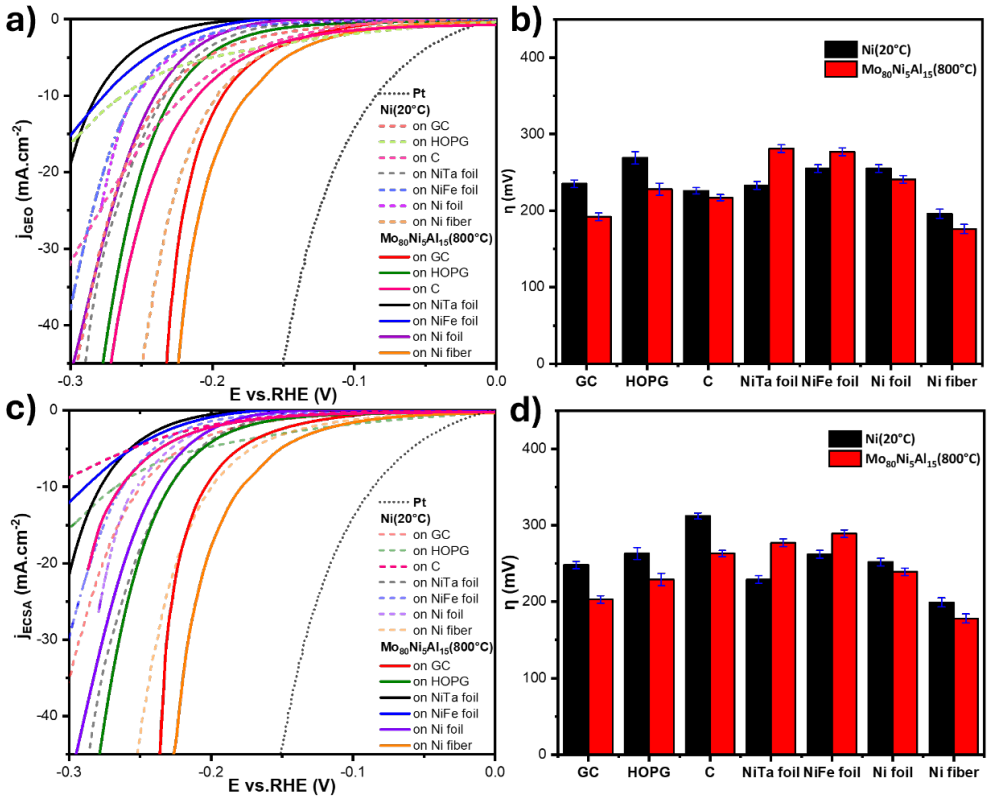

Figure 1 (a) Polarization curves of $Mo_{80}Ni_5Al_{15}$ (800 °C) and Ni (20 °C) thin films deposited on various substrates, with current density normalized to geometric surface area j_{GEO}. *(b)* Corresponding bar chart summarizing overpotential values at j = –10 mA·cm^{-2} (geometric area basis). *(c)* Polarization curves of the same samples normalized to the electrochemically active surface area j_{ECSA}. *(d)* Bar chart of overpotential values at j = –10 mA·cm^{-2} based on ECSA-normalized current densities.

Figure 1 a shows the polarization curves of all prepared samples normalized to geometric area. The overpotential values at a current density of -10 mA.cm² are summarized in *Table 1*. Among all tested samples, the $Mo_{80}Ni_5Al_{15}$(800°C) alloy deposited on Ni fiber exhibited the lowest overpotential (−176 mV), approaching that of Pt (~−80 mV under identical conditions). Also, pure Ni prepared on nickel fiber achieved excellent results (-196 mV). Additionally, the alloy $Mo_{80}Ni_5Al_{15}$ (800°C) deposited on the glassy carbon (GC) substrate exhibited relatively low catalytic activity (−188 mV) compared to other tested configurations [5]. As illustrated in *Figure 1 b*, $Mo_{80}Ni_5Al_{15}$(800°C) alloys exhibit lower overpotentials than pure Ni on the identical substrates. However, $Mo_{80}Ni_5Al_{15}$ alloy on NiTa and NiFe foils represented an exception. The overpotentials for pure Ni (−233 mV and −255 mV, respectively) were lower than those for the corresponding alloys (−280 mV for NiTa and −276 mV for NiFe).

To more accurately assess the HER catalytic activity of $Mo_{80}Ni_5Al_{15}$ and Ni thin films, the polarization curves were normalized to the electrochemically active surface area j_{ECSA} (*Figure 1 c*). These allow a direct comparison of the intrinsic catalytic activity between different substrates. The corresponding overpotentials at $j = -10\ mA \cdot cm^{-2}$ (normalized to ECSA) are shown in the bar graph in *Figure 1 d* and summarized in *Table 1*. The catalyst $Mo_{80}Ni_5Al_{15}$(800 °C)/ Ni fiber showed enhanced catalytic performance (-178 mV). This elevated catalytic activity can be attributed to the porous structure of the nickel fiber. This substrate provided a larger electrochemically active surface area and more suitable catalytic sites for HER. The porous network maximizes interaction with the electrolyte, contributing to both activity and stability. The results confirm the importance of ECSA normalization for the objective evaluation of thin film electrocatalysts.

Table 1 Summary values of overpotential (η) of $Mo_{80}Ni_5Al_{15}$ (800°C) and Ni (20°C) on various substrates series for hydrogen evolution reaction in 1M NaOH.

	η (mV) @ j_{GEO} (-10 mA.cm^{-2})	η (mV) @ j_{ECSA} (-10 mA.cm^{-2})	η (mV) @ j_{GEO} (-10 mA.cm^{-2})	η (mV) @ j_{ECSA} (-10 mA.cm^{-2})
	Ni prepared at 20°C on various substrates		$Mo_{80}Ni_5Al_{15}$ prepared at 800°C on various substrates	
GC	-235	-248	-188	-203
HOPG	-263	-264	-226	-229
C	-221	-312	-212	-263
NiTa foil	-233	-229	-280	-277
NiFe foil	-255	-262	-276	-289
Ni foil	-255	-252	-239	-239
Ni fiber	-196	-199	-176	-178

The XPS was performed. High-resolution XPS measurements were conducted using a SPECS PHOIBOS 100 hemispherical analyzer equipped with a monochromatic Al Kα source (1486.6 eV) operating at 200 W. All measurements were performed at room temperature under ultra-high vacuum (~10^{-8} mbar).

Our XPS results (*Figure 2*) confirmed the successful formation of the $Mo_{80}Ni_5Al_{15}$ alloy with detectable oxidation states corresponding to Mo^0, Mo^{6+}, Ni^0, Ni^{3+}. XPS spectra demonstrate complete oxidation from Ni^0 to Ni^{3+} after electrochemical testing, implying higher oxidation stability. This observation is catalytically significant. Ni^{3+} species are reported to exhibit stronger reactant binding and lower activation barriers for HER compared to Ni^0 or Ni^{2+} [7], study exhibits that higher-valent Ni^{3+} (and Co^{2+}) contribute to HER activity through enhanced water dissociation and proton adsorption.

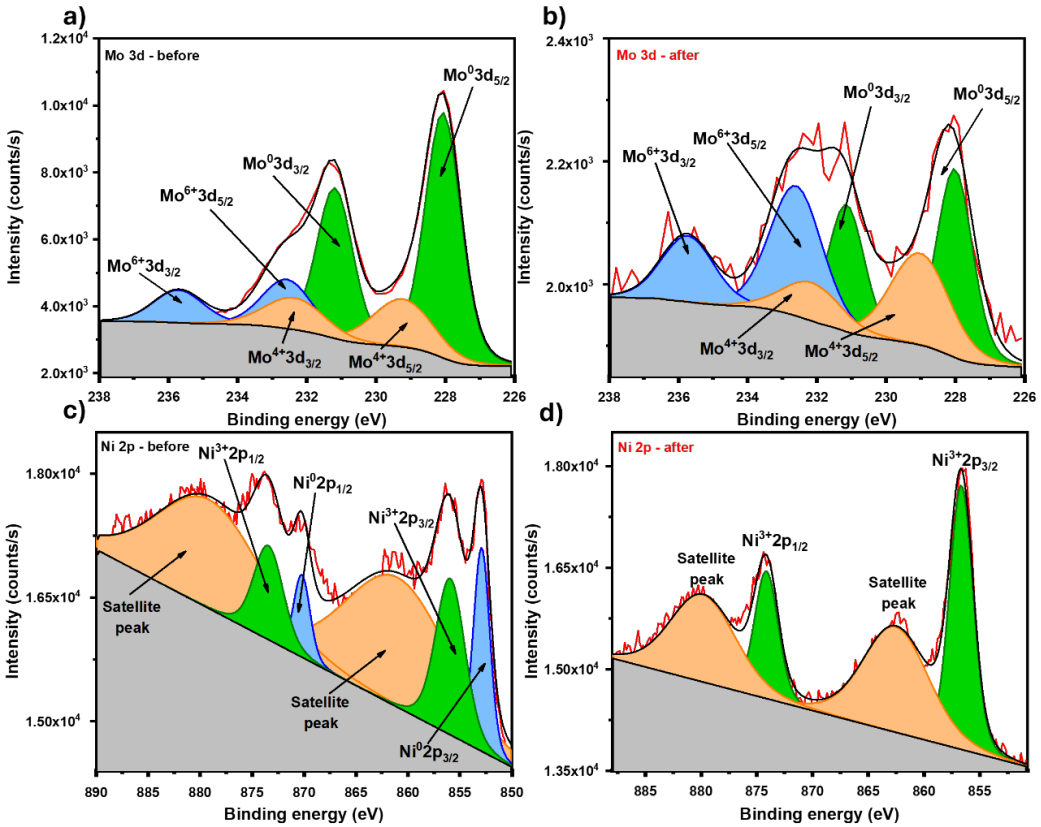

Figure 2 High resolution Mo3d XPS spectra of sample Mo80Ni5Al15 (800°C) on Ni fiber before *(a)* and after measurement *(b)*. High resolution Ni2p XPS spectra of sample Mo80Ni5Al15 (800°C) on Ni fiber before *(c)* and after measurement *(d)*.

Acknowledgements
Funded by the EU NextGenerationEU through the Recovery and Resilience Plan for Slovakia under the project No. 09I03-03-V04-00385.

References

[1] J.A. Turner, "Sustainable hydrogen production." *Science*, vol. 305, no. 5686, pp. 972-974, 2004, doi: 10.1126/science.1103197.
[2] Y. Zheng, Y. Jiao, M. Jaroniec, S. Z. Qiao, "Advancing the electrochemistry of the hydrogen-evolution reaction through combining experiment and theory." *Angewandte Chemie International Edition*, vol. 54, no.1, pp. 52-65, 2015, doi: 10.1002/anie.201407031.
[3] T. B. Ferriday, P. H. Middleton, M. L. Kolhe, "Review of the hydrogen evolution reaction—A basic approach." *Energies*, vol. 14, no. 24, pp. 8535, 2021, doi: 10.3390/en14248535.
[4] H. A. Firouzjaie, W. E. Mustain, "Catalytic advantages, challenges, and priorities in alkaline membrane fuel cells. " *ACS catalysis*, vol. 10, no.1, pp. 225-234, 2019, doi: 10.1021/acscatal.9b03892.
[5] R. Bodnarova, V. Latyshev, S. Vorobiov, M. Lisnichuk, H. You, V. Komanicky, "Improved catalytic activity of MoxNiyAlz thin films as electrocatalyst for hydrogen evolution reaction in alkaline media." *International Journal of Hydrogen Energy*, vol. 49, pp. 506-217, 2024, doi: 10.1016/j.ijhydene.2023.08.173.
[6] R. Bodnarova, M. Kozejova, V. Latyshev, S. Vorobiov, M. Lisnichuk, H. You, M. Gregor, V. Komanicky, "Study of synergistic effects and compositional dependence of hydrogen evolution reaction on MoxNiy alloy thin films in alkaline media." *Molecular Catalysis*, vol. 528, pp. 1124721, 2022, doi: 10.1016/j.mcat.2022.112481.
[7] F. Tsai, Y. Deng, Ch. Pao, J. Chen, J. Lee, K. Laic and W. Liaw, "The HER/OER mechanistic study of an FeCoNi-based electrocatalyst for alkaline water splitting." *Journal of Materials Chemistry A*, vol. 8, no. 19, pp. 9939-9950, 2020, doi: 10.1039/D0TA01877E.

Tuning Sulphur Confinement and Redox Kinetics in Li–S Batteries through Metal-Dependent MOF-74 Frameworks

D. Capkova[a,b], T. Kazda[b], N. Kiraly[c], A. Strakova Fedorkova[d], M. Almasi[c,*]
[a] Department of Chemical Sciences, Bernal Institute, University of Limerick, V94 T9PX Limerick, Ireland
[b] Department of Electrical and Electronic Technology, Faculty of Electrical Engineering and Communication, Brno University of Technology, Technická 10, CZ-616 00, Brno, Czech Republic
[c] Department of Inorganic Chemistry, Faculty of Sciences, Pavol Jozef Šafárik University in Košice, Moyzesova 11, SK-040 01, Košice, Slovak Republic
[d] Department of Physical Chemistry, Faculty of Sciences, Pavol Jozef Šafárik University in Košice, Moyzesova 11, SK-040 01, Košice, Slovak Republic
* miroslav.almasi@upjs.sk

Lithium–sulphur (Li–S) batteries are widely regarded as one of the most promising next-generation electrochemical energy storage systems owing to their exceptionally high theoretical specific capacity of 1675 mAh g^{-1} and energy density approaching 2600 Wh kg^{-1}, which significantly surpasses the performance limits of conventional lithium-ion batteries. The abundance, low cost, and environmental friendliness of sulphur further enhance the attractiveness of Li–S chemistry for large-scale applications, ranging from electric vehicles to grid-scale energy storage. Nevertheless, despite decades of research, the practical deployment of Li–S batteries remains hindered by several intrinsic challenges. The dissolution and uncontrolled migration of intermediate lithium polysulphides (Li_2S_x, $4 \leq x \leq 8$) between the cathode and anode induce the so-called shuttle effect, resulting in severe active material loss, low Coulombic efficiency, and poor cycling stability. Additionally, the substantial volumetric expansion of sulphur during lithiation, its inherently low electrical conductivity, and the sluggish redox kinetics of polysulphide conversion collectively compromise rate capability and long-term durability. Addressing these limitations requires the rational design of advanced cathode host materials capable of physically confining sulphur, chemically binding soluble polysulphides, and catalytically accelerating their redox transformations.

Metal–organic frameworks (MOFs), a class of crystalline porous coordination polymers composed of metal ions and organic linkers, have recently emerged as highly versatile materials for electrochemical energy storage. Their exceptionally high surface areas, tunable porosities, and rich chemical functionalities enable precise control over ion transport and interfacial interactions. Among the broad family of MOFs, the MOF-74 topology (also known as CPO-27), based on the 2,5-dioxido-1,4-benzenedicarboxylate linker and divalent metal cations, is of particular interest. MOF-74 possesses one-dimensional hexagonal channels with pore apertures of approximately 11 Å, ideally suited to accommodate S_8 molecules. More importantly, its frameworks expose a high density of coordinatively unsaturated metal sites (CUSs) along the channel walls. These Lewis-acidic sites provide strong binding to polar polysulphide species, thereby enabling simultaneous physical confinement and chemical anchoring. Furthermore, the incorporation of catalytically active transition metals into the MOF-74 framework offers the possibility to accelerate polysulphide redox kinetics, thereby mitigating shuttle effects and enhancing overall cell efficiency.

In this study, we systematically investigated the role of different divalent metal centres, namely Mg(II), Fe(II), and Ni(II), in determining the structural stability, sulphur confinement ability, and electrochemical performance of S/MOF-74 composite cathodes. Mg and Fe were selected as earth-abundant and environmentally benign elements with favourable cost profiles, while Ni was introduced due to its well-established catalytic activity and redox versatility in electrochemical systems. The MOF-74(M) frameworks were synthesised via solvothermal methods, subjected to solvent-exchange activation to remove strongly bound DMF molecules, and subsequently impregnated with sulphur. Composite electrodes containing sulphur, MOF-74, and conductive carbon were fabricated and extensively characterised by powder X-ray diffraction (PXRD), thermogravimetric analysis (TGA), nitrogen adsorption–desorption, scanning electron microscopy (SEM), infrared spectroscopy (FTIR), elemental analysis, and high-resolution X-ray photoelectron spectroscopy (XPS). Their electrochemical behaviour was further probed using cyclic voltammetry (CV), galvanostatic cycling, rate capability tests, and electrochemical impedance spectroscopy (EIS).

Thermogravimetric analysis revealed distinct differences in thermal stability among the three frameworks. MOF-74(Mg) exhibited the highest stability, maintaining structural integrity up to 400 °C, followed by MOF-74(Ni) stable up to 300 °C, whereas MOF-74(Fe) showed decomposition at significantly lower temperatures (~200 °C). These observations correlated directly with optimal activation conditions before sulphur loading: high-temperature activation (200–250 °C) was required for Ni and Mg frameworks to achieve maximum porosity, whereas Fe-based MOF-74 necessitated milder activation at 60 °C to prevent structural collapse. Nitrogen physisorption confirmed that the activated Mg and Ni analogues reached specific surface areas exceeding 1100 m^2 g^{-1}, while Fe-based samples displayed optimal values only under mild conditions. Incorporation of sulphur into the frameworks led to a drastic reduction in surface area and pore volume, confirming effective pore filling and confinement.

PXRD analysis confirmed that all as-synthesised and solvent-exchanged MOF-74(M) samples retained their crystalline structure and characteristic honeycomb topology, with no evidence of structural degradation during activation. In composite cathodes, the diffraction patterns were dominated by crystalline sulphur, yet the presence of the MOF-74 phase was still discernible, confirming structural stability throughout the electrode fabrication process. Complementary FTIR measurements further corroborated the integrity of the frameworks, while the emergence of characteristic sulphur vibrational modes validated successful sulphur incorporation.

XPS provided valuable insight into the nature of sulphur–metal interactions across the MOF-74 series. For S/MOF-74(Ni), a pronounced binding energy shift of the S 2p peaks indicated strong interaction between sulphur species and Ni(II) centres, consistent with significant electronic perturbation and stabilisation of polysulphides. In S/MOF-74(Mg), dual spectral features suggested both Mg–sulphur interactions and partial formation of oxidised sulphur species. Conversely, S/MOF-74(Fe) displayed only minimal shifts relative to elemental sulphur, suggesting weaker interactions. The hierarchy of sulphur binding strength, Ni > Mg > Fe, correlated well with the subsequent electrochemical performance.

Electrochemical testing revealed substantial differences among the three composite systems (see *Figure 1*). Cyclic voltammetry showed characteristic sulphur redox peaks near 2.3 V and 2.0 V for all electrodes, yet the stability and reproducibility of these signals varied. The S/MOF-74(Ni) electrode exhibited well-defined and stable redox features across repeated scans, whereas S/MOF-74(Fe) displayed significant current fluctuations indicative of unstable reaction kinetics. Rate capability tests further distinguished the samples: while all three electrodes delivered initial capacities around 600–650 mAh g^{-1} at 0.2 C, the capacity retention at higher C-rates was markedly superior for S/MOF-74(Ni). At 2 C, it sustained capacities above 300 mAh g^{-1}, while Mg- and Fe-based analogues dropped more severely. Importantly, when returned to 0.2 C, Ni-containing electrodes largely recovered their initial performance, highlighting excellent structural resilience and reversibility.

Long-term galvanostatic cycling provided the most striking contrast. The S/MOF-74(Ni) cathode achieved a reversible capacity of 465 mAh g^{-1} with a negligible fading rate of 0.001% per cycle over 200 cycles, corresponding to an outstanding capacity retention of 99.75%. In contrast, the S/MOF-74(Mg) electrode retained only 77.96% of its capacity over the same period, while the Fe analogue suffered catastrophic fading, retaining a mere 2.78% of capacity after 200 cycles. Coulombic efficiencies mirrored these trends: Ni- and Mg-based electrodes exhibited average efficiencies around 89–90%, whereas Fe-based systems were plagued by persistent parasitic reactions linked to insufficient polysulphide confinement. These findings are consistent with the stronger sulphur–metal interactions observed in XPS and demonstrate the critical role of catalytic activity and binding strength in governing long-term stability.

The excellent performance of S/MOF-74(Ni) can be attributed to the synergistic combination of physical confinement within the microporous channels, chemical anchoring of polysulphides at Lewis acidic Ni sites, and catalytic acceleration of their redox transformations. This synergy suppresses the shuttle effect, enhances sulphur utilisation, and stabilises cycling behaviour. The Mg analogue benefits from strong confinement and high thermal stability but lacks sufficient catalytic activity, resulting in moderate but less durable performance. The Fe analogue, although earth-abundant, proved unsuitable due to its poor stability and weak interactions with polysulphides.

Beyond the intrinsic comparison among metal centres, these results underscore broader design principles for MOF-based sulphur hosts. First, optimisation of activation conditions is critical to maximising accessible surface area without compromising framework integrity. Second, the choice of central metal profoundly influences not only the physical stability but also the electronic environment and catalytic potential, which in turn dictate polysulphide adsorption and redox kinetics. Third, effective composite design, combining MOFs with conductive carbon and polymer binders, remains essential to overcome the intrinsic low conductivity of sulphur and MOF matrices.

In conclusion, this work demonstrates that the integration of sulphur into MOF-74(Ni) yields a highly stable and efficient composite cathode material for Li–S batteries, outperforming its Mg and Fe analogues in terms of both cycling stability and rate capability. The findings establish a clear correlation between framework stability, sulphur–metal interactions, and electrochemical performance, providing fundamental insights into the design of next-generation cathode hosts. By highlighting the decisive role of catalytic metal centres, this study paves the way for rational tailoring of MOF-based materials to achieve synchronised sulphur confinement, polysulphide adsorption, and redox acceleration.

From a practical perspective, the demonstrated performance metrics already exceed those of commercial lithium-ion batteries, suggesting that MOF-based composites such as S/MOF-74(Ni) could form the basis of future high-energy-density devices with improved durability and efficiency. Future efforts should focus on optimising sulphur loading under lean electrolyte conditions, exploring multi-metallic MOF-74 variants for synergistic effects, and evaluating the scalability and cost-effectiveness of electrode fabrication. Collectively, these advances could bring Li–S batteries closer to commercial reality, enabling sustainable and high-performance energy storage solutions for the electrified future.

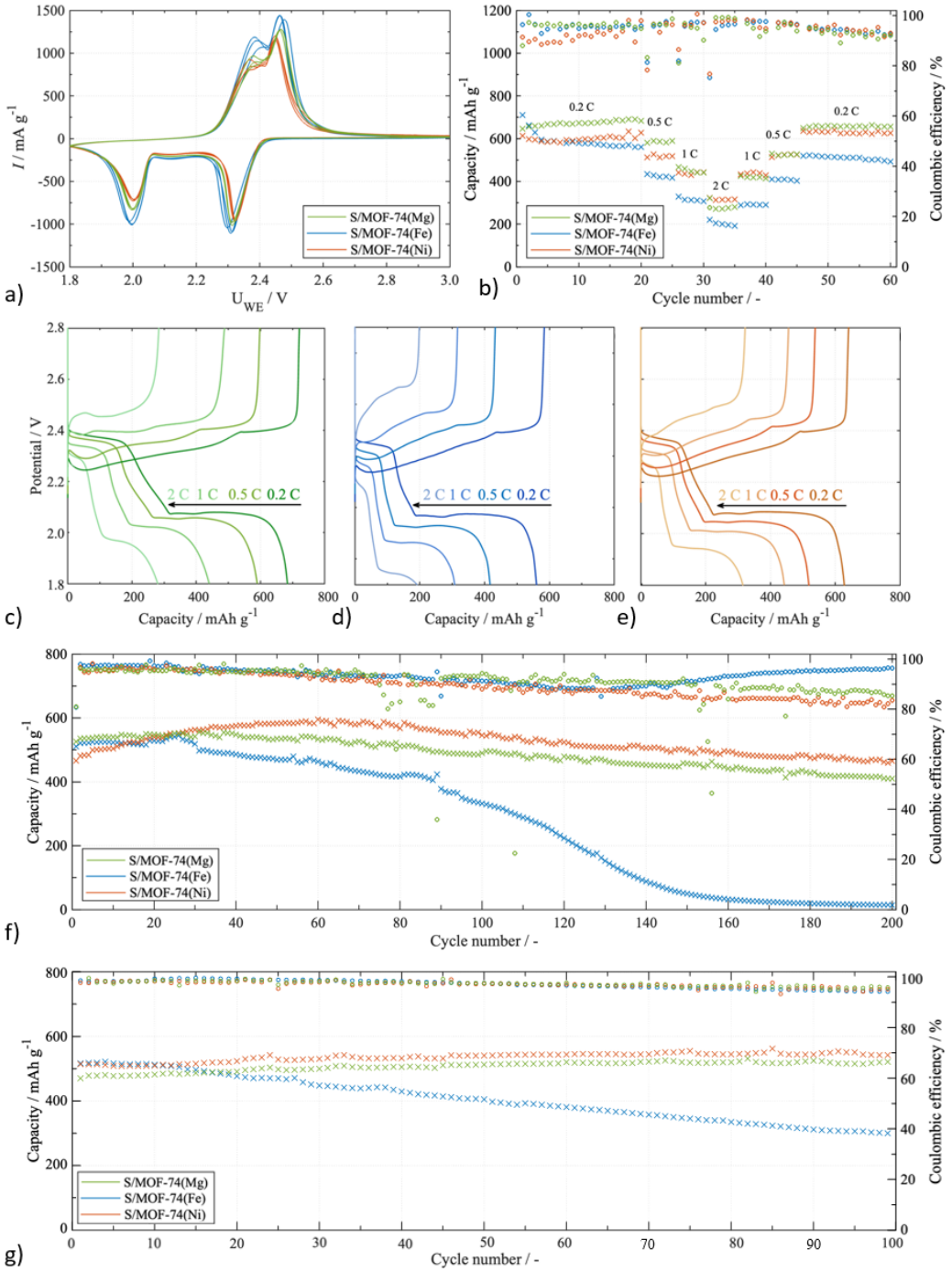

Figure 1 a) CV curves at 0.1 mV s^{-1} of S/MOF-74(Mg), S/MOF-74(Fe), and S/MOF-74(Ni). *b)* Rate capabilities tested at different C-rates of S/MOF-74(Mg), S/MOF-74(Fe), and S/MOF-74(Ni). Voltage profiles at various C-rates for *c)* S/MOF-74(Mg) cathode, *d)* S/MOF-74(Fe) cathode, and *e)* S/MOF-74(Ni) cathode. Cycling properties and Coulombic efficiency at *f)* 0.5 C for 200 cycles and *g)* 1 C for 100 cycles.

Acknowledgements
This work was supported by the EU NextGenerationEU through the Recovery and Resilience Plan for Slovakia under the project SUNFLOWERS No. 09I02-03-V01-00022.

Optimising Electrochemical Deposition of Hydroxyapatite Coatings for Ti6Al4V Medical Implants

V. Cakyova[a,*], R. Orinakova[a]
[a] Department of Physical Chemistry, Faculty of Science, P. J. Šafárik University in Košice, Moyzesova 11, 041 54, Košice, Slovak republic
* viktoria.cakyova@student.upjs.sk

Craniofacial defects can arise from traumatic injuries, congenital malformations, infections, or oncological therapies, creating a significant medical, social and economic burden worldwide. To address these challenges, craniofacial implants are used to restore both the structural and functional integrity of damaged tissues [1]. However, these implants face important complications, including peri-implant soft tissue reactions, implant failure, infections, or impaired bone remodelling. Ideally, implants for craniofacial repair should exhibit biosafety, biocompatibility, mechanical stability, osteoinductive or osteoconductive properties, and support both hard and soft-tissue integration while remaining easy to fabricate and sterilise. Various classes of implants, such as metal-based, ceramic, and polymeric biomaterials, have been used to meet these requirements, each with specific advantages and limitations [2], [3].

Titanium implants are widely used in craniofacial surgery due to their biocompatibility, mechanical strength, imaging compatibility, and corrosion resistance. Despite these advantages, titanium and its alloys face several limitations that compromise their long-term performance. Their bio-inert surface inhibits osseointegration, often resulting in fibrotic encapsulation rather than bone bonding. In addition, titanium exhibits poor tribological behaviour, generating wear debris that may trigger inflammation, while long-term exposure to physiological fluids can release metallic ions, reducing local biocompatibility. These challenges have driven the development of surface modification strategies aimed at enhancing the biological and functional performance of titanium implants without compromising their bulk properties [4], [5].

Among these strategies, the deposition of bioceramic coatings is one of the most effective approaches. Bioinert ceramics, such as alumina and zirconia, improve mechanical stability but show limited interaction with bone. In contrast, bioactive ceramics, particularly calcium phosphates and bioglass, strongly promote osseointegration. Hydroxyapatite (HA, $Ca_{10}(PO_4)_6(OH)_2$) has emerged as the most widely applied coating due to its chemical and structural similarity to bone mineral (Ca/P ratio 1.67), excellent osteoconductivity and the ability to serve as a barrier against metal ion release. HA coatings accelerate bone healing, improve implant fixation, and significantly improve long-term clinical success [6], [7].

Several techniques are used to deposit HA coatings onto titanium, such as plasma spraying, micro-arc oxidation, hydrothermal treatment, sol-gel, electrophoretic or electrochemical deposition, and biomimetic approaches. Electrochemical deposition stands out among these methods due to the ability to produce uniform and precisely controlled coatings. Still, electrochemical deposition outcomes are influenced by multiple factors, including deposition time, current density, electrolyte concentration, temperature, pH and other variables. These parameters collectively determine the properties of the resulting HA layer, making systematic investigation essential for optimising coating performance and enhancing implant functionality in biomedical applications [8], [9].

The investigation of different deposition parameters (*Table 1*) in order to optimise coating adhesion, morphology, and bioactivity of the prepared ceramic coatings is therefore crucial for the development of the implant material.

Table 1 Main electrochemical deposition parameters for hydroxyapatite coatings on Ti6Al4V and their influence on coating properties [7]

Deposition parameter	Influence on coating	Typical values used for Ti6Al4V
Deposition time	▪ Determines coating thickness and morphology ▪ Prolonged times increase thickness but may reduce adhesion or introduce cracking	10 – 60 min
Current density	▪ Controls growth rate, crystallinity, and adhesion ▪ Excessive values can cause porous, brittle coatings	1 – 20 mA/cm^2
Electrolyte concentration	▪ Regulates ion availability, influencing phase composition, homogeneity, and the Ca/P ratio of the coating	5 – 50 mM Ca^{2+}, PO_4^{3-}
Temperature	▪ Higher temperature improves crystallinity and uniformity ▪ Excessive heat may destabilize HA phases	25 – 70 °
pH level	▪ Strongly affects phase stability and deposition outcome	4 – 6 (commonly~5)
Applied potential/voltage	▪ Controls nucleation rate and adhesion strength ▪ Higher potentials accelerate deposition but can compromise quality	-1.2 – -2.0 V vs. SCE
Surface preparation	▪ Roughness and pre-treatment improve adhesion and uniformity of HA coating	▪ Sandblasting ▪ Etching ▪ Polishing

Acknowledgements
This work was supported by the Slovak Research and Development Agency under the project APVV-24-0033 and APVV-20-0278.

References
[1] M. Kauke-Navarro, L. Knoedler, S. Knoedler, C. Deniz, L. Stucki, and A. F. Safi, "Balancing beauty and science: a review of facial implant materials in craniofacial surgery," 2024, *Frontiers Media SA*. doi: 10.3389/fsurg.2024.1348140.
[2] O. Mishchenko, A. Kopchak, D. Chernohorskyi, V. Deineka, N. Waloszczyk, M. Pogorielov and W. Simka, "Craniofacial reconstruction using 3D personalized implants with enhanced surface properties: Technological and clinical aspects," *Applied Surface Science Advances*, vol. 16, Aug. 2023, doi: 10.1016/j.apsadv.2023.100437.
[3] M. Ureel, S. Corthals, R. Coopman, H. Vermeersch, and N. Brusselaers, "Implant failure of facial prostheses: systematic review and meta-analysis," *Int J Oral Maxillofac Surg*, vol. 54, no. 9, pp. 881–895, Sep. 2025, doi: 10.1016/j.ijom.2025.03.016.
[4] J. Li, T. Zhang, Z. Liao, Y. Wei, R. Hang, and D. Huang, "Engineered functional doped hydroxyapatite coating on titanium implants for osseointegration," Nov. 01, 2023, *Elsevier Editora Ltda*. doi: 10.1016/j.jmrt.2023.09.239.
[5] C. E. Wen, W. Xu, W. Y. Hu, and P. D. Hodgson, "Hydroxyapatite/titania sol-gel coatings on titanium-zirconium alloy for biomedical applications," *Acta Biomater*, vol. 3, no. 3 SPEC. ISS., pp. 403–410, 2007, doi: 10.1016/j.actbio.2006.10.004.
[6] A. Jaafar, C. Hecker, P. Árki, and Y. Joseph, "Sol-gel derived hydroxyapatite coatings for titanium implants: A review," Dec. 01, 2020, *MDPI AG*. doi: 10.3390/bioengineering7040127.
[7] P. R. Dev, C. P. Anand, D. S. Michael, and P. Wilson, "Hydroxyapatite coatings: a critical review on electrodeposition parametric variations influencing crystal facet orientation towards enhanced electrochemical sensing," Sep. 06, 2022, *Royal Society of Chemistry*. doi: 10.1039/d2ma00620k.
[8] P. Puranto, M. P. Kamil, K. P. Suwondo, A. D. Mellinia, A. N. Avivin, I. M. Ulfah, M. Kozin, "Unveiling the pH influence: Enhancing hydroxyapatite-coated titanium biomedical implants through electrochemical deposition," *Ceram Int*, vol. 50, no. 8, pp. 13412–13421, Apr. 2024, doi: 10.1016/j.ceramint.2024.01.253.
[9] R. Gorejová, R. Oriňáková, Z. Orságová Králová, T. Sopčák, I. Šišoláková, M. Schnitzer, M. Kohan and R. Hudák, "Electrochemical deposition of a hydroxyapatite layer onto the surface of porous additively manufactured Ti6Al4V scaffolds," *Surf Coat Technol*, vol. 455, Feb. 2023, doi: 10.1016/j.surfcoat.2022.129207

Electrochemical Determination of Ciprofloxacin Using a GaTCPP(Ni)-Modified Screen-Printed Carbon Electrode

J. Demeterova[a,*], J. Shepa[a] , N. Kiraly[b], M. Almasi[b], I. Sisolakova[a],
[a] Department of Physical Chemistry, Pavol Jozef Šafárik University in Košice, Moyzesova 11, 040 01 Košice, Slovak Republic
[b] Department of Inorganic Chemistry, Pavol Jozef Šafárik University in Košice, Moyzesova 11, 040 01 Košice, Slovak Republic
* jana.demeterova@student.upjs.sk

Introduction

Antibiotics are among the most significant groups of drugs used to treat bacterial infections. However, their extensive use in medicine, veterinary practice, and agriculture leads to the frequent occurrence of residues in environmental and biological samples, which may contribute to the growth of antimicrobial resistance [1]. Consequently, it is necessary to develop reliable methods for the detection of antibiotics in different samples, including biological fluids and environmental matrices.

Ciprofloxacin, a broad-spectrum fluoroquinolone, is frequently detected in environmental and biological samples [2]. This is problematic, as it may disturb bacterial populations and promote the development of resistant bacteria. In recent decades, electrochemical determination of analytes has become a major area of research. The main advantages of this approach are high sensitivity, selectivity, low cost, low sample consumption, and rapid response time, which make it highly suitable for on-site [3]. The use of screen-printed carbon electrodes (SPCEs) in combination with metal–organic frameworks (MOFs) can significantly improve the electrochemical performance of sensors [4].

Experimental

A gallium–porphyrin framework (GaTCPP) was synthesized and post-synthetically metalated with Ni(II) ions to obtain GaTCPP(Ni). For electrode modification, 0.0020 g of GaTCPP(Ni) was dispersed in 0.25 mL ethanol and 0.25 mL Nafion (1:8, Nafion:ethanol) and homogenized by ultrasonication for 20 min. Subsequently, 0.75 µL of the suspension was drop-cast onto the working surface of a screen-printed carbon electrode (SPCE) and left to dry at room temperature. The morphology of bare and GaTCPP(Ni)-modified SPCEs was examined by scanning electron microscopy (SEM) and confocal microscopy. Electrochemical measurements were performed in phosphate-buffered saline (PBS, pH 7.4) using cyclic voltammetry (CV) and differential pulse voltammetry (DPV) with successive additions of ciprofloxacin standard solutions.

Results and discussion

SEM images revealed morphological changes after modification with GaTCPP(Ni), with visible MOF particles distributed across the working electrode surface. Based on confocal microscopy images, the surface roughness increased from 1.35 µm to 3.36 µm, the surface area from 0.32 mm² to 0.37 mm², and the maximum height from 18.6 µm to 25.52 µm. The stability of the GaTCPP(Ni)-Nafion/SPCE sensor was assessed by repeated cycling in the $[Fe(CN)_6]^{3-}/[Fe(CN)_6]^{4-}$ redox system, showing only a minor decrease in current response (11.48%). The reproducibility was excellent, with a relative standard deviation (RSD) of 3.39% (*Figure 1 A*). The sensor also showed high selectivity against common interferents such as cysteine, glucose, ascorbic acid, urea, and sucrose (*Figure 1 B*).

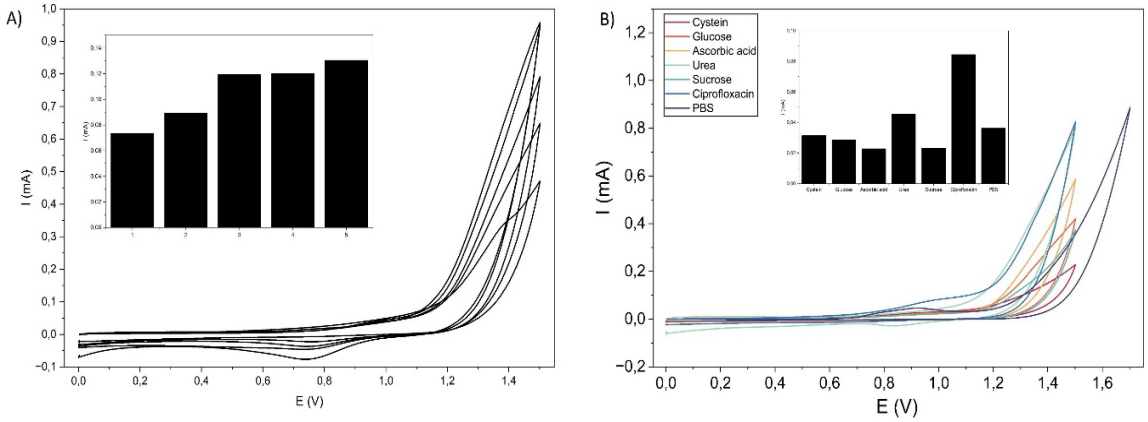

Figure 1 (A) Cyclic voltammograms illustrating reproducibility of the GaTCPP(Ni)-Nafion/SPCE electrode during five consecutive measurements of ciprofloxacin (300 µM), with stable current responses confirmed by the bar chart inset. *(B)* Electrochemical responses of the modified electrode toward ciprofloxacin in the presence of common interferents (cysteine, glucose, ascorbic acid, urea, sucrose, and PBS), showing a significantly higher signal for ciprofloxacin compared to other species.

Based on CV/DPV measurements, a linear response to ciprofloxacin was observed in the 200–1000 µM range. The sensitivity and limit of detection (LOD) were 6.5 µA/mM and 145 µM for CV, and 34.5 µA/mM and 118 µM for DPV, respectively (*Figure 2 A, B*). These results demonstrate that the GaTCPP(Ni)-modified SPCE is a promising platform for ciprofloxacin determination in real samples and highlights the potential of porphyrin-based MOFs for the development of electrochemical antibiotic sensors.

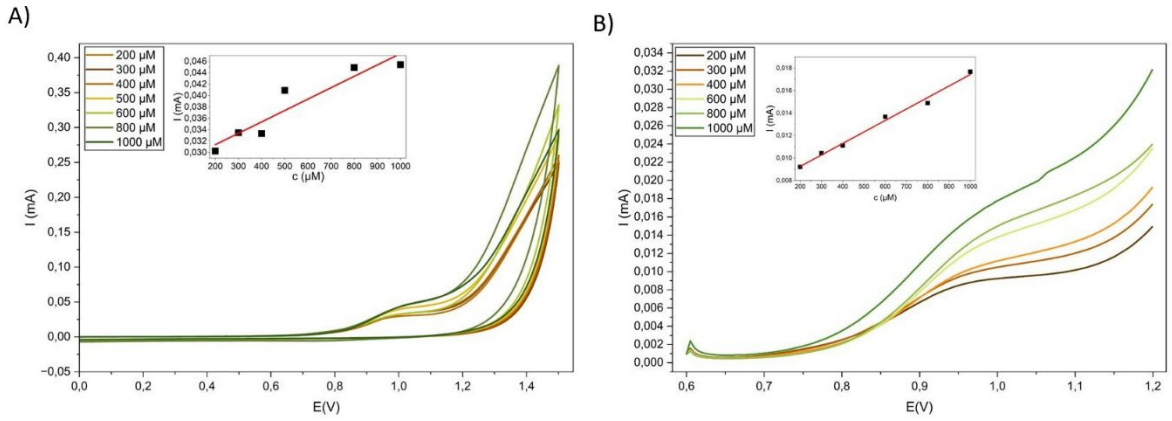

Figure 2 (A) Cyclic voltammetry (CV) curves in PBS for ciprofloxacin in the concentration range 200–1000 µM with corresponding calibration plot (inset). *(B)* Differential pulse voltammetry (DPV) curves in PBS for ciprofloxacin in the concentration range 200–1000 µM with corresponding calibration plot (inset).

Acknowledgements
This research was sponsored by the NATO Science for Peace and Security Programme under grant id. G6106.

References

[1] D. G. J. Larsson and C. F. Flach, "Antibiotic resistance in the environment," 2022. doi: 10.1038/s41579-021-00649-x.
[2] P. C. Sharma, A. Jain, S. Jain, R. Pahwa, and M. S. Yar, "Ciprofloxacin: Review on developments in synthetic, analytical, and medicinal aspects," 2010. doi: 10.3109/14756360903373350.
[3] D. Zabitler, E. Ülker, K. Turan, N. Ö. Erdoğan, and G. Aydoğdu Tığ, "Electrochemical Sensor for Biological Samples Monitoring," 2025, *Springer*. doi: 10.1007/s11244-025-02080-5.
[4] N. Kajal, V. Singh, R. Gupta, and S. Gautam, "Metal organic frameworks for electrochemical sensor applications: A review," *Environ Res*, vol. 204, Mar. 2022, doi: 10.1016/j.envres.2021.112320.

Electron Tomography: Unlocking 3D Structure of Solid Materials

V. Girman[a,b,*], P. Sovak[a], J. Bednarcik[a,c]
[a] Department of Solid State Physics, Pavol Jozef Šafárik University in Košice, Park Angelinum 9, 040 01 Košice
[b] Institute of Materials Research, Slovak Academy of Science, Watsonova 47, 040 01 Košice
[c] Institute of Experimental Physics, Slovak Academy of Science, Watsonova 47, 040 01 Košice
* vladimir.girman@upjs.sk

Modern materials are inherently complex, with structural features extending across all three spatial dimensions. Capturing these characteristics through three-dimensional (3D) analysis is essential for understanding the relationship between structure and function. The transmission electron microscope (TEM), although a widely used and versatile tool for structural characterization, inherently projects a 3D object into a two-dimensional (2D) image. This conversion almost inevitably results in the loss of critical structural information along one dimension. An effective solution to this limitation is the application of electron tomography (ET) directly in the TEM, which enables 3D reconstruction of micro- and nanoscale objects and provides insights inaccessible from 2D projection images alone [1]. This is particularly valuable for heterogeneous or irregularly shaped nanomaterials. In general, ET is a technique that derives 3D structural information from a tilt series of 2D projections. It has steadily matured into a high-resolution characterization method in materials science, offering sub-nanometer resolution. ET has thus progressed from a marginal imaging tool to a flagship method for quantitative 3D analysis [2]. The transformative impact of ET was formally recognized with the 2017 Nobel Prize in Chemistry, awarded "*for developing cryo-electron microscopy for the high-resolution structure determination of biomolecules in solution*" [3].
The fundamental principle of ET is straightforward: a large set of 2D images is acquired at defined tilt angles over a wide angular range, from which a 3D reconstruction of the structure is obtained. As schematically illustrated in *Figure 1*, three key steps are involved: 1.) *Data acquisition*. Projections must be acquired with high precision, using a properly tuned electron beam. The tilt series is typically recorded in angular increments of 1–2°. Larger increments lead to information loss and must be compensated by appropriate reconstruction algorithms. The maximum possible tilt range should be employed, ideally ±90°. 2.) *Alignment*. Acquired projections require correction for imperfections. Unsuitable images must be excluded, the rotation axis must be accurately aligned, and positional shifts between consecutive projections are corrected, commonly using cross-correlation. 3.) *Reconstruction*. Following alignment, a 3D volume is reconstructed from the 2D projections. The most widely used approaches are weighted back-projection (WBP) and iterative methods, particularly the simultaneous iterative reconstruction technique (SIRT) [4]. Alternative algorithms continue to be developed, providing ongoing improvements in reconstruction fidelity and efficiency.

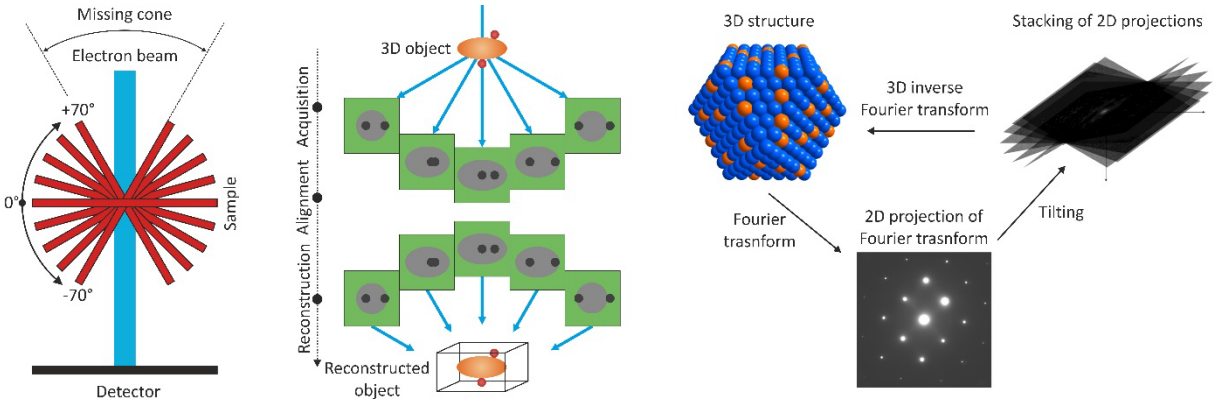

Figure 1 From the left: Schematic illustration of specimen tilting during tomography, direct image reconstruction, and image reconstruction from reciprocal space.

From a mathematical point of view, ET is based on the Radon transform, which models a projection as a line integral through an object, providing the forward model that connects measured tilt-series images to the sought 3D volume. For a 2D object $f(x,y)$, the Radon transform is

$$R\,f(p,\theta) = \int_{-\infty}^{\infty}\int_{-\infty}^{\infty} f(x,y)\;\delta\;(p - x\cos\theta - y\sin\theta)\;dxdy$$

where $f(x,y)$ is density function of 2D slice, $Rf(p,\theta)$ is projection along a line distant p from the origin, rotated at an angle θ, and δ is Dirac delta function. The Fourier transform of Radon transform obeys the Central slice theorem,

important for all reconstruction algorithms, stating that the 1D Fourier transform of a projection at angle θ equals a central slice through the 2D Fourier transform of f at the same [5]. In principle, two approaches to 3D imaging can be considered for ET. They differ in terms of the method and conditions of data collection and the complexity of reconstruction: Image and diffraction tomography.

Image tomography

This way of tomography is performed using direct 2D projections acquired by an image detector, most commonly through the High-Angle Annular Dark-Field imaging technique, which suppresses the effects of dynamical diffraction typical of TEM observations. Without this suppression, the reconstruction of the three-dimensional structure would be significantly affected by artifacts, particularly at tilt angles fulfilling the Bragg diffraction condition. The 2D projections must therefore be obtained with the highest possible accuracy to minimize the occurrence of artifacts during reconstruction. The minimum tilt range for the specimen is approximately ±70°. At lower angular coverage, the negative influence of the missing cone artifact becomes increasingly pronounced. *Figures 2* and *3* present examples of image-based ET: a carbon fiber decorated with CoP nanoparticles and a TiO_2 nanotube, respectively.

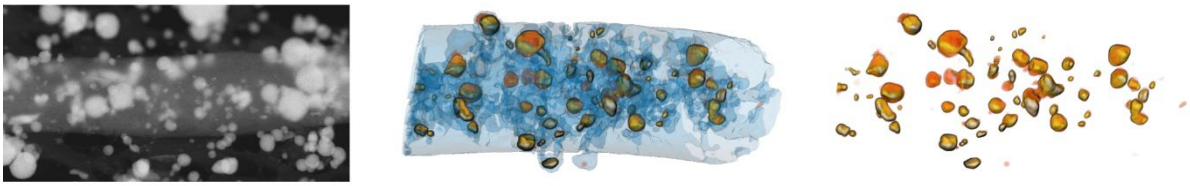

Figure 2 Carbon fibre decorated with CoP nanoparticles. From the left: TEM image, reconstructed segment of fibre and visualization of CoP nanoparticles distribution (V. Girman, Ana B. Hungría, Miguel L. Haro).

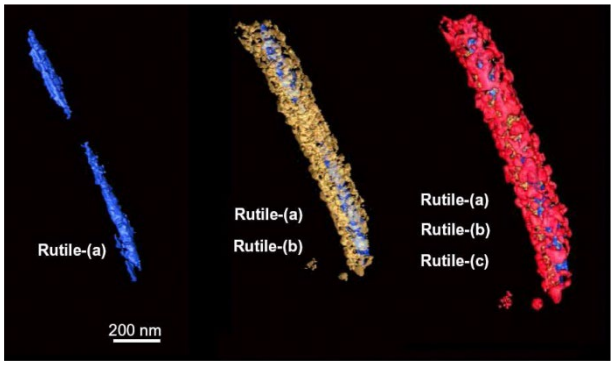

Figure 3 Segmentation of reconstructed TiO_2 nanotubes (Courtesy of Ana B. Hungría).

Diffraction tomography

Proceeding solely through the reconstruction of object projections is often sufficient for image analysis. However, there are cases where it is essential to map the reciprocal space of the specimen as accurately as possible using tomographic slices. In crystallography in particular, the combination of tomography with electron diffraction has been only marginally exploited, yet it is highly probable that this integration will determine the future direction of electron crystallography of inorganic compounds in the coming years [6]. This ET technique is employed for the reconstruction and analysis of the atomic structure of specimens. Tomographic data collection takes place in reciprocal space. In standard diffraction analysis, the outcome consists of one or more slices through reciprocal space. This approach, however, has a significant drawback: a single slice captures only a limited number of reflections. This limitation is illustrated in *Figure 4* (left), which represents the reciprocal lattice. Each red plane corresponds to a slice through reciprocal space, i.e., an individual diffraction pattern, intersecting only a minimal fraction of reciprocal lattice points. This drawback is overcome by diffraction tomography. In *Figure 4* (right), the coverage of reciprocal space is shown in red. In off-zone orientations, far fewer reflections are excited, which markedly reduces multiple scattering, allowing the use of the kinematic diffraction approximation for crystal structure determination. The entire process of diffraction data collection is several times faster, and the subsequent analysis is considerably more accurate. Using this method, a large volume of reciprocal space is covered, and the acquired slices are reconstructed into a 3D map. From this reciprocal space map, the arrangement of atoms in the unit cell can be derived. Notably, even a relatively limited angular range of approximately ±50° may be sufficient

for successful application of this technique. *Figure 5* demonstrates the solution of the paracetamol unit cell structure obtained through reciprocal-space tomography reconstruction.

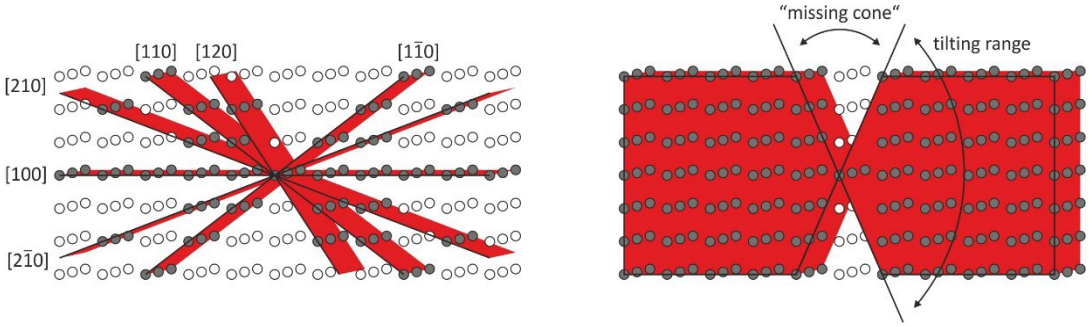

Figure 4 Reciprocal space coverage. From the left: selected area diffraction and diffraction tomography.

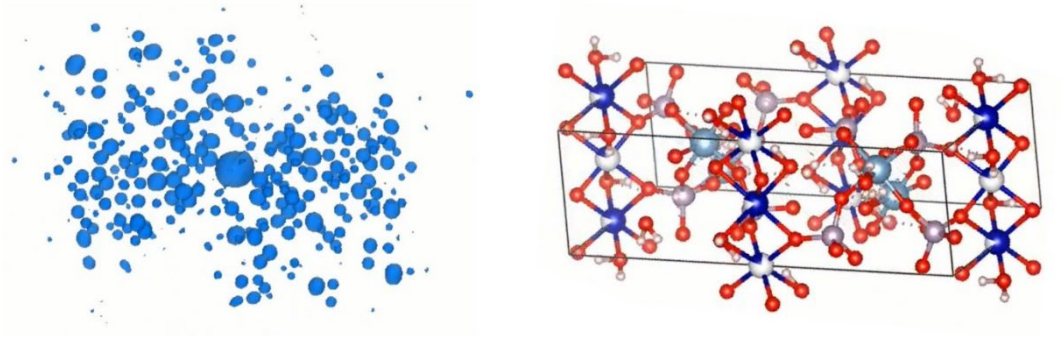

Figure 5 Reciprocal space in 3D and reconstructed unit cell of paracetamol (Courtesy of M. Klementová).

Electron tomography in TEM enables true 3D reconstructions, thereby eliminating projection overlap and uncovering otherwise inaccessible morphological features and connectivity. Quantitative parameters such as volume fraction, surface area, curvature, and tortuosity can be systematically determined. Pores, fibrous networks, and composite architectures are resolved, while core–shell structures, crystallographic faceting, and the three-dimensional dispersion of nanoparticles are revealed with high fidelity. In crystalline microstructures, ET provides detailed information on precipitate morphologies, grain- and triple-junction connectivity, as well as 3D networks of cracks and voids. When combined with diffraction contrast or Z-contrast imaging, ET further permits the localization and characterization of crystal defects, including twins, stacking faults, and dislocation arrays, within the reconstructed volume. In comparison with conventional 2D TEM, ET significantly reduces interpretational ambiguity by allowing visualization of the material from arbitrary viewing directions. Collectively, these capabilities establish electron tomography as a powerful methodology for correlating nanoscale architecture with macroscopic properties across a broad spectrum of advanced materials, including metallic alloys, ceramics, porous frameworks, functional oxides, intermetallic compounds, and structural as well as functional composites.

Acknowledgements
This research was funded by the EU NextGenerationEU through the Recovery and Resilience Plan for Slovakia under the project No. 09I03-03-V03-00034.

References
[1] P. Ercius, O. Alaidi, M. J. Rames and G. Ren, " Electron Tomography: A Three-Dimensional Analytic Tool for Hard and Soft Materials Research," *Adv. Mater.*, vol. 27, no. 38, pp. 5638–5663, Oct. 2015, doi: 10.1002/adma.201501015.
[2] R. Hovden and D. A. Muller, " Electron tomography for functional nanomaterials," *MRS Bulletin,* Vol. 45, Issue 4, pp. 298-304, Apr. 2020, doi: 10.1557/mrs.2020.87.
[3] https://www.nobelprize.org/prizes/chemistry/2017/press-release/, (29.09.2025).
[4] B. Goris, T. Roelandts, K. J. Batenburg, H. H. Mezerji and S. Bals," Advanced reconstruction algorithms for electron tomography: From comparison to combination," *Ultramicroscopy*, vol. 127, pp. 40-47, Apr. 2013, doi: 10.1016/j.ultramic.2012.07.003.
[5] A. C. Kak and M. Slaney, *Principles of Computerized Tomographic Imaging*, IEEE, Inc., NY: IEEE Press, ISBN: 0-87942-198-3, 1987.

[6] X. Zhou, S. Hovmoller and P. Oleynikov, *Electron Crystallography – Electron Microscopy and Electron Diffraction*, CPI Group, UK: Oxford University Press, ISBN: 978-0-19-958020-0, 2012.
12.

Analysis of Ceramic Layers Electrodeposited on Zinc Powders for Biodegradable Implant Preparation

R. Gorejova[a,*], I. Mojzisova[a], R. Orinakova[a]
[a] Department of Physical Chemistry, Faculty of Science, Pavol Jozef Šafárik University, Moyzesova 11, 040 11 Košice, Slovak Republic
* radka.gorejova@upjs.sk

Zinc (Zn) has emerged as a promising and attractive alternative to commonly used metals such as iron (Fe) and magnesium (Mg), which are typically employed in the fabrication of medical biodegradable materials [1], [2]. These materials are designed to provide temporary support to damaged bone tissue during the regeneration process inside the patient's body and gradually dissolve once their supportive function is fulfilled. However, since locally elevated concentrations of released Zn^{2+} ions can trigger unwanted toxic reactions[3], [4], zinc must be modified -despite its many advantages - to prevent undesirable biological effects after implantation.
In this study, Zn metal powders were coated with a ceramic hydroxyapatite (HAp) layer, intended as a starting material for the preparation of biodegradable implants. The addition of this ceramic coating is expected to slow down the degradation of the material in a controlled manner, thereby reducing the toxic impact of degradation products while simultaneously enhancing osteogenesis [5], [6]. The HAp-modified Zn powders were prepared using two approaches: a biomimetic method in simulated body fluid (SBF) and an electrochemical deposition process from a solution containing $Ca(NO_3)_2 \cdot 4H_2O$ and $NH_4H_2PO_4$.
The aim of this work was to analyze the chemical composition and atomic ratios of the prepared ceramic layer. The powders were studied using electron microscopy combined with EDS analysis. *Figure 1 a-c* shows the chemical composition of powders obtained by electrochemical deposition, while *Figure 1 d-f* presents those prepared by the biomimetic method. In both cases, the presence of phosphorus and calcium is clearly visible, confirming the formation of the ceramic layer. However, the detected atomic ratios of these elements deviate from the stoichiometric CaP ratio (1.67), and therefore, further investigation of the powders is required to confirm the presence of HAp.

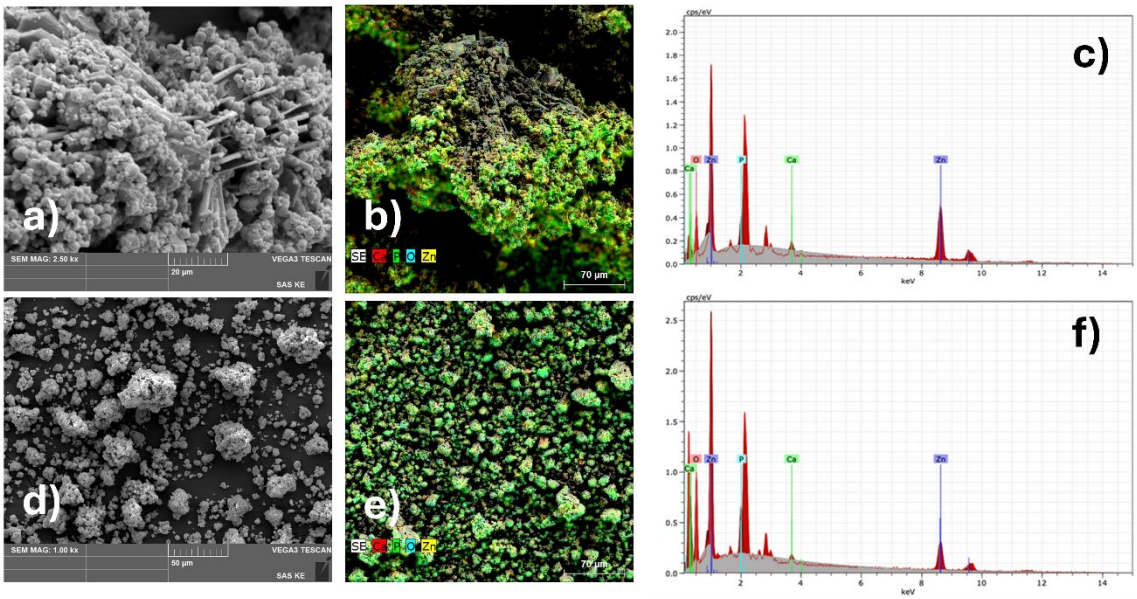

Figure 1 SEM images of zinc-ceramic powders prepared electrochemically (*a*) and via biomimetic route (*d*) with corresponding EDS chemical composition analysis (electrochemical route (*b,c*) and biomimetic preparation (*e,f*)).

Acknowledgements
This work was funded by the EU NextGenerationEU through the Recovery and Resilience Plan for Slovakia under the project ZETA no. 09I03-03-V04-00010.

References

[1] Y. Liu, Y. Zheng, X.-H. Chen, J.-A. Yang, H. Pan, D. Chen, L. Wang, J. Zhang, D. Zhu, S. Wu, K. W. K. Yeung, R.-C. Zeng, Y. Han and S. Guan, "Fundamental Theory of Biodegradable Metals—Definition, Criteria, and Design," *Adv Funct Mater*, vol. 29, no. 18, pp. 1–21, 2019, doi: 10.1002/adfm.201805402.
[2] J. Cheng, B. Liu, Y. H. Wu, and Y. F. Zheng, "Comparative invitro study on pure metals (Fe, Mn, Mg, Zn and W) as biodegradable metals," *J Mater Sci Technol*, vol. 29, no. 7, pp. 619–627, 2013, doi: 10.1016/j.jmst.2013.03.019.
[3] J. Ma, N. Zhao, and D. Zhu, "Endothelial Cellular Responses to Biodegradable Metal Zinc," *ACS Biomater Sci Eng*, vol. 1, no. 11, pp. 1174–1182, 2015, doi: 10.1021/acsbiomaterials.5b00319.
[4] P. K. Bowen, J. Drelich, and J. Goldman, "Zinc Exhibits Ideal Physiological Corrosion Behavior for Bioabsorbable Stents," *Advanced Materials*, vol. 25, no. 18, pp. 2577–2582, May 2013, doi: 10.1002/adma.201300226.
[5] W. S. W. Harun, R. I. M. Asri, J. Alias, F. H. Zulkifli, K. Kadirgama, S. A. C. Ghani and J. H. M. Shariffuddin, "A comprehensive review of hydroxyapatite-based coatings adhesion on metallic biomaterials," Feb. 01, 2018, *Elsevier Ltd*. doi: 10.1016/j.ceramint.2017.10.162.
[6] V. S. Kattimani, S. Kondaka, and K. P. Lingamaneni, "Hydroxyapatite–-Past, Present, and Future in Bone Regeneration," *Bone Tissue Regen Insights*, vol. 7, pp. 9–19, Jan. 2016, doi: 10.4137/btri.s36138.

Optimized Non-Enzymatic Electrochemical Sensor based on Polypyrrole-Copper Nanoparticles for Cholesterol Determination

F. Chovancova[a,*], I. Sisolakova[a]
[a] Department of Physical Chemistry, Faculty of Science, Pavol Jozef Šafárik University, Moyzesova 11, 04011 Košice, Slovak Republic
* frederika.chovancova1@student.upjs.sk

Cholesterol, an indispensable steroid present in the human body, acts as a precursor for different biological substrates such as bile acid, vitamin D and different hormones. It is used to form structures inside the cell membrane for cell protection and interaction with the external environment [1,2]. Maintaining normal cholesterol levels, typically between 140-200 mg/100 mL in human bodily fluids, is vital, as deviations can lead to severe health complications like hypolipoproteinemia or, conversely, hypertension and arteriosclerosis [3,4,5]. The accumulation of cholesterol in blood serum increases the risk of several diseases such as stroke, nephrotic syndrome, myocardial infarction, cerebral thrombosis, atherosclerosis and hepatobiliary disease [6,5]. Given these severe health implications, the regular monitoring of cholesterol levels is crucial for early detection and prevention of cardiovascular and cerebrovascular conditions [7].

In recent decades, biosensing has gained considerable traction due to its capacity for developing selective sensing systems to identify target analytes. Bioactive macromolecules, frequently employed as biomarkers, hold significant importance in clinical diagnostics. Biosensors offer a valuable approach for the rapid and cost-effective detection of biomolecules in samples, characterized by their high sensitivity and specificity. These enhanced capabilities stem from the integrated recognition unit within the biosensor, which is typically biological, such as enzymes or antibodies. However, these biological recognition elements present challenges, including instability under operational conditions, limited shelf life, and the expense and complexity associated with antibody production. To address these limitations, electrode systems utilizing screen-printing technology have emerged as a viable alternative to conventional solid electrodes for the quantification of various compounds. Their advantages, such as low cost, widespread availability, portability, ease of fabrication, and commercial accessibility, make screen-printed electrodes suitable for the rapid and sensitive electroanalysis of numerous target analytes. Consequently, three distinct electrode systems have been identified as promising candidates for the design of point-of-care devices and for applications in both environmental and clinical analysis. The demand for accurate, rapid, and cost-effective detection methods for critical biomarkers, such as cholesterol, necessitates the continued development of advanced biosensing platforms [8].

Non-enzymatic electrochemical sensors for cholesterol determination often leverage the unique properties of nanomaterials, such as conducting polymers and metal oxides, to achieve high sensitivity and selectivity without the inherent instability of enzyme-based systems [9,10]. Conductive polymers possess distinctive attributes, including elevated conductivity, superior thermal resilience, straightforward synthesis, environmental robustness, and biocompatibility. Their high conductivity is attributed to the presence of conjugated electrons or an alternating arrangement of single and double bonds within their molecular frameworks [11,12]. Polypyrrole, polyaniline, and polythiophene are among the most advantageous conductive polymers, with polypyrrole exhibiting the highest conductivity when compared to these materials. PPy has been the subject of research for diverse applications, including electronic devices, sensors, and batteries, owing to the broad utility of chemically synthesized PPy and its inherent properties like thermal stability and conductivity [13,14,15].

The influence of various species on the pyrrole during the electrochemical polymerisation process and its subsequent impact on the electrochemical properties of the resulting sensor were investigated. To enhance the performance of the sensor. This optimization focused on leveraging the inherent advantages of conducting polymers like polypyrrole, including their heightened sensitivity, selectivity, and reproducibility. Specifically, polypyrrole exhibits high electrical conductivity through the movement of positively charged defect structures known as polarons, a property critical for effective biosensor development [16].

We studied the electropolymerization of polypyrrole membranes using cyclic voltammetry at a potential window from -0.3 V to 1.2V at scan rate 10mV/s for one cycle. The process of electropolymerization was investigated, with a particular focus on the effect of dopants presented in medium. Three varieties of pyrrole solutions were studied: 0.1 M pyrrole solution in the presence of 0.1 M potassium chloride (KCl); next, 0.1 M pyrrole in the presence of 0.1 M sulphuric acid (H_2SO_4), and the last one, a combination of 0.1 M pyrrole and 0.1 M sulphuric acid with the addition of 0.1 M potassium chloride. This systematic investigation of dopant effects on polypyrrole electropolymerization is crucial for optimizing the film's morphology and electrochemical properties, which directly influence its performance in non-enzymatic biosensing applications. These dopants, particularly chloride, are known to significantly impact the conductivity of polypyrrole by compensating for electron vacancies in the polymer backbone during the doping process. Polymer membrane were modifed by copper nanoparticles to enhance their electrochemical activity and provide additional catalytic sites for improved cholesterol detection, as copper nanoparticles are known to exhibit excellent electrocatalytic properties. The integration of copper

nanoparticles into the polypyrrole matrix further facilitates electron transfer kinetics and increases the active surface area, both critical factors for enhancing the sensitivity and reducing the detection limit of the non-enzymatic cholesterol biosensor. As is shown in *Figure 1*, the current response for 10 mM cholesterol oxidation on the surface of modified electrodes, the most promising results were obtained with the polypyrrole in KCl and copper nanoparticle (SPCE_PPy_KCl_Cu) composite for cholesterol determination. In comparison of electrodes SPCE_PPy_H_2SO_4_Cu and SPCE_PPy_H_2SO_4_Cu, almost any of current response for cholesterol oxidation at E= 0.2 V wasn´t observed.

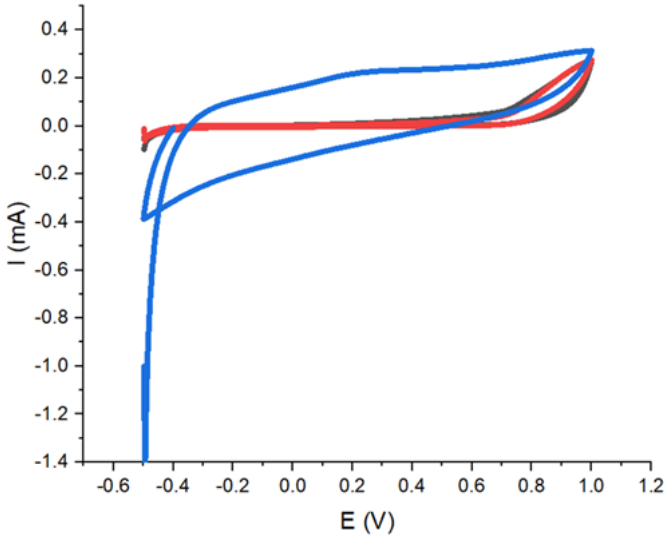

Figure 1 Cyclic voltammogram of modifications screen-printed carbon electrode (SPCE) with PPy film and Copper nanoparticles on current response for 10 mM cholesterol in 0.1M NaOH and PBS. SPCE_PPy_KCl_H_2SO_4_Cu (black line), SPCE_PPy_H_2SO_4_Cu (red line) and SPCE_PPy_KCl_Cu (blue line) at potential window from -0.5 V to 1 V at 50 mV/s.

This indicates that the presence of chloride ions during electropolymerization, coupled with copper nanoparticle incorporation, significantly enhances the electrocatalytic activity towards cholesterol oxidation. Further exploration of the synergistic effects between chloride doping and copper nanoparticle integration could lead to the development of highly sensitive and selective non-enzymatic biosensors for cholesterol.

Acknowledgements
This research was sponsored by the NATO Science for Peace and Security Programme under grant id. G6106 and Funded by the EU NextGenerationEU through the Recovery and Resilience Plan for Slovakia under the project No. 09I03-03-V05-00008.

References
[1] W. Xia, H. Wang, X. Zhou, Y. Wang, L. Xue, B. Cao and J. Song, “The role of cholesterol metabolism in tumor therapy, from bench to bed,” Front. Pharmacol., vol. 14. Frontiers Media, Apr. 06, 2023. doi: 10.3389/fphar.2023.928821.
[2] B. D. Geest and M. Mishra, “New Perspectives on Cholesterol and Lipoprotein Metabolism,” Int. Mol. Sci., vol. 24, no. 14, p. 11298, Jul. 2023, doi: 10.3390/ijms241411298.
[3] P. T. Nguyen, Y. I. Kim, and M. I. Kim, “Reagent-Free Colorimetric Cholesterol Test Strip Based on Self Color-Changing Property of Nanoceria,” Front. Chem. , vol. 8, Sep. 2020, doi: 10.3389/fchem.2020.00798.
[4] V. Joshi, S. Hussain, S. Dua, N. Arora, S.H. Mir, G. Rydzek and T. Senthilkumar “Oligomer Sensor Nanoarchitectonics for ‘Turn-On’ Fluorescence Detection of Cholesterol at the Nanomolar Level,” Molecules , vol. 27, no. 9, p. 2856, Apr. 2022, doi: 10.3390/molecules27092856.
[5] H. M. Yadav, J. D. Park, H. C. Kang, and J. J. Lee, “Recent development in nanomaterial-based electrochemical sensors for cholesterol detection,” Chemosensors , 2021. doi: 10.3390/chemosensors9050098.
[6] N. Ruecha, W. Siangproh, and O. Chailapakul, “A fast and highly sensitive detection of cholesterol using polymer microfluidic devices and amperometric system,” Talanta , vol. 84, no. 5, p. 1323, Mar. 2011, doi: 10.1016/j.talanta.2011.02.040.
[7] V. Dharmawan, I. Rahmawati, A. R. Sanjaya, B. E. Dewi, E. Saepudin, and T. A. Ivandini, “A High Selective and Sensitive Spectrophotometric Cholesterol Detection Using B-Cyclodextrin/Fe3O4 Composite as the Identification Agent,” Int. J. Technol., vol. 16, no. 2, p. 672, Mar. 2025, doi: 10.14716/ijtech.v16i2.7176.

[8] J. H. T. Luong, T. Narayan, S. Solanki, and B. D. Malhotra, "Recent Advances of Conducting Polymers and Their Composites for Electrochemical Biosensing Applications," J. Funct. Biomat., vol. 11, no. 4. Multidisciplinary Digital Publishing Institute, p. 71, Sep. 25, 2020. doi: 10.3390/jfb11040071.
[9] S. Deivanayaki, P. Jayamurugan, S. Ashokan, V.G. Krishnan, B. Yogeswari, M. Ubaidullah, B. Pandit, G.V.S.S. Sarma, H.K. Narsetti, "Growth of non-enzymatic cholesterol biosensor using TiO2 decorated graphene oxide with bare GCE and PPy-GCE," J. Indian Chem. Soc., vol. 100, no. 3, p. 100906, Jan. 2023, doi: 10.1016/j.jics.2023.100906.
[10] X. Li, Z. Zhang, and F. Li, "Flexible electrochemical sensors based on nanomaterials: Constructions, applications and prospects," Chem. Eng. J., p. 158101, Nov. 2024, doi: 10.1016/j.cej.2024.158101.
[11] Md. A. Shahid, Md M. Rahman, Md. T. Hossain, I. Hossain, Md.S. Sheikh, Md.S. Rahman, N. Udin, S.W. Donne and Md.I.U. Hoque, "Advances in Conductive Polymer-Based Flexible Electronics for Multifunctional Applications," Journal of J. Compos. Sci., vol. 9, no. 1, p. 42, Jan. 2025, doi: 10.3390/jcs9010042.
[12] J. Qiu, Z. Lu, X. Qian, J.Yao, C. Han, Z. Wu, H. Ye, G. Shan, Q. Zheng, K. Xu, and M. Du, "Highly conductive polymer with vertical phase separation for enhanced bioelectronic interfaces," Flex. Electron., vol. 9, no. 1, Jul. 2025, doi: 10.1038/s41528-025-00441-4.
[13] A. Sardar and P. S. Gupta, "Polypyrrole based nanocomposites for supercapacitor applications: A review," AIP Conf. Proc., American Institute of Physics, p. 30020, Jan. 01, 2018. doi: 10.1063/1.5032355.
[14] Y. Sood, K. Singh, H. Mudila, P.E. Lokhande, L. Singh, D. Kumar, A. Kumar, N.M. Mubarak and M.H. Dehghani, "Insights into properties, synthesis and emerging applications of polypyrrole-based composites, and future prospective: A review," Heliyon , vol. 10, no. 13. Elsevier BV, Jun. 27, 2024. doi: 10.1016/j.heliyon.2024.e33643.
[15] A. Dube, S. J. Malode, A. N. Alodhayb, K. Mondal, and N. P. Shetti, "Conducting Polymer-Based Electrochemical Sensors: Progress, Challenges, and Future Perspectives," Talanta Open , vol. 11, p. 100395, Dec. 2024, doi: 10.1016/j.talo.2024.100395.
[16] B. D. Malhotra and Md. A. Ali, "Biopolymeric Nanostructures," in Nanomaterials for Biosensors , 2018. doi: 10.1016/b978-0-323-44923-6.00004-2.

Screen-Printed Electrode Modified by Polymer Membrane and Metal Oxides Nanoparticles as Platform for Electrochemical Cholesterol Sensor

F. Chovancova[a,*], I. Sisolakova[a]
[a] Department of Physical Chemistry, Faculty of Science, Pavol Jozef Šafárik University, Moyzesova 11, 04011 Košice, Slovak Republic
* frederika.chovancova1@student.upjs.sk

This work focuses on developing a robust and highly sensitive electrochemical platform for the direct detection of cholesterol, specifically utilizing screen-printed electrodes functionalized with polymer membranes and further modified with metal or metal oxide nanoparticles. The integration of conductive polymers, such as polypyrrole, offers enhanced electron transfer pathways, while the incorporation of nanoparticles, including copper oxide or nickel oxide, significantly boosts the electrochemical reactivity towards cholesterol, given its inherently low redox activity [1,2].

Cholesterol is an essential lipid molecule, vital for cell membrane integrity, hormone synthesis, and bile acid production, yet elevated levels, particularly of low-density lipoprotein cholesterol, are directly implicated in the pathogenesis of atherosclerosis and subsequent cardiovascular diseases [3]. The determination of cholesterol levels is therefore critical for clinical diagnosis of conditions like heart problems and thrombosis [4]. Consequently, the development of accurate, rapid, and cost-effective methods for cholesterol detection is of paramount importance for preventative healthcare and disease management [3,5]. Conventional methods for cholesterol quantification, such as enzymatic colorimetric assays, often suffer from limitations including complex sample preparation, long analysis times, and susceptibility to interferences. This underscores the growing need for advanced biosensing platforms that offer high sensitivity, selectivity, and rapid analysis for point-of-care diagnostics, thereby facilitating timely medical interventions and improving patient outcomes [3,6] . This necessitates the exploration of innovative sensing technologies, with electrochemical sensors emerging as a promising alternative due to their inherent advantages such as low cost, portability, high sensitivity, and rapid response [7].

This approach aims to circumvent the limitations of traditional enzymatic biosensors by enabling a non-enzymatic detection mechanism, thus enhancing stability and extending the operational lifespan of the sensing platform [8]. The proposed method addresses the current challenges in cholesterol detection, such as the expense and time-consuming nature of conventional techniques, by offering a rapid, cost-effective, and robust alternative [9]. This novel architecture, leveraging the synergistic properties of conductive polymers and metal oxide nanoparticles, promises improved analytical performance characteristics, including lower limits of detection and wider linear ranges. Furthermore, the direct electrochemical oxidation of cholesterol eliminates the need for expensive and unstable enzymes, leading to a more practical and sustainable diagnostic tool [10]. The high chemical and environmental stability, biocompatibility, and unique optoelectronic and sensing properties of nanomaterials, particularly metal and metal oxide nanoparticles, are crucial for advancing these biosensing applications [7]. . Moreover, the integration of these nanomaterials with screen-printed electrodes provides a miniaturized and mass-producible sensing platform suitable for point-of-care diagnostics, due to their excellent catalytic and electrocatalytic properties [3,7]. This synergistic combination facilitates superior signal transduction and amplified detection capabilities, thereby enabling the development of highly efficient non-enzymatic cholesterol biosensors with enhanced sensitivity and specificity. This advanced platform leverages the inherent advantages of screen-printed electrodes for mass production and portability, further augmenting their performance through the controlled deposition of these nanocomposites [2]. This strategy allows for the development of highly stable and reproducible sensors, overcoming the limitations of enzymatic systems, such as enzyme degradation and limited shelf life [11,12]. The focus on non-enzymatic detection not only mitigates these enzymatic drawbacks but also broadens the applicability of these sensors in diverse matrices where enzyme activity might be compromised [10,13].

This work shows the Screen-Printed electrode modified by pyrrole and metal oxide nanoparticles, especially copper oxide effectively oxidazed the cholesterol. Cholesterol was dissolved in Phosphate-Buffer Saline in presence of surfactant to improve its solubility. Various of concentrations were chosen for direct cholesterol determination – from 2.5 mM to 10 mM. Standard level of cholesterol in at adult human is lover than 5.2 mM.. As promising electrochemical method to detect various cholesterol concentrations, chronoamperometry was choosed. The experimental parameters were optimase as constant potential 0.2 V for 150s as is shown in Fig. 1 (left).

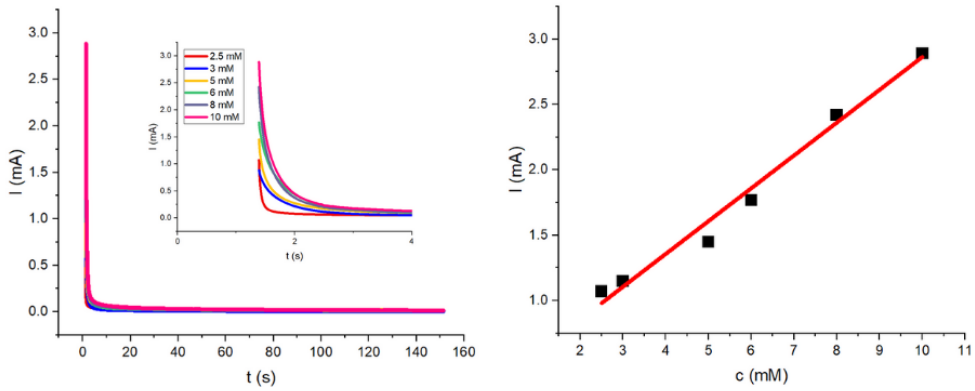

Figure 1 Choronoamperogram for various of cholesterol concentrations (2.5mM red line, 3mM blue line, 5mM yellow line, 6mM green line, 8mM purple line and 10 mM magenta line) in PBS and 0.1M NaOH at E= 0.2 V and t= 150 s (left). Fitted linear regresion of current response versus concentration (right).

Based on the obtained data, the linear regression between current response and concentration was found to be R^2 = 0.98 (*Figure 1*, right). This linearity highlights the sensor's capability for precise quantitative analysis within a physiologically relevant range, demonstrating its potential for accurate diagnostic applications. Based on the obtained data, analytical parameters were calculated as Limit of Detection (LOD), Linear Range and Sensitivity. LOD was calculated according to Equation (1):

$$LOD = 3.3\ SD/S \quad (1)$$

where SD means Standard Deviation of response and S represents the Slope of the calibration curve. The calculated LOD is 0.23 mM, and the sensitivity of the prepared sensor is 0.25 mA/mM. These analytical figures of merit demonstrate the sensor's robust performance, particularly in terms of its ability to detect cholesterol concentrations relevant to early disease markers reliably.

Acknowledgements
Funded by the EU NextGenerationEU through the Recovery and Resilience Plan for Slovakia under the project No. 09I03-03-V05-00008.

References
[1] C. B. A. Hassine, H. Kahri, and H. Barhoumi, "Development of non-enzymatic cholesterol electrochemical sensor based on CuO(NPs)-Polyaniline-Murexide composite," *Res Sq.* doi: 10.21203/rs.3.rs-255899/v1.
[2] Z. G. Shiri, S. M. Zebarjad, and K. Janghorban, "Evaluation and Comparison of Nio/Cuo Nanocomposite and Nio Nanofibers as Non-Enzymatic Electrochemical Cholesterol Biosensor," *SSRN Electronic Journal* , Jan. 2022, doi: 10.2139/ssrn.4082770.
[3] V. Narwal, R. Deswal, B. Batra, V. Kalra, R. Hooda, M. Sharma and J.S. Rana, "Cholesterol biosensors: A review," *Steroids* , 2019. doi: 10.1016/j.steroids.2018.12.003.
[4] M. Alagappan, S. Immanuel, R. Sivasubramanian, and A. Kandaswamy, "Development of cholesterol biosensor using Au nanoparticles decorated f-MWCNT covered with polypyrrole network," *Arab. J. Chem.*, vol. 13, no. 1, p. 2001, Mar. 2018, doi: 10.1016/j.arabjc.2018.02.018.
[5] S. Söylemez, Y. A. Udum, M. Kesik, C. G. Hızlıateş, Y. Ergün, and L. Toppare, "Electrochemical and optical properties of a conducting polymer and its use in a novel biosensor for the detection of cholesterol," *Sens. Actuators B Chem* , vol. 212, p. 425, Feb. 2015, doi: 10.1016/j.snb.2015.02.045.
[6] O. Demkiv, W. Nogala, N. Stasyuk, N. M. Grynchyshyn, B. Vus, and M. Gonchar, "The Peroxidase-like Nanocomposites as Hydrogen Peroxide-Sensitive Elements in Cholesterol Oxidase-Based Biosensors for Cholesterol Assay," *J. Funct. Biomater.*, vol. 14, no. 6, p. 315, Jun. 2023, doi: 10.3390/jfb14060315.
[7] H. M. Yadav, J. Park, H. C. Kang, and J. Lee, "Recent Development in Nanomaterial-Based Electrochemical Sensors for Cholesterol Detection," *Chemosensors* , vol. 9, no. 5, p. 98, Apr. 2021, doi: 10.3390/chemosensors9050098.
[8] K. M. Janani, L. A. Kumar, and M. Alagappan, "Novel MoS2-decorated Cu2O hybrid nanoparticles for enhanced non-enzymatic electrochemical cholesterol detection," *Nanotechnology* , vol. 35, no. 19, p. 195101, Jan. 2024, doi: 10.1088/1361-6528/ad22b3.
[9] S. Deivanayaki, P. Jayamurugan, S. Ashokan, V.G. Krishan, B. Yogeswari, M. Ubaidullah, B. Pandit, G.V.S.S. Sarma, H.K. Narsetti, "Growth of non-enzymatic cholesterol biosensor using TiO2 decorated graphene oxide with bare GCE and PPy-GCE," *J. Indian Chem. Soc.*, vol. 100, no. 3, p. 100906, Jan. 2023, doi: 10.1016/j.jics.2023.100906.

[10] M. A. Sha, P. C. Meenu, H. Haspel, and Z. Kónya, "Metal-based non-enzymatic systems for cholesterol detection: mechanisms, features, and performance," *RSC Advances* , vol. 14, no. 34. Royal Society of Chemistry, p. 24561, Jan. 01, 2024. doi: 10.1039/d4ra04104f.
[11] O. E. Carp, M. Pinteală, and A. Arvinte, "Innovative Non-Enzymatic Electrochemical Quantification of Cholesterol," *Sensors* , vol. 22, no. 3, p. 828, Jan. 2022, doi: 10.3390/s22030828.
[12] A. Wisitsoraat, C. Karuwan, K. Wong-ek, D. Phokharatkul, P. Sritongkham, and A. Tuantranont, "High sensitivity electrochemical cholesterol sensor utilizing a vertically aligned carbon nanotube electrode with electropolymerized enzyme immobilization," *Sensors* , 2009, doi: 10.3390/s91108658.
[13] M. A. Yassin, A.F. Abou-Hadid, H.M. Mousa, C.H. Park, C.S. Kim, A.Salem and M.A. Mattar, "Enzymeless electrochemical detection of hydrogen peroxide using NiO octahedron decorated 3D graphene hydrogel," *Sci. Rep.,* vol. 15, no. 1, Aug. 2025, doi: 10.1038/s41598-025-10472-6.

Point-of-Care Electrochemical Multisensors for Simultaneous Detection of Antibiotics in Blood

P. Jarcuska[b,*], I. Sisolakova[a], J. Shepa[a], O. Zahornacky[b], R. Orinakova[a]

[a] Department of Physical Chemistry, Pavol Jozef Šafárik University in Košice, Moyzesova 11, 040 01, Košice, Slovak republic

[b] Department of Infectology and Travel Medicine at the L. Pasteur University Hospital Košice, Slovakia, Pavol Jozef Šafárik University in Košice, Rastislavova 43, 040 01, Košice, Slovak republic

* pavol.jarcuska@upjs.sk

Antibiotics have transformed medicine since their widespread adoption in the mid-20th century, saving millions of lives by treating bacterial infections that were previously lethal. However, over the decades their use has greatly expanded—not only in human medicine, but also in veterinary practice, agriculture, aquaculture, and livestock production—leading to widespread misuse, overprescription, and environmental discharge, and thereby contributing to the alarming rise of antimicrobial resistance (AMR). Recent global estimates show that AMR already imposes a substantial mortality and morbidity burden worldwide [1, 2].

Globally, human antibiotic consumption is estimated at tens of billions of defined daily doses (DDD) per year, with considerable geographical variation and increasing trends in many low- and middle-income countries. In the European Union, surveillance data demonstrate wide heterogeneity and problematic patterns of antibiotic use across member states [3]. In the United States, the Centers for Disease Control and Prevention (CDC) estimate that at least 30% of all antibiotic prescriptions are unnecessary or suboptimal [4, 5]. The World Health Organization warns that AMR is among the top ten global public health threats, projecting that without effective interventions, resistant infections could cause millions of deaths annually by 2050 [2, 6].

Misuse of antibiotics not only accelerates the selection of resistant strains but also results in residual and sub-therapeutic concentrations persisting in body fluids and tissues. Monitoring antibiotic levels in blood or plasma—therapeutic drug monitoring (TDM) - is therefore essential for optimizing dosage, avoiding toxicity or underdosing, and reducing the risk of resistance development. In clinical settings, TDM is routinely applied to certain narrow-therapeutic-index drugs (e.g., aminoglycosides, vancomycin), but is rarely used for most antibiotics due to cost, complexity, and lack of rapid detection methods [7, 8].

Current analytical approaches—such as liquid chromatography–tandem mass spectrometry (LC–MS/MS), high-performance liquid chromatography (HPLC), immunoassays, or microbiological assays—offer excellent sensitivity and specificity, but require expensive instrumentation, laborious sample preparation, and centralized laboratories. These constraints make them unsuitable for point-of-care (POC) decision-making or frequent monitoring in resource-limited settings. Even with recent advances in automated LC–MS/MS, costs, turnaround times, and the need for trained personnel remain major barriers to routine bedside implementation [9, 10].

Among emerging diagnostic platforms, electrochemical sensors stand out due to their inherent advantages: high sensitivity, rapid response, miniaturization potential, low power requirements, relative affordability, and compatibility with portable electronics. In recent years, substantial progress has been achieved in electrochemical detection of antibiotics - particularly through novel electrode materials such as metal nanoparticles, carbon nanomaterials, metal - organic frameworks, molecularly imprinted polymers, and aptamers. These innovations are pushing detection limits into the nM–pM range while improving selectivity and response times [11, 12].

Our developed electrochemical sensors represent a revolutionary approach to therapeutic antibiotic monitoring. Unlike conventional techniques, they enable ultra-rapid analysis when an entire measurement, including software-based evaluation, is completed in approximately 15 seconds.

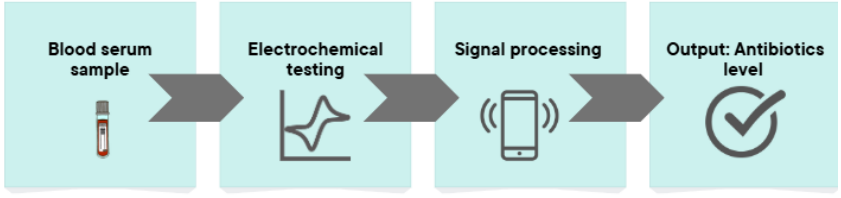

Figure 1 Steps of electrochemical antibiotics detection.

They are also highly cost-effective, with the current price per test not exceeding €2; by applying our own electrode printing, costs can be reduced by up to two-thirds. A further advantage is the multisensor concept (*Figure 2*), which enables simultaneous detection of up to four different antibiotics in a single sample. This capability is particularly valuable in polymicrobial infections or in patients receiving combination antibiotic therapies. The

unique combination of speed, affordability, and multiplexed detection paves the way for real-world clinical implementation and even field use, fundamentally reshaping the paradigm of antibiotic treatment monitoring.

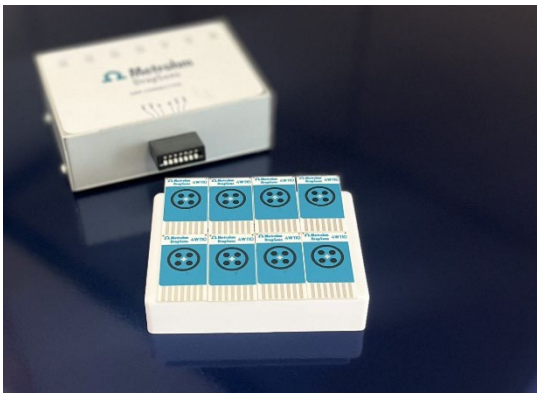

Figure 2 Electrochemical Multisenzor.

Nevertheless, translating electrochemical sensors to direct blood-based monitoring presents challenges: matrix complexity (interfering species, proteins), electrode fouling, stability, selectivity in the presence of multiple electroactive compounds, and calibration in biologically relevant ranges. Addressing these issues, alongside rigorous clinical validation, remains an active research frontier and a decisive step toward transforming these promising tools into robust clinical diagnostics [13].

Acknowledgements
This work was funded by the EU NextGenerationEU through the Recovery and Resilience Plan for Slovakia under the project No. 09-I05-03-V02-00047.

References
[1] C. J. L. Murray, K. S. Ikuta, F. Sharara, L. Swetschinski, G. R. Robles Aguilar, A. Gray, C. Han, C. Bisignano, P. Rao and E. Wool, "Global burden of bacterial antimicrobial resistance in 2019: a systematic analysis," *Lancet*, vol. 399, no. 10325, pp. 629–655, 2022, doi: 10.1016/S0140-6736(21)02724-0.
[2] World Health Organization, "Antimicrobial resistance: fact sheet," WHO, Geneva, 2023. [Online]. Available: https://www.who.int/news-room/fact-sheets/detail/antimicrobial-resistance
[3] European Centre for Disease Prevention and Control (ECDC), *Antimicrobial consumption in the EU/EEA: Annual epidemiological report for 2024*, Stockholm: ECDC, 2024. [Online]. Available: https://www.ecdc.europa.eu/en/publications-data
[4] K. E. Fleming-Dutra, A. L. Hersh, D. J. Shapiro, M. A. Bartoces, E. P. Enns, T. M. File Jr, J. A. Finkelstein, J. S. Gerber, D. Y. Hyun, J. A. Linder, M. H. Lynfield, N. Mangione-Smith, J. S. Polgreen, L. H. Raebel, A. M. Sanchez, T. M. Schroeck, A. A. Simmering, K. E. Suda, A. M. Thomas, A. M. Zetts and R. M. Hicks., "Prevalence of inappropriate antibiotic prescriptions among US ambulatory care visits, 2010–2011," *JAMA*, vol. 315, no. 17, pp. 1864–1873, 2016, doi: 10.1001/jama.2016.4151.
[5] Centers for Disease Control and Prevention (CDC), *Antibiotic use in the United States, 2022 update: Progress and opportunities*, Atlanta, GA: CDC, 2022. [Online]. Available: https://www.cdc.gov/antibiotic-use
[6] World Health Organization, *No time to wait: Securing the future from drug-resistant infections. Report to the UN Secretary-General*, Geneva: WHO, 2019. [Online]. Available: https://www.who.int/publications/i/item/no-time-to-wait
[7] J. A. Roberts, M. H. Abdul-Aziz, J. Lipman, J. W. Mouton, A. A. Vinks, T. W. Felton, W. W. Hope, A. Farkas, M. N. Neely, J. J. Schentag, G. Drusano, O. R. Frey, U. Theuretzbacher and J. L. Kuti, "Individualised antibiotic dosing for patients who are critically ill: challenges and potential solutions," *Lancet Infect. Dis.*, vol. 14, no. 6, pp. 498–509, 2014, doi: 10.1016/S1473-3099(14)70036-2.
[8] M. H. Abdul-Aziz, C. McDonald, S. C. Wallis, *et al.*, "Antimicrobial therapeutic drug monitoring in critically ill adult patients: a position paper," *Int. J. Antimicrob. Agents*, vol. 55, no. 2, p. 105840, 2020, doi: 10.1016/j.ijantimicag.2019.11.001.
[9] S. Jünger, A. Brinkmann, C. Wyen, *et al.*, "Automated LC–MS/MS: ready for clinical routine?," *Clin. Mass Spectrom.*, vol. 28, p. 100208, 2023, doi: 10.1016/j.clinms.2023.100208.
[10] H. Zhang, J. He, Y. Zhou, *et al.*, "Recent advances in LC–MS/MS for therapeutic drug monitoring of antibiotics," *J. Pharm. Biomed. Anal.*, vol. 165, pp. 252–264, 2019, doi: 10.1016/j.jpba.2018.12.022.
[11] M. Frigoli, S. Scarano, and M. Minunni, "Electrochemical sensors for antibiotic detection: a review," *Sensors*, vol. 24, no. 3, p. 1225, 2024, doi: 10.3390/s24031225.
[12] X. Gong, J. Li, Y. Chen, *et al.*, "Advances in the electrochemical detection of antibiotics: from novel materials to point-of-care devices," *Sensors*, vol. 25, no. 2, p. 578, 2025, doi: 10.3390/s25020578.

[13] A. Hassan, A. E. Radi, and K. A. El-Shaikh, “Electrochemical sensing of antibiotics in complex biological matrices: challenges and prospects,” *Biosens. Bioelectron.*, vol. 176, p. 112925, 2021, doi: 10.1016/j.bios.2020.112925.

Electrochemical Detection of Antibiotics

N. Jasnakova[a,*], J. Shepa[a], I. Shepa[b], I. Sisolakova[a]
[a] Department of Physical Chemistry, Faculty of Science, Pavol Jozef Šafárik University, Moyzesová 11, 04011 Košice, Slovak Republic
[b] Institute of Materials Research, Slovak Academy of Sciences, vvi, Watsonova 47, 040 01 Košice, Slovak Republic
* nikola.jasnakova@upjs.sk

Introduction

The increasing demand for sustainable technologies and rapid diagnostics highlights the urgent need for innovative sensor solutions. Among today's most critical challenges is the escalating threat of antibiotic resistance, projected to rise by nearly 70% between 2022 and 2050. This global health concern stems from the declining efficacy of antibiotics, allowing bacteria to spread with highly resistant structures that undermine conventional therapies [1]. Vancomycin, a glycopeptide antibiotic, remains a last-resort treatment for severe Gram-positive infections such as pneumonia, sepsis, endocarditis, and osteomyelitis. Its mechanism of action involves disrupting peptidoglycan synthesis, altering membrane permeability, and interfering with bacterial RNA synthesis. However, inappropriate or excessive use in both human and veterinary medicine accelerates the development of resistance, with residues entering the food chain and the environment [2, 3].
This research aims to develop advanced electrochemical sensors for the sensitive detection of vancomycin in biological fluid and infusion solutions. The sensor is expected to exhibit hight sensitivity, selectivity and reproductibility. Ultimately, our goal is to design multisensor platforms capable of monitoring a broad spectrum of antibiotics, contributing to safer healthcare practices and sustainable environmental protection.

Experiment

This study focused on the modification of a conventional screen-printed carbon electrode (SPCE, DropSens). The electrode was modified by applying 10 µM of solution, composed of 0.03 g $AuCl_3$, 0.03 mL HCl, and 25 mL KCl. Electrochemical deposition was subsequently performed for 15 cycles, resulting in the fabrication of an AuNP-modified SPCE sensor. The properties of the modified sensor were measured in 5 mM $K_3Fe(CN)_6/K_4Fe(CN)_6$ in 1 M KCl.
Further electrochemical measurements were carried out using a 500 µM vancomycin in PBS solution, with the pH adjusted to 13 using NaOH solution. The mechanism of vancomycin interaction on the gold-modified electrode was thoroughly investigated, including studies based on the polarization rate to elucidate kinetic behaviour. Calibration curves were constructed over a range of concentrations, employing various electrochemical techniques, including cyclic voltammetry (CV), differential pulse voltammetry (DPV), and chronoamperometry (CHA). Finally, stability and reproducibility tests were conducted to assess the performance and reliability of the modified sensor.

Results and discussion

Morphology of SPCE modified by AuNPs was studied by scanning electrone microscopy (SEM). As shown in the *Figure 1*, the AuNP-modified SPCE electrodeposited during 5, 10, and 15 cycles revealed progressive changes in surface morphology. Remarkably, after 15 cycles, the electrode surface exhibited well-defined aggregates of gold nanoparticles, representing the most effective modification and underscoring the impact of repeated cycling on electrode surface structuring.

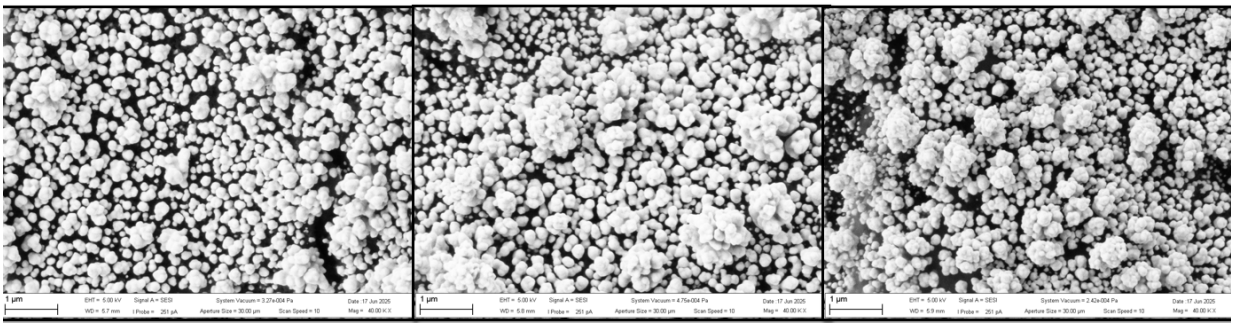

Figure 1 AuNP-modified electrode during 5, 10, and 15 cycles, analyzed by SEM at 40,000× magnification.

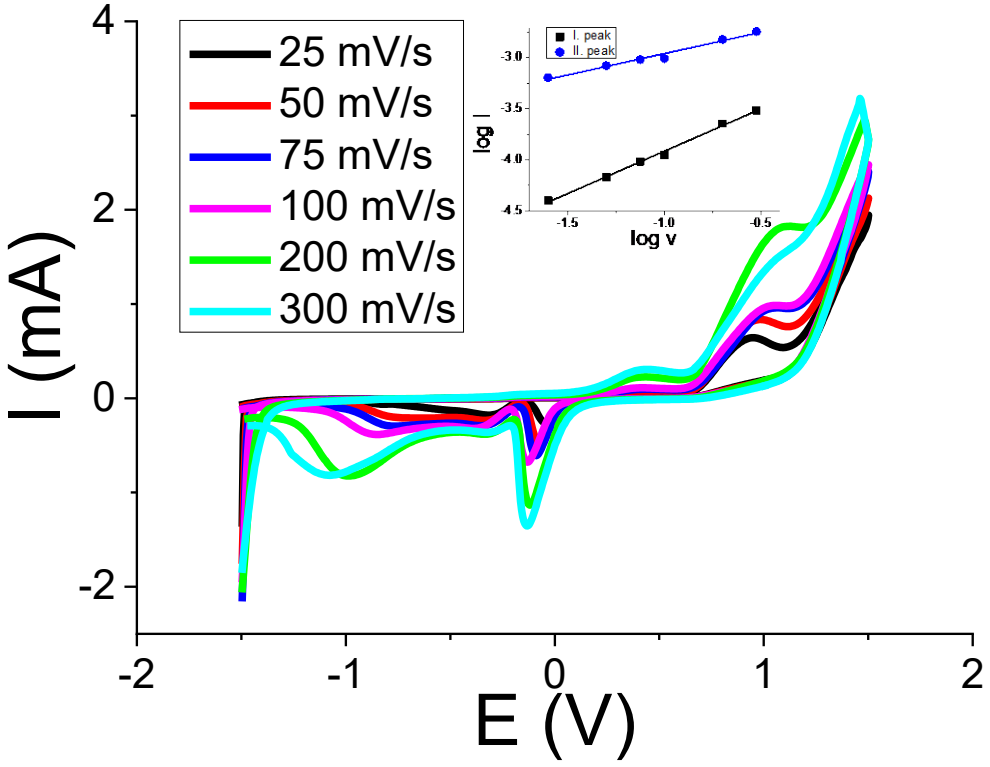

Figure 2 Electrochemical response of the AuNP-modified SPCE sensor for vancomycin detection at varying scan rates from 25 to 300 mV/s.

Prepared electrodes were studied via cyclic voltammetry at different scan rates to study mechanism of electrochemical reaction (*Figure 2*). Cyclic voltammograms for vancomycin detection display 2 well defined oxidation peaks at the potential 0.5 V and 1 V. The oxidation potential shift to the higher values, which indicates irreversible or quasireversible process. The logarithmic dependence of polarization rate on current revealed that first oxidation process was limited by adsorption onto the electrode surface (slope value – 0.82), and second step was limited by diffusion of electroactive species to the elctrode surface. Precise quantification of vancomycin across a range of concentrations in a samples will further be performed using CV, DPV, or CHA. The sensor could be applicable from local delivery in orthopedic implants[4], through surgical administration[5], to intraoperative irrigation[6], providing precise real-time vancomycin monitoring and enhancing treatment optimization and postoperative infection prevention.

The AuNP/SPCE sensor still under development, represents a highly promising advancement in vancomycin monitoring. Its precision, versatility, and adaptability across concentration ranges suggest it could become an essential tool for enhancing safety and treatment effectiveness in surgical and orthopedic practice.

Acknowledgements

This work was funded by the EU NextGenerationEU through the Recovery and Resilience Plan of the Slovak Republic under project no. 09-I05-03-V02-00047.

References

[1] S. V. Khairnar, A. Das, D. Oupický, M. Sadykov, and S. Romanova, “Strategies to overcome antibiotic resistance: silver nanoparticles and vancomycin in pathogen eradication,” RSC Pharmaceutics, vol. 2, no. 3, pp. 455–479, 2025, doi: 10.1039/D4PM00314D.

[2] W. D. Adane, B. S. Chandravanshi, Y. Chebude, and M. Tessema, “A novel electrochemical sensor (Au-Ag-ANCCs/r-GO/poly(L-histidine)/GCE) for the simultaneous determination of vancomycin and ceftriaxone residues in chicken meat, fish, and milk samples,” Chemical Engineering Journal, vol. 497, p. 154808, Oct. 2024, doi: 10.1016/j.cej.2024.154808.

[3] M. Pourmadadi, M. Shirazi, M. Jafari, A. Rahdar, and S. A. de Alencar, “Nanoscaled drug delivery carriers for the targeted delivery of vancomycin: Overcoming bacterial resistance through advanced formulation strategies,” J Drug Deliv Sci Technol, vol. 114, p. 107454, Dec. 2025, doi: 10.1016/j.jddst.2025.107454.

[4] S. Kim, A. R. Bishop, M. W. Squire, W. E. Rose, and H.-L. Ploeg, “Mechanical, elution, and antibacterial properties of simplex bone cement loaded with vancomycin,” J Mech Behav Biomed Mater, vol. 103, p. 103588, Mar. 2020, doi: 10.1016/j.jmbbm.2019.103588.

[5] S.-T. Wang, H.-H. Lin, Y.-C. Yao and P.-H. Chou, "Vancomycin powder mixed with autogenous bone graft and bone substitute may decrease the deep surgical site infections in elective lumbar instrumented fusion surgery for degenerative disorders: a prospective randomized study," The Spine Journal, vol. 25, no. 9, pp. 1866–1876, Sep. 2025, doi: 10.1016/j.spinee.2025.05.001.
[6] N. B. Hinckley, M. C. Klanderman, and K. J. Renfree, "Tissue Concentrations of Vancomycin Achieved by Regional Perfusion Versus Intravenous Prophylaxis in Upper Extremity Surgery: A Randomized Controlled Trial," *J Hand Surg Am*, vol. 50, no. 5, pp. 560–567, May 2025, doi: 10.1016/j.jhsa.2025.02.003.

Functional Nanomaterials For Aqueous Zn-Ion Batteries: The Emerging Alternative of Li-Ion

L. Kavan[a]
[a] J. Heyrovsky Institute of Physical Chemistry, Academy of Sciences of the Czech Republic, Dolejskova 3, CZ-182 23 Prague 8, Czech Republic
* kavan@jh/inst.cas.cz

Introduction and Motivation

Aqueous dual-ion (Zn/Li) batteries offer a compelling balance of safety, cost, and sustainability, positioning themselves among promising alternatives to the conventional Li-ion batteries [1]. By coupling the abundance and intrinsic safety of the zinc/water interface with the high energy density of lithium metal oxides or phosphates, these systems embody a hybrid strategy with significant potential. During operation, Zn^{2+} and Li^{+} ions simultaneously participate in charge storage: zinc dissolves to Zn^{2+} at the negative electrode while Li^{+} is extracted from the cathode during discharge, with the process reversed upon charging.
The inherent drawbacks of aqueous electrolytes, i.e. easy hydrogen/oxygen evolution, corrosion, and Zn dendrite formation, can be largely mitigated using water-in-salt electrolytes (WiSE) instead of traditional electrolyte solutions with smaller salt concentrations [2]. In the WISE, the mass ratio of salt to water exceeds unity. At the extreme end, molten hydrates can be formed, in which the molar ratio of salt to water drops below three. Zinc chloride, one of the most soluble inorganic salts ever, is of particular relevance in this context. An example is $ZnCl_2 \cdot 2.33\ H_2O$, which melts above 10 °C.

Results and Discussion

The paper will present the first systematic study of electrochemical materials, including substrates, active electrode compounds, and electrolyte components, relevant to Zn/Li dual-ion batteries employing $ZnCl_2$-based WiSE. Among the investigated substrates, titanium offers the widest electrochemical stability window in this WiSE. By contrast, carbon, commonly used as an additive and substrate, is unstable at potentials above ~2.2 V vs. Zn^{2+}/Zn, raising concerns about its suitability for high-voltage electrode materials such as $LiMnPO_4$. On the other hand, carbon-coated $LiFePO_4$ (olivine) is a robust, highly stable positive electrode material in WiSE, exhibiting both good charge capacity and cycling performance. Its formal potential shifts positively with increasing Li^{+} concentration in the electrolyte.

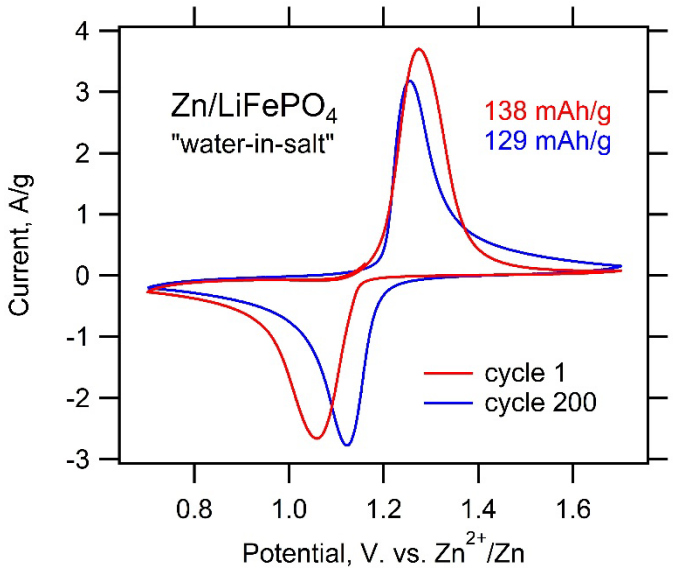

Figure 1 Cyclic voltammograms of $LiFePO_4$ in WiSE electrolyte; scan rate 1 mV/s. The electrolyte composition is 15 m $ZnCl_2$ + 1m LiCl. The positive electrode is a battery-grade $LiFePO_4$ (Roth) mixed with Timcal carbon black C65 and PVDF. The negative and reference electrodes are from Zn/metal. Two-hundred cycles were tested, the plots show the 1st and 200th cycle for easier reading.

Our study also highlights the often-overlooked impact of electrolyte impurities. Trace amounts of Mn^{2+}, commonly present in commercial-grade $ZnCl_2$, can mimic the electrochemical signatures of $LiMnPO_4$, potentially leading to misinterpretation of results [3]. Conversely, the intentional addition of Mn^{2+} to WiSE gives rise to a new battery chemistry reminiscent of redox-flow systems.

Acknowledgments
This work was financially supported by the project "The Energy Conversion and Storage", funded as project No. CZ.02.01.01/00/22_008/0004617 by Programme Johannes Amos Comenius, call Excellent Research

References
[1] Y. Ran, F. Dong, S. Sun and Y. Lei, "Aqueous Zinc-Based Batteries: Active Materials, Device Design, and Future Perspectives", *Adv. Energy Mater.*, vol. pp. 2406139, 2025, doi: 10.1002/aenm.202406139.
[2] B. Zhang, J. Yao, C. Wu, Y. Li, J. Liu, J. Wang, T. Xiao, T. Zhang, D. Cai, J. Wu, Z.W. Seh, S. Xi, H. Wang, W. Sun, H. Wan and H.J. Fan, "Electrolyte Design for Reversible Zinc Metal Chemistry", *Nat. Commun.*, vol. 16 pp. 71, 2025, doi: 10.1038/s41467-024-55657-1.
[3] T. Supiňková, M. Zukalová, N. Kakavas, J. Xu, W. Niu, F.T. Eickemeyer, M. Graetzel and L. Kavan, "Electrolyte effects and stability of Zn/Li dual-ion batteries with water-in-salt electrolytes", *J. Power Sourc.*, vol. 655 pp. 237983, 2025, doi: 10.1016/j.jpowsour.2025.237983.

Azo-Ligands in Metal–Organic Frameworks for catalytic and energy applications

N. Kiraly[a,*], V. Zelenak[a], M. Almasi[a]
[a] Department of Inorganic Chemistry, Institute of Chemistry, Faculty of Science UPJS, Moyzesova 11, 041 54 Kosice, Slovak Republic
* nikolas.kiraly@upjs.sk

The study of azo-containing ligands in the construction of metal–organic frameworks (MOFs) at Pavol Jozef Šafárik University has progressed markedly over time. The earliest efforts centered on the synthesis of the layer-pillared framework $\{[Zn_2(OH)(AZPY)(BDC)_{1.5}]\cdot H_2O\}_n$, where 4,4′-azobispyridine (AZPY) served as a bridging unit alongside 1,4-benzenedicarboxylate (BDC) [1]. This material exhibited an interpenetrated bilayer architecture connected through neutral (4,4)-grid-type sheets, yielding one-dimensional channels extending in the [011] direction. Gas sorption studies confirmed the uptake of nitrogen and carbon dioxide, with CO_2 adsorption reaching 1.04 mmol g^{-1} at 273 K.

Building on this foundation, ternary Cu(II) coordination polymers were prepared, including $\{[Cu(\mu_2\text{-}AZPY)(H_2BTC)_2]\}_n$ and $\{[Cu(\mu_2\text{-}AZPY)(\mu_2\text{-}HBTC)(H_2O)]\cdot AZPY\}_n$. Both frameworks utilized benzene-tricarboxylate (BTC) linkers, with their final architectures strongly dependent on the employed synthetic route, whether solvothermal or diffusion-based [2].

More recent investigations have incorporated extended azo-carboxylate linkers, particularly H_4MTA (methanetetrayltetrakis(benzene-4,1-diyl)tetrabenzoic acid), which enabled the design of MOFs with tailored porosities and functional properties. Frameworks such as ZnMTA $\{[Zn_2(MTA)]\cdot 4H_2O\cdot 3DMF\}_n$ and CdMTA $\{[Cd_2(MTA)]\cdot 5H_2O\cdot 4DMF\}_n$ were obtained, exhibiting high BET surface areas (up to 1057 $m^2\cdot g^{-1}$) and notable CO_2 and CH_4 adsorption capacities under high-pressure conditions [3].

Parallel work expanded into alkaline-earth systems, producing SrMTA $\{[Sr_2(MTA)(H_2O)]\cdot H_2O\cdot 4DMF\}_n$ and BaMTA $\{[Ba_2(MTA)(H_2O)]\cdot H_2O\cdot 4DMF\}_n$. These compounds were isostructural, containing one-dimensional channels (~11 × 10 Å²). SrMTA achieved a surface area of 1321 $m^2\cdot g^{-1}$ and adsorbed up to 22.4 wt.% CO_2 at 0 °C [4]. A Pb(II)-based analogue, PbMTA $\{[Pb_2(MTA)]\cdot 2DMF\cdot 8H_2O\}_n$, confirmed by single-crystal X-ray diffraction, showed moderate CO_2 uptake (6.3 wt.% at 0 °C) but excellent reusability as a catalyst in Knoevenagel condensation reactions.

Among the most structurally sophisticated systems is the ZrMTA framework $\{[Zr_6(\mu_3\text{-}O)_8(H_2O)_8(\mu_8\text{-}MTA)_2]\cdot xDMF\cdot yH_2O\}_n$. This material integrates robust Zr_6O_8 clusters and contains multiple pore systems with apertures as large as 24.26 × 22.28 Å². Combining high porosity, remarkable stability, and versatile adsorption properties, ZrMTA represents a landmark in MOF development within this research program. Additional studies produced lanthanide-containing analogues, LnMTA $\{[Ln_4(MTA)_3]\cdot xH_2O\cdot yDMF\}_n$ (Ln = Pr, Nd, Gd, Er), crystallizing in tetragonal lattices with channels exceeding 12 Å. These exhibited thermal stability up to 380 °C and selective CO_2 uptake, with capacities of 33 $cm^3\ g^{-1}$ for PrMTA and 24 $cm^3\ g^{-1}$ for NdMTA.

Ongoing efforts are now directed toward the synthesis of new tritopic azo-carboxylate ligands—H_3TDT, H_3MATAB, and H_3TBDTA—which feature extended π-conjugation and multiple azo linkages. These novel linkers, not yet explored in MOF chemistry, are being introduced into frameworks with s-, p-, d-, and f-block metals. Their directional coordination ability and electron-rich azo groups are expected to yield porous coordination networks with improved adsorption selectivity, light-responsiveness, and catalytic potential. This forward-looking approach underlines the university's strategy to expand the family of azo-functionalized MOFs and explore their applications in energy storage, CO_2 capture, and environmentally relevant catalytic processes.

Acknowledgements
This research was created with the support of grant EU NextGenerationEU through the Recovery and Resilience Plan for Slovakia under the project No. 09I03-03-V05-00008 (VVGS-ESGV-2923).

References

[1] V. Zeleňák, Z. Vargová, M. Almáši, A. Zeleňáková and J. Kuchár, *Microporous and Mesoporous Materials*, 2010, 129, 354–359.
[2] M. Almáši, V. Zeleňák, A. Zeleňáková, Z. Vargová and I. Císařová, *Inorganic Chemistry Communications*, 2016, 74, 66–71.
[3] M. Almáši, N. Király, V. Zeleňák, M. Vilková and S. Bourrelly, *RSC Advances*, 2021, 11, 20137–20150.
[4] N. Király, D. Capková, R. Gyepes, N. Vargová, T. Kazda, J. Bednarčík, D. Yudina, T. Zelenka, P. Čudek, V. Zeleňák, A. Sharma, V. Meynen, V. Hornebecq, A. Straková Fedorková and M. Almáši, *Nanomaterials*, 2023, 13, 234.

Multiporous HKUST-1 in Knoevenagel Condensation Reactions

N. Kiraly[a], N. Vargova[a,*], R. Serbin[b], G. Zelenkova[c], T. Zelenka[c], M. Almasi[a]
[a] Department of Inorganic Chemistry, Institute of Chemistry, Faculty of Science, University of Pavol Jozef Safarik in Kosice, Moyzesova 11, 041 54 Kosice, Slovak Republic
[b] Department of Analytical Chemistry, Institute of Chemistry, Faculty of Science, University of Pavol Jozef Safarik in Kosice, Moyzesova 11, 041 54 Kosice, Slovak Republic
[c] Department of Chemistry, Faculty of Science, University of Ostrava, 30. Dubna 22, CZ-702 00 Ostrava, Czech Republic
* nikolas.kiraly@upjs.sk

Metal–organic frameworks (MOFs) are a class of crystalline porous solids consisting of metal ions or clusters coordinated to polytopic organic linkers, resulting in periodic three-dimensional structures. Due to their large surface area, adjustable pore dimensions, and high thermal and chemical stability, MOFs have gained substantial attention for use in gas adsorption, catalysis, targeted drug delivery, and sensing applications [1]. In heterogeneous catalysis, MOFs offer distinct advantages because their modular structures permit rational tuning of active sites via alteration of both metal centers and organic linkers. This allows for the enhancement of catalytic activity and selectivity in key transformations, including oxidation, hydrogenation, and condensation reactions [2].
In this study, two types of copper-based MOFs exhibiting micro- and mesoporous characteristics, denoted as HKUST-1(A) and HKUST-1(B), were synthesized and investigated for their catalytic performance. The frameworks were synthesized via a solvothermal approach employing trimesic acid (H_3BTC) and copper(II) nitrate trihydrate [$Cu(NO_3)_2 \cdot 3H_2O$] dissolved in *N,N′*-dimethylformamide (DMF). To induce hierarchical porosity, various concentrations of cetyltrimethylammonium bromide (CTAB) and citric acid were introduced as structure-directing agents. After 10 minutes of sonication, the mixture was heated at 75 °C for 24 hours. The resulting crystalline blue products were separated by filtration and washed with DMF.
The subsequent removal of templating agents was conducted in multiple steps. Initially, the materials were treated with a 1 M solution of ammonium nitrate in an ethanol–water mixture (1:2 v/v) at 60 °C for 24 hours. This step was followed by decantation and further washing with fresh ethanol–water (1:2 v/v) under ambient conditions for another 24 hours. A final purification stage was carried out using Soxhlet extraction with methanol for a duration of three days. Fourier-transform infrared spectroscopy (FTIR) confirmed both the successful formation of the frameworks and the effective removal of the structure-directing agents (*Figure 1*).
Nitrogen adsorption–desorption measurements were employed to analyze the porosity and specific surface areas of the synthesized materials. HKUST-1(A) exhibited a hierarchical architecture consisting of both micropores and mesopores, whereas HKUST-1(B) demonstrated predominantly mesoporous characteristics. The BET surface areas were determined to be 1534 $m^2 \cdot g^{-1}$ for HKUST-1(A) and 1709 $m^2 \cdot g^{-1}$ for HKUST-1(B), confirming the successful application of a cooperative templating strategy that integrates microporous frameworks within mesopore walls.

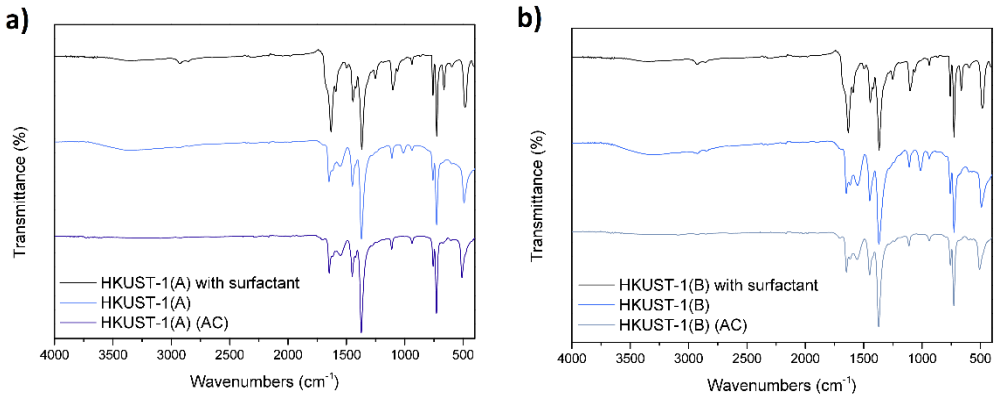

Figure 1 FTIR spectra illustrating the as-synthesized, surfactant-extracted, and fully activated samples of *(a)* HKUST-1(A) and *(b)* HKUST-1(B).

The catalytic efficiency of the activated MOF samples was assessed through the Knoevenagel condensation of benzaldehyde (PhCHO) with malononitrile, used as a model reaction. Several reaction parameters—including the type of solvent (toluene, acetonitrile, and xylene), reaction temperature (60 °C, 80 °C, and 100 °C), and catalyst amount (25 mg and 50 mg)—were optimized. The most effective reaction conditions involved the use of toluene as the solvent, a reaction temperature of 80 °C, and a catalyst loading of 50 mg.

Under these optimized conditions, a series of substituted benzaldehydes bearing electron-withdrawing groups at the ortho (2-F, 2-Cl, 2-Br, 2-NO_2) and para (4-F, 4-Cl, 4-Br, 4-NO_2) positions were investigated. Across all tested substrates, HKUST-1(B) consistently exhibited superior catalytic activity relative to HKUST-1(A). Among the ortho-substituted aldehydes, the highest conversion (96%) was observed for 2-nitrobenzaldehyde, while 4-chlorobenzaldehyde showed the highest conversion (97%) among the para-substituted series. In contrast, the maximum yields achieved with HKUST-1(A) were 84% for 2-fluorobenzaldehyde and 91% for 4-chlorobenzaldehyde.

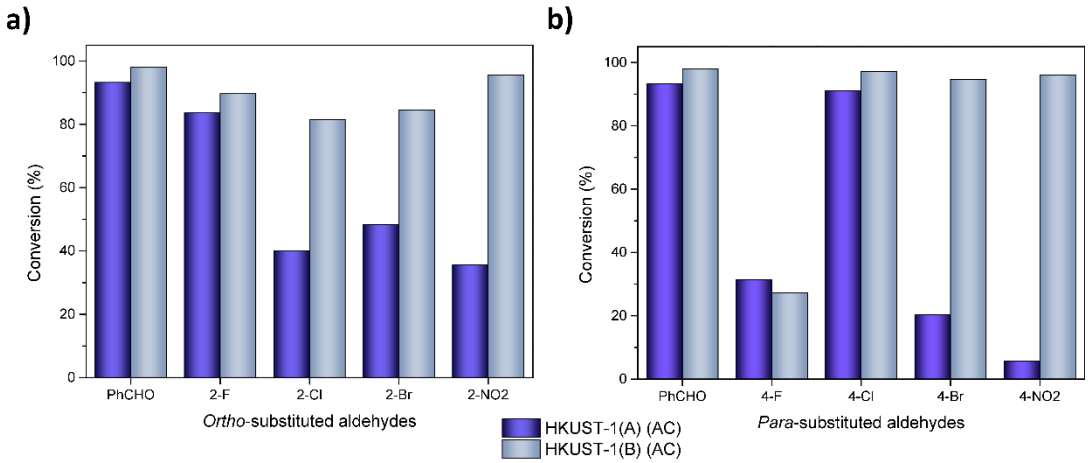

Figure 2 Comparative catalytic performance of *(a)* HKUST-1(A) and *(b)* HKUST-1(B) in the Knoevenagel condensation using ortho- and para-substituted aromatic aldehydes.

Acknowledgements
This research was created with the support of EU NextGenerationEU through the Recovery and Resilience Plan for Slovakia under the project No. 09I03-03-V05-00008 (ESGV-2923).

References
[1] D. Yang, B. C. Gates, ACS Catal. **9** (2019) 1779-1798.
[2] Y-S. Wei, M. Zhang, R. Zou, Q. Wu, Chem. Rev. **120** (2020) 12089-12174.

Tailored Viologen Derivatives with Variable Alkyl Chains for Enhanced Redox-Flow Battery Performance

N. Kiraly[a,*], M. Zelinska[a], M. Vilkova[b], A. Strakova Fedorkova[c], J. Asenjo[d], M. Almasi[a]
[a] Department of Inorganic Chemistry, Institute of Chemistry, Faculty of Science, University of Pavol Jozef Safarik in Kosice, Moyzesova 11, 041 54 Kosice, Slovak Republic
[b] Department of NMR, Institute of Chemistry, Faculty of Science, University of Pavol Jozef Safarik in Kosice, Moyzesova 11, 041 54 Kosice, Slovak Republic
[c] Department of Physical Chemistry, Institute of Chemistry, Faculty of Science, University of Pavol Jozef Safarik in Kosice, Moyzesova 11, 041 54 Kosice, Slovak Republic
[d] *InoBat Energy, Tomasikova 30, 821 01 Bratislava, Slovakia*
* nikolas.kiraly@upjs.sk

The ongoing global transition toward renewable energy requires energy storage technologies capable of operating at large scale. Lithium-ion batteries (LIBs), which currently dominate applications ranging from portable electronics to electric vehicles and grid systems, provided 8.8 GWh of stationary storage capacity in 2019, compared with only 0.25 GWh delivered by redox-flow batteries (RFBs). Despite their widespread use, LIBs face several drawbacks, including high maintenance expenses, safety risks, and the limited availability of lithium resources. These limitations have intensified the demand for alternative technologies. For long-term grid storage, systems must combine durability, low cost, high cycling stability, and strong round-trip efficiency, yet installation and operational costs continue to present barriers.

The European Strategic Energy Technology (SET) Plan has established clear 2030 objectives for stationary energy storage, targeting a cost of 0.05 €/kWh per cycle and a lifetime of at least 10,000 cycles over 20 years. In this context, RFBs represent a highly promising class of technologies for sustainable energy management. Their architecture, which separates power output (determined by the electrochemical stack) from energy capacity (dictated by electrolyte volume), offers significant advantages. These include modular design, scalability, relatively low maintenance requirements, and long service life. An RFB typically consists of three essential parts: external electrolyte reservoirs, electrochemical stacks, and a pumping system. Active redox species stored in solution circulate between the tanks and stack, where reversible electrochemical reactions occur. Although RFBs generally display lower volumetric energy and power density than LIBs, they compensate with high round-trip efficiency, deep discharge capability, rapid response, and reduced environmental impact, particularly in aqueous systems [1,2].

In this study, a series of viologen derivatives were synthesized and evaluated for potential use as electrolyte components in RFBs. The compounds prepared were 4,4′-([4,4′-bipyridine]-1,1′-diium-1,1′-diyl) derivatives bearing ethanoate, butanoate, pentanoate, and heptanoate substituents. All four species were synthesized under uniform solvothermal conditions in *N,N′*-dimethylformamide at 100 °C for 48 h in an inert atmosphere. The procedure involved the alkylation of 4,4′-bipyridine with the corresponding ethyl bromoesters (ethyl 4-bromoethanoate, -butanoate, -pentanoate, or -heptanoate), followed by acid-catalyzed de-esterification in hydrobromic acid solution to afford the viologen dicarboxylic acids as final products.

The isolated yields of the synthesized derivatives varied, reflecting the influence of subtle changes in the synthetic pathway. A detailed comparison of the yields and the impact of structural modifications will be presented in the poster contribution at the upcoming conference.

Acknowledgements
Funded by the EU NextGenerationEU through the Recovery and Resilience Plan for Slovakia under the project SUNFLOWERS No. 09I02-03-V01-00022.

References
[1] Arévalo-Cid, P.; Dias, P.; Mendes, A.; Azevedo, J. Redox flow batteries: anew frontier on energy storage. Sustainable Energy & Fuels 2021, 5 (21),5366–5419.
[2] Yao, Y.; Lei, J.; Shi, Y.; Ai, F.; Lu, Y.-C. Assessment methods andperformance metrics for redox flow batteries. Nature Energy 2021, 6 (6), 582–588. (https://doi.org/10.1039/d1se00839k)
(https://doi.org/10.1038/s41560-020-00772-8)

Electrochemical Multisensor for Bioanalytes Determination

S. Kiraly[a,*], I. Sisolakova[a], J. Shepa[a], M. Varga[b], G. Urban[b,c], R. Orinakova[a]
[a] Department of Physical Chemistry, Pavol Jozef Šafárik University in Košice, Moyzesova 11, 040 01, Košice, Slovak republic
[b] INNOVLAB startup centrum of Deutsche Telekom IT Solutions s.r.o, Moldavská cesta 8b, 040 11, Košice, Slovak republic
[c] Faculty of Electrical Engeneering and Informatics, Technical University Košice, Letná 1/9, 042 00 Košice-Sever, Slovenská republika
* sona.kiraly@upjs.sk

Rapid, selective, and cost-effective detection of bioanalytes plays a crucial role in modern diagnostics, particularly for diseases such as diabetes mellitus. Traditional analytical methods, while highly accurate, are often expensive, technically demanding, and unsuitable for point-of-care applications or use outside specialized laboratories. In this context, electrochemical sensors have emerged as an attractive alternative due to their simplicity, high sensitivity, portability, and potential for miniaturization. These characteristics make them a promising technology for fast, low-cost, and reliable bioanalytical measurements [1, 2].
This research focuses on the development of non-enzymatic electrochemical multisensors (*Figure 1*) designed for the detection of clinically relevant biomolecules, including glucose, insulin, cholesterol, ascorbic acid, and antibiotics. The primary aim is to optimize individual sensors as a foundational step toward their integration into a multi-analyte sensing platform. Such an approach could enable simultaneous monitoring of several bioanalytes in real-world samples, enhancing diagnostic capabilities and reducing analysis time.

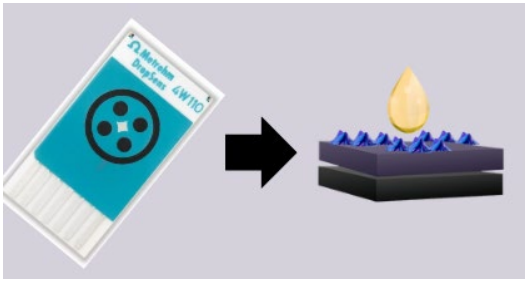

Figure 1 Electrochemical Multisenzor.

The sensors under development are based on carbon electrodes fabricated via screen-printing (SPCE) and further modified with polymeric membranes (e.g., chitosan, polypyrrole) and metallic nanoparticles (Ni, Cu, Au), which replace the enzymatic components typically used in traditional biosensors. Electrochemical characterization indicates that the appropriate combination of polymer and metal nanoparticle significantly enhances sensitivity, stability, and selectivity of the sensors. Detection limits can reach below 10 nM, while maintaining rapid response times (<10 s) and high reproducibility, demonstrating strong analytical performance.
These findings establish a solid foundation for the development of integrated multi-sensor devices capable of simultaneous detection of multiple bioanalytes in complex biological matrices outside of laboratory settings. Such devices could provide practical, real-time diagnostic solutions for clinical and point-of-care applications, paving the way toward more accessible and versatile bioanalytical platforms**.**

Acknowledgements
Funded by the EU NextGenerationEU through the Recovery and Resilience Plan for Slovakia under the project No. 09-I05-03-V02-00047.

References
[1] I. Šišoláková, J. Hovancová, R. Oriňaková, A. Oriňak, L. Trnková, D. R. García, and J. Radoňak, “Influence of a polymer membrane on the electrochemical determination of insulin in nanomodified screen printed carbon electrodes,” *Bioelectrochemistry*, vol. 130, p. 107326, Dec. 2019, doi: 10.1016/j.bioelechem.2019.06.011.
[2] N. Amini, M. B. Gholivand, and M. Shamsipur, “Electrocatalytic determination of traces of insulin using a novel silica nanoparticles–Nafion modified glassy carbon electrode,” *J. Electroanal. Chem.*, vol. 714, pp. 70–75, Feb. 2014, doi: 10.1016/j.jelechem.2013.12.015

Comparative Evaluation of Enriched Iron Implants for Bone Substitution in a Rat Tibial Defect Model

M. Kozar[a,*], B. Siskova[a], E. Tomovcikova[a], R. Gorejova[b], R. Orinakova[b]
[a] Small Animal Clinic, The University of Veterinary Medicine and Pharmacy in Košice, 040 01 Košice, Slovak Republic
[b] Department of Physical Chemistry, Pavol Jozef Šafárik University in Košice, Moyzesova 11, 040 01, Košice, Slovak republic
* martin.kozar@uvlf.sk

Bone defect healing is a complex process influenced by biological and mechanical factors [1,2]. While small defects may regenerate spontaneously, critical-sized defects require additional interventions such as bone grafts or biomaterials [2]. Orthopedic surgery has advanced significantly over the past decades, not only in diagnostic methods and surgical approaches but also in materials science. Traditional metal implants made of stainless steel or titanium have long been the standard for fracture fixation. Despite their advantages, these materials still carry risks for patients, such as infection, the need for a secondary surgery to remove the implant, and potential biological complications related to corrosion or ion release. These limitations have resulted in extensive research into biodegradable materials that provide adequate mechanical support during healing and later degrade gradually without the need for reoperation. Autografts remain the gold standard, but their use is limited by donor site morbidity and restricted availability [3, 4]. Allografts and synthetic substitutes carry risks of immune rejection or infection [5, 6]. Biodegradable implants offer an attractive alternative as they are gradually resorbed and replaced by new bone, thus avoiding secondary removal surgery [7-9]. Polymers offer good biocompatibility but lack sufficient strength for hard tissue applications [10-12]. On the other hand, biodegradable metals, such as magnesium- and iron-based alloys, offer superior mechanical integrity, though they require better control over degradation rates [7, 13, 14]. Ceramics, especially hydroxyapatite, are valuable as bioactive coatings that enhance implant integration [15-17].

Current research focuses on the development of iron-based porous implants with tailored corrosion and mechanical properties [13, 18]. The present study describes the design and in vivo evaluation of a novel sponge-like iron-based biodegradable implant intended for bone replacement, demonstrating promising potential for orthopedic applications [18].

The experimental study focused on the use of iron implants in a rat model (Rattus norvegicus, Wistar strain), after creating a standardized full-thickness bone defect in the tibia.

Three implant groups were used:

1. Pure iron implant,
2. Iron implant enriched with hydroxyapatite,
3. Iron implant enriched with gentamicin,
4. Control group without internal bridging of the bone stumps.

The methodology was focused on evaluating inflammatory markers during the first 21 days after defect creation and implantation of the biodegradable material. Monitoring and evaluation of metallic material incorporation into bone tissue and its degradation were carried out over a 365-day period following surgery.

Another essential aspect was the gene expression analysis for:

- Collagen type I alpha 1 (COL1A1),
- Osteocalcin,
- Osteopontin,
- Osteonectin,
- Arbp (acidic ribosomal phosphoprotein P0).

One of the key evaluation components was macroscopic assessment of:

- The bone defect status,
- Osteointegration and degradation of the iron implants,
- Bridging of the bone defect,
- Reaction of the surrounding structures.

In the macroscopic evaluation, the greatest reactivity of the surrounding structures at the defect site was observed in the group with gentamicin-enriched iron implants, manifested as a strong inflammatory reaction, poor incorporation into the bone stump, and increased postoperative complications.

The most notable ingrowth of new tissue through the iron implant was observed from day 180 in the group with hydroxyapatite-enriched implants.

When evaluating the use of pure iron implants, several limitations emerged:

- Formation of cartilaginous pseudo-tissue as the initial stage of callus formation,
- Loss of stability of the pure implant,

- Delayed osteointegration due to the reactivity of surrounding structures during degradation,
- Increased inflammatory response after implantation.

As a starting point for further research, the focus should be on developing a porous structural matrix made from multiple materials with different stiffness and resorption times, aimed at creating biocomposites for bone tissue replacement.

Acknowledgements
This work was supported by the project APVV-20-0278 of the Slovak Research and Development Agency and by the project KEGA 012UVLF-4/2025 of the Cultural and Educational Grant Agency of the Ministry of Education, Culture and Sports of the Slovak Republic.

References
[1] I. Blumenfeld, S. Srouji, Y. Lanir, D. Laufer and E. Livne, "Enhancement of bone defect healing in old rats by TGF-b and IGF-1," *Exp. Gerontol*., vol. 37, no. 4, pp. 553–565, Apr. 2002, doi: 10.1016/s0531-5565(01)00215-7.
[2] C.R. Perry, "Bone repair techniques, bone graft, and bone graft substitutes", *Clin. Orthop. Relat. Res.*, vol. 360, pp. 71-86, Mar. 1999, doi: 10.1097/00003086-199903000-00010.
[3] G. Liu, L. Zhao, W. Zhang, L. Cui, W. Liu and Y. Cao, "Repair of goat tibial defects with bone marrow stromal cells and betatricalcium phosphate", *J. Mater. Sci. Mater. Med.*, vol. 19, no. 6, pp. 2367-2376, Jun. 2008, doi: 10.1007/s10856-007-3348-3.
[4] F.C. den Boer, B.W. Wippermann, T.J. Blokhuis, P. Patka, F.C. Bakker and H.J. Haarman, "Healing of segmental bone defects with granular porous hydroxyapatite augmented with recombinant human osteogenic protein-1 or autologous bone marrow", *J. Orthop. Res.,* vol. 21, pp. 521–528, May 2003, doi: 10.1016/S0736-0266(02)00205-X.
[5] M.W. Chapman, R. Bucholz and R. Cornell, "Treatment of acute fractures with a collagen-calcium phosphate graft material. A randomized clinical trial", *J. Bone. Jt. Surg. Am.,* vol. 79, no.4, pp. 495–502, Apr. 1997, doi: 10.2106/00004623-199704000-00004.
[6] R.W. Lindsey, Z. Gugala, E. Milne, M. Sun, F.H. Gannon and L.L. Latta, "The efficacy of cylindrical titanium mesh cage for the reconstruction of a critical-size canine segmental femoral diaphyseal defect", *J. Orthop. Res.*, vol. 24, no. 7, pp. 1438-1453, Jul. 2006, doi: 10.1002/jor.20154.
[7] A.R. Khan, N.S. Grewal, C. Zhou, K. Yuan, H.J. Zhang and J. Zhang, "Recent advances in biodegradable metals for implant applications: Exploring in vivo and in vitro responses", *Bioact. Mater.,* vol. 20, 105126, 2023, doi: 10.1016/j.rineng.2023.101526.
[8] A.M. Ibrahim, P.G. Koolen, K. Kim, G.S. Perrone, D.L. Kaplan and S.J. Lin, "Absorbable biologically based internal fixation", *Clin. Podiatr. Med. Surg.,* vol. 32, no. 1, pp. 61–72, Jan. 2015, doi: 10.1016/j.cpm.2014.09.009.
[9] M.B. Kannan, "Hydroxyapatite coating on biodegradable magnesium and magnesium-based alloys", in *Mucalo M, ed. Hydroxyapatite (HAp) for Biomedical Applications. Woodhead Publishing: Sawston*, UK, 2015, pp. 289–306, ISBN 978-1-78242-033-0.
[10] R. Song, M. Murphy, CH. Li, K. Ting, CH. Soo and Z. Zheng, "Current development of biodegradable polymeric materials for biomedical applications", *Drug. Des. Devel. Ther.*, vol. 24, no. 12, pp. 3117-3145, Sep. 2018, doi: 10.2147/DDDT.S165440.
[11] A. Prasad, "Bioabsorbable polymeric materials for biofilms and other biomedical applications: Recent and future trends", *Mater. Today. Proc.,* vol. 44, pp. 2447–2453, 2021, doi: 10.1016/j.matpr.2020.12.489.
[12] D. Eberli, " Tissue Engineering", in *BoD—Books on Demand: Norderstedt, Germany*, 2010, ISBN 978-953-51-4553-0.
[13] F. Zivic, N. Grujovic, E. Pellicer, J. Sort, S. Mitrovic, D. Adamovic and M. Vulovic, "Biodegradable Metals as Biomaterials for Clinical Practice: Iron-Based Materials", in *Biomaterials in Clinical Practice. Springer*, 2018, pp. 225–280, doi: https://doi.org/10.1007/978-3-319-68025-5.
[14] J. Espiritu, M. Meier and J.M. Seitz, "The current performance of biodegradable magnesium- based implants in magnetic resonance imaging: A review", *Bioact. Mater*., vol. 6, pp. 4360–4367, Apr. 2021, doi: 10.1016/j.bioactmat.2021.04.012.
[15] L. Liu and T.J. Webster, "Nanotechnology for reducing orthopedic implant infections: Synthesis, characterization, and properties", in *Orthopedic Biomaterials. Springer, Cham*, 2017, pp. 31–62, doi: 10.1007/978-3-319-73664-8.
[16] M. Saini, Y. Singh, P. Arora, V. Arora and K Jain, "Implant biomaterials: A comprehensive review*", World. J. Clin. Cases.*, vol. 16, no. 3(1), pp. 52-57, Jan. 2015, doi: 10.12998/wjcc.v3.i1.52.
[17] J.S. Al-Sanabani, A.A. Madfa and F.A. Al-Sanabani, "Application of calcium phosphate materials in dentistry," *Int. J. Biomater,* 2013: 876132, Jun. 2013, doi: 10.1155/2013/876132.
[17] B. Wegener, A. Sichler, S. Milz, CH. Sprecher, K. Pieper, W. Hermanns, V. Jansson, B. Nies, B. Kieback, P. Ernst Müller, V. Wegener and P. Quadbeck, "Development of a novel biodegradable porous iron-based implant for bone replacement", *Sci. Rep.*, vol. 4, no. 10(1), p. 9141, Jun. 2020, doi: 10.1038/s41598-020-66289-y.

9th International Conference on Novel Materials Fundamentals and Applications
High Tatras, 12.10.-15.10.2025

Electrolyte/Sulphur Ratio Optimization for Lithium–Sulphur Batteries

J. Lescinsky[a,*], D. Capkova[b], A. Strakova Fedorkova[a]
[a] Department of Physical Chemistry, Faculty of Sciences, Pavol Jozef Šafárik University in Košice, Moyzesova 11, 04154 Kosice, Slovak Republic
[b] Department of Chemical Sciences, Bernal Institute, University of Limerick, V94 T9PX Limerick, Ireland
* jakub.lescinsky@student.upjs.sk

Introduction

Since the widespread deployment of renewable energy sources such as solar and wind, the demand for high-capacity and cost-effective energy storage systems has rapidly increased. Conventional lithium-ion (Li-ion) batteries, which have dominated the portable electronics and electric vehicle markets for the past three decades, are now reaching their theoretical energy density limits and face sustainability issues due to critical raw material demands [1,2].

Lithium–sulphur (Li–S) batteries have therefore attracted great attention as next-generation energy storage systems, owing to their exceptionally high theoretical specific capacity (1675 $mAhg^{-1}$), high gravimetric energy density (up to 2500 $Whkg^{-1}$), low cost, and environmental benignity of sulphur [3,4]. Despite these advantages, several challenges hinder commercialization: the intrinsic insulating nature of sulphur and its reduction products, the ~80% volume expansion upon lithiation, polysulfide dissolution and migration (shuttle effect), and the instability of the lithium metal anode [5,6].

One of the most decisive practical parameters is the electrolyte-to-sulphur (E/S) ratio, which directly determines sulphur utilization, energy density at the cell level, and cycling stability [7]. While high electrolyte contents enable efficient sulphur redox kinetics, they penalize gravimetric energy density. Conversely, lean electrolyte operation often leads to high polarization, poor cycling life, and severe capacity fading [8,9]. Therefore, a systematic optimization of the E/S ratio, together with the choice of separator, is essential for designing commercially relevant Li–S systems.

Experimental

Cathodes containing 60 wt.% sulphur were prepared using a carbon host matrix and coated onto aluminium foil as current collectors. The electrodes were assembled into coin-type half-cells with lithium metal anodes.

The effect of electrolyte content was studied across a wide range of **E/S ratios (5–55 µL mg^{-1})**. Two separators were investigated: a commercial polyolefin membrane (Celgard® 2325) and a glass fiber separator (Whatman GF/A). Electrolytes were ether-based, optimized for polysulfide solubility and ionic transport. Electrochemical characterization included cyclic voltammetry (CV, 0.1 mV s^{-1}) (*Figure 1*), galvanostatic charge/discharge cycling (GCPL) at different C-rates(*Figure 2 a,2 b*). Before cycling, the morphology of both electrodes and separators was examined by scanning electron microscopy (SEM) (*Figure 3*), while the compositional analysis using energy-dispersive X-ray spectroscopy (EDX) was performed only for the electrodes.

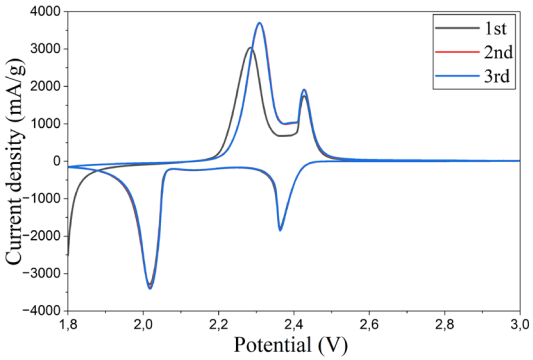

Figure 1 Cyclic voltammogram of a cell with an E/S ratio of 55 µl/mg and a GF/A separator at a scanning speed of 0.1 mV/s.

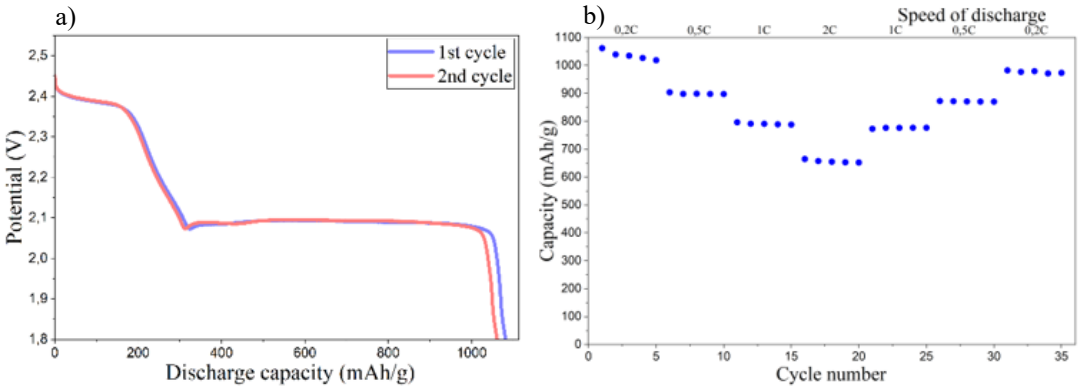

Figure 2 Characteristics of cell discharge with an E/S ratio of 55 µl/mg and a GF/A separator *2 a)* first two discharge cycles at a discharge rate of 0.1C; *2 b)* maximum discharge capacities of cycles during galvanostatic cycling at different current loads.

Results and Discussion

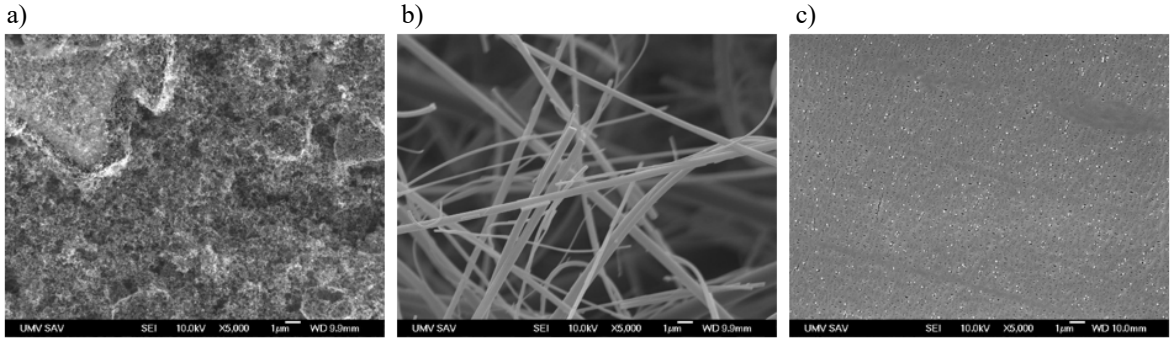

Figure 3 SEM images of 3a) electrode surface; 3b) GF/A separator; 3c) separator Celgard® 2325.

Cells with the **GF/A separator** demonstrated superior electrochemical performance compared to those with Celgard® 2325. The higher porosity and wettability of GF/A provided improved electrolyte distribution and polysulfide retention, resulting in reduced polarization and enhanced cycle stability.

The best performance was achieved for an **E/S ratio of 40 µL mg^{-1}** with GF/A(Tab.1), which exhibited high initial discharge capacities and stable capacity retention over extended cycling. CV curves revealed well-defined redox peaks at ~2.35 V and ~2.1 V, corresponding to the two-step reduction of S_8 to soluble polysulfides and subsequently to insoluble Li_2S_2/Li_2S. GCPL confirmed that GF/A-based cells maintained higher specific capacities and Coulombic efficiency compared to Celgard® 2325.

At low E/S ratios (5–15 µL mg^{-1}), both separators showed severe capacity fading, indicating the difficulty of maintaining efficient redox reactions under electrolyte-deficient conditions. SEM/EDX analyses revealed uniform sulphur distribution in cathodes.

These findings are consistent with recent reports emphasizing the critical role of electrolyte economy. Huang et al. [8] demonstrated that tuning electrode porosity reduces the minimal sustainable E/S ratio from ~4 µL mg^{-1} to ~2 µL mg^{-1}. Cho et al. [9] showed that Lewis-acidic additives rejuvenate lean electrolytes, enabling stable cycling even at ultra-low E/S ratios. Furthermore, separator engineering—such as surface-modified glass fiber membranes—has been shown to effectively mitigate polysulfide shuttling [10,11].

Table 1 Comparison of discharge capacities of the studied electrodes at different current loads.

Typ separátora		GF/A		Celgard® 2325	
Pomer E/S ($\frac{\mu l}{mg}$)		55	40	25	15
Číslo cyklu	C-rate (C)	Kapacita($\frac{mAh}{g}$)			
1	0,2	836,0	1062,1	725,6	594,1
6	0,5	711,5	903,9	576,2	465,5
11	1	640,3	796,5	453,5	363,3
16	2	553,5	664,7	321,1	259,8
21	1	644,1	773,2	406,6	337,7
26	0,5	717,2	872,6	499,6	419,3
31	0,2	774,2	982,6	620,3	515,7
Zachovanie kapacity (%)		91,9	92,5	85,4	87,1

Conclusion

This study highlights the crucial importance of the electrolyte-to-sulphur ratio and separator type for practical Li–S battery performance. The optimal configuration—**GF/A separator with an E/S ratio of 40 µL mg⁻¹**—provided the best balance between sulphur utilization, capacity retention, and electrolyte efficiency.

The results underscore the need for integrated strategies combining electrolyte minimization with separator and electrolyte engineering to achieve high energy density and long cycle life. Future research should focus on reducing the E/S ratio below 10 µL mg^{-1} without sacrificing electrochemical stability, potentially through advanced electrolyte formulations, functional separator coatings, and interlayer designs.

Acknowledgements

This work was funded by the Recovery and Resilience Plan for Slovakia under the project SUNFLOWERS no. 09I02-03-V01-00022.

References

[1] Tarascon, J.M., Armand, M. Issues and challenges facing rechargeable lithium batteries. Nature, 414, 359–367 (2001).
[2] Goodenough, J.B., Park, K.S. The Li-ion rechargeable battery: A perspective. J. Am. Chem. Soc., 135, 1167–1176 (2013).
[3] Ji, X., Nazar, L.F. Advances in Li–S batteries. J. Mater. Chem., 20, 9821–9826 (2010).
[4] Manthiram, A., et al. Lithium–sulphur batteries: progress and prospects. Adv. Mater., 32, 2003666 (2020).
[5] Li, J., et al. Engineering strategies for suppressing the shuttle effect in lithium–sulphur batteries. Nano Energy, 99, 107399 (2022).
[6] Yari, S., et al. Performance benchmarking and analysis of lithium–sulphur batteries under practical conditions. Nat. Commun., 16, 2542 (2025).
[7] Ma, C., et al. Green production of biomass-derived carbons for Li–S batteries. Nanomaterials, 13, 1768 (2023).
[8] Huang, Z., et al. Balancing sulphur utilization and electrolyte demand in Li–S batteries. J. Power Sources, 623, 235678 (2025).
[9] Cho, H., et al. Interconvertible and rejuvenated Lewis acidic electrolyte additive for lean Li–S batteries. Nat. Commun., 16, 3211 (2025).
[10] Hwang, J.Y., et al. Advanced cathodes for practical lithium–sulphur batteries. Acc. Mater. Res., 6, 2025.
[11] "Advancements in Glass Fiber Separator Technology for Lithium–Sulfur Batteries." ACS Omega, 9, 45678–45689 (2024).

Adsorption of Gases by Carbon Nanomaterials

M. Lhotka[a,*], L. Mastny[b]
[a] Department of Inorganic Technology, Faculty of Chemical Technology, University of Chemistry and Technology, Prague, Technická 5, 166 28, Prague 6, Czech Republic
[b] Department of Inorganic Chemistry, Faculty of Chemical Technology, University of Chemistry and Technology, Prague, Technická 5, 166 28, Prague 6, Czech Republic
* miloslav.lhotka@vscht.cz

Carbon materials (biochar) is a highly porous, fine, carbon-rich material produced via pyrolysis from various feedstock materials of organic origin. Plant biomass can be transferred into biochar *via* pyrolysis and can be further used as a sorbent agent in soils. This paper focuses on the textural characterization of biochar. The aim of the study is to generalize the influence of agriculture residues and temperature of pyrolysis on biochar yield, surface properties and pore composition and to determine the properties of biochar predicting its behaviour in soil. The plant biomass for pyrolysis was harvested in a relatively small area close to Příbram region (Czech Republic). The biomass of herbaceous and wood plants was treated by slow pyrolysis at 5 temperatures (400 – 600°C) to prepare biochar. Winter wheat (straw and grains), maize, meadow grass and wood poplar bark were used as feedstock [1]. The biochar samples were characterized using adsorption of nitrogen and carbon dioxide. The specific surface area (S_{BET} and $S_{t\text{-}plot}$), micropore analysis and distributions of volume mesopores were measured on 3Flex surface analyzers (Micromeritics, USA) using the gas sorption technique (N_2 at 77 K). The adsorption isotherms were fitted by using the Brunauer-Emmett-Teller (BET) method for specific surface area, the micropore volume by the t-plot method, the pore-size distribution by the Barrett-Joyner-Halenda (BJH) method for mesopores and the Horvath-Kawazoe method for micropores. The micropore volume and isosteric heats of adsorption were measured on ASAP 2050 analyzers (Micromeritics, USA) using the gas sorption technique (CO_2 at 273-333 K). All samples of biochar showed adsorption isotherms of Ib and IVa types (IUPAC classification), the samples thus represent a mixture of micropores and mesopores with classical type of hysteresis loop H4 (IUPAC classification), which corresponds to slit pores. The final value of specific surface area varied according to the material used for its production. The S_{BET} generally increased logarithmically with the temperature of pyrolysis, e.g. for wood poplar bark the values increased from 124.4 $m^2\ g^{-1}$ to 428.1 $m^2\ g^{-1}$, for maize from 4.75 to 105.05 $m^2\ g^{-1}$. The highest surface area was found in biochar from wood poplar bark (511 $m^2\ g^{-1}$); the herbaceous material provided specific surface area of 192 $m^2\ g^{-1}$ (wheat straw). By processing data from the adsorption isotherms of biochar using t-plot, it was found that the specific surface area of mesopores ($S_{t\text{-}plot}$) is significantly lower than the specific surface area determined by the BET method. The microporous structure was predominant for biochars (predicting possible sorption abilities) prepared at increasing pyrolysis temperature, the volume of micropores was more developed. In this study, novel results concerning complex biochar analysis were obtained. In conclusion, the texture properties of biochar play a key role in understanding the influence of feedstock and pyrolysis conditions.

References

[1] Lehmann, J., Joseph, J., Biochar for environmental management: science and technology, Earthscan, London (2009).
[2] Břendová K, Száková J, Lhotka M, Krulikovská T, Punčochář M and Tlustoš P,: Biochar physicochemical parameters as a result of feed-stock material and pyrolysis temperature: predictable for the fate of biochar in soil?, *Environ Geochem Health* vol. 39, pp. 1381–1395, 2017
[3] Sedlakova M., Szakova J., Lhotka M., Hailegnaw N.S., Holeckova Z., Pracke K., Robledo-Mahon T., Tlustos P.: Changes in soil carbon and nitrogen accessibility with the application of biochars with different morphological and physical characteristics. *Journal of Soils and Sediments* vl. 21, pp. 1644–1658, 2021

Environmentally Friendly Biginelli Reaction and Electrosynthetic Hydrolysis of Dihydropyrimidinones

T. J. Liska[a,*], M. Parackova[a], R. Orinakova[a], M. Vilkova[a]
[a] Institute of Chemistry, Faculty of Science, Pavol Jozef Šafárik University in Košice, Moyzesova 11, 040 01 Košice, Slovak Republic
* tomas.jan.liska@student.upjs.sk

Introduction

A central goal of modern chemistry is the discovery of novel and affordable biologically active substances that can improve the potency of therapeutic agents while minimizing or even eliminating adverse side effects. Statistical analyses reveal that more than 85% of known bioactive compounds are heterocyclic molecules, with the majority containing nitrogen atoms. The prevalence of heterocycles is not coincidental: their structural diversity and electronic properties enable a wide range of interactions, including dipole–dipole contacts, hydrogen bonding, and π–π stacking, all of which are fundamental to molecular recognition in biological systems. These features underline the critical role of heterocycles in drug discovery and rational design of new pharmaceuticals. Consequently, heterocyclic chemistry has become a cornerstone of pharmaceutical research, driving the development of innovative synthetic methodologies and accelerating the identification of promising therapeutic candidates [1, 2, 3].

One of the most powerful modern strategies for the synthesis of heterocyclic compounds is the use of multicomponent reactions (MCRs). These are one-pot processes in which more than two starting materials react together, with most of their atoms incorporated into the final product [4]. Remarkably, scientists have even accomplished a seven-component reaction by exploiting the distinct chemoselectivities of the Ugi–Mumm and Ugi–Smiles reactions, generating highly diverse peptide- and glycopeptide-like structures [5]. Owing to their efficiency and versatility, MCRs have found widespread applications in medicinal chemistry, natural product synthesis, and materials science. Compared to conventional multistep approaches, MCRs offer several key advantages: convergent synthesis in a single step, excellent atom- and pot-economy, rapid construction of complex molecules from simple building blocks, facile access to large compound libraries by varying starting materials, and the potential for post-MCR modifications that enable the generation of novel ring systems and substitution patterns. Their generally mild conditions also align with greener and more sustainable synthetic practices [6]. Many fundamental MCRs are classic name reactions, including the Ugi, Passerini, van Leusen, Strecker, Hantzsch, and Biginelli reactions, along with numerous modern variations. Importantly, the initial products of these reactions often serve as synthetic hubs that can be elaborated into a vast diversity of cyclic and acyclic scaffolds through secondary transformations. As a result, libraries of drug-like advanced compounds can typically be prepared in only one to three synthetic steps [7].

Organic synthesis is a central discipline for the bottom-up construction and late-stage diversification of molecular compounds, enabling transformative advances in medicinal chemistry, drug development, materials science, and the chemical and pharmaceutical industries. Over the past decade, researchers have increasingly embraced new enabling technologies such as photochemistry, artificial intelligence, mechanochemistry, and flow chemistry. In contrast, molecular electrosynthesis remained relatively underexplored until recently. Organic electrochemistry, once considered a niche technique, has now begun to overcome many of its earlier limitations. Its roots trace back to the 19th century, with Faraday's electrolysis of acetic acid to hydrocarbons and Kolbe's electrochemical decarboxylative dimerization. In the early 20th century, Hickeling further advanced the field by proposing potentiostatic control of reactions instead of constant-current electrolysis [8]. As illustrated in *Figure 1*, electrosynthesis has seen a remarkable resurgence in recent years and is gaining increasing popularity.

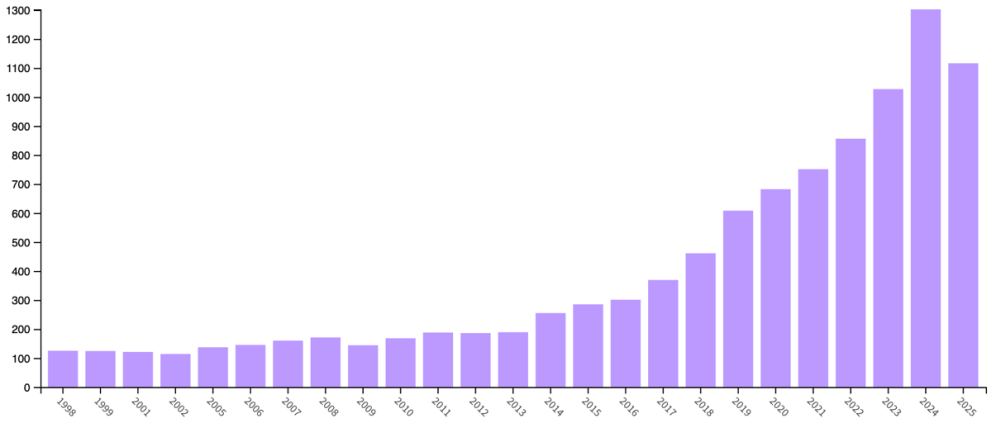

Figure 1 Number of published articles with keyword "electrosynthesis" on Web of Science (WoS). Accessed 30.09.2025.

Results and discussion

The synthesis of dihydropyrimidinone (DHPM, **1**), the product of the Biginelli multicomponent reaction (MCR), was carried out using three reactants: 4-hydroxybenzaldehyde (**2**), ethyl acetoacetate (**3**), and urea (**4**), as shown in *Figure 1*. Replacing conventional methods with greener protocols is an important objective from both economic and ecological perspectives. One approach involves the use of biodegradable catalysts that are readily available, naturally occurring, safe, and efficient. In this work, L-tartaric acid (**5**) was selected as the catalyst [9]. A further application of green chemistry principles was the choice of solvent. The Environmental, Health, and Safety (EHS) assessment method identifies potential hazards of chemical substances during early process design, while Life Cycle Assessment (LCA) quantifies emissions and resource use throughout a solvent's life cycle. Ethanol ranks highly in both assessments, and was therefore used as the reaction medium [10]. Under these conditions, the reaction afforded the target product in nearly quantitative yield.

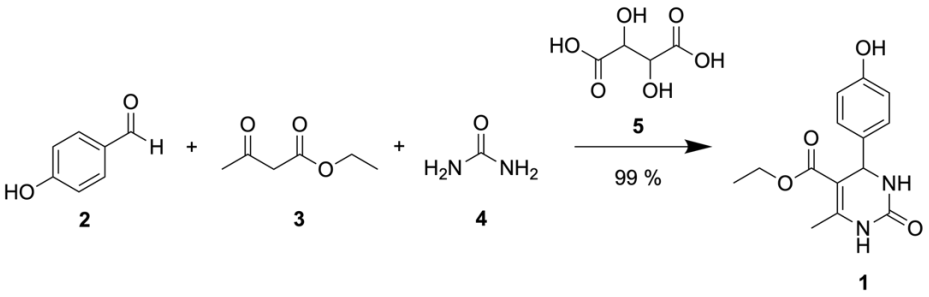

Figure 2 Multicomponent synthesis of dihydropyrimidinone **1**.

The second stage of the study focused on modification of the ethyl ester group (*Figure 2*), which has been reported to be resistant to hydrolysis and nucleophilic attack. Our investigations confirmed this observation: compound **1** remained stable even under strongly basic conditions (pH > 14, 100 °C, 48 h), with only ~1% of the ester hydrolyzed. In contrast, application of electrosynthetic methods enabled ester cleavage under much milder conditions. The electrochemical hydrolysis was conducted potentiostatically at 1.2 V in aqueous solution (pH = 12.5) using a Pt | Pt electrode system at room temperature. After 10 h, product **6** was obtained in a yield of 15%.

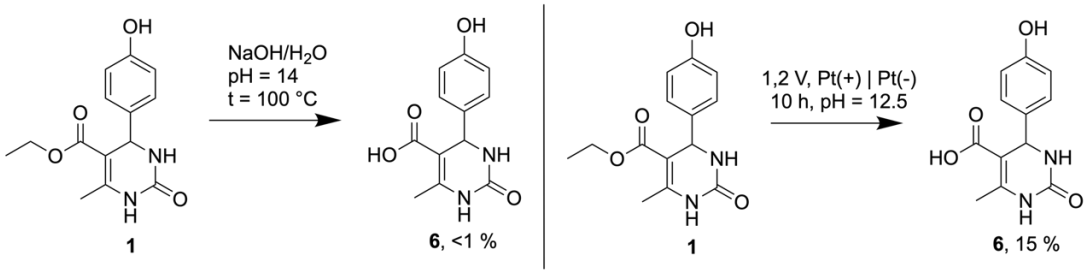

Figure 3 Hydrolysis of ester moiety employing conventional route (left) and electrochemical route (right).

Conclusion

Dihydropyrimidinones (DHPMs) are versatile heterocyclic scaffolds accessible through the Biginelli reaction and serve as valuable synthetic hubs for the development of diverse structures with applications in both medicinal and materials chemistry. While numerous studies have focused on improving DHPM synthesis – ranging from the use of environmentally benign catalysts to precious metal-based systems – our work has emphasized greener conditions. This approach proved highly effective, affording the target DHPM in nearly quantitative yield. In contrast, modification of the DHPM core remains a greater challenge, with far fewer reports available in the literature. Here, we have demonstrated a novel strategy to functionalize the DHPM scaffold under exceptionally mild and sustainable conditions, employing only water and NaOH for ester hydrolysis. This advance highlights the potential of combining multicomponent synthesis with green electrochemical methods to expand the chemical space of DHPM derivatives. Ongoing optimization of the hydrolysis step aims to further improve the reaction efficiency and yields.

Acknowledgements

Part of the research results was obtained using the computational resources procured in the national project National competence centre for high performance computing (project code: 311070AKF2) funded by European Regional Development Fund, EU Structural Funds Informatization of society, Operational Program Integrated Infrastructure, by Internal Scientific Grant System "PF Výskum UPJŠ" of Pavol Jozef Šafárik University in Košice (vvgs-2023-3039) and by the Grant Agency of the Ministry of Education, Science, Research and Sport of the Slovak Republic: KEGA Grant No. 008UPJS-4/2023.

References

[1] M. M. Heravi and V. Zadsirjan, 'Prescribed drugs containing nitrogen heterocycles: an overview', Nov. 23, 2020, *Royal Society of Chemistry*. doi: 10.1039/d0ra09198g.
[2] I. Pibiri, 'Recent Advances: Heterocycles in Drugs and Drug Discovery', Sep. 01, 2024, *Multidisciplinary Digital Publishing Institute (MDPI)*. doi: 10.3390/ijms25179503.
[3] J. A. . Joule and K. . Mills, *Heterocyclic chemistry*. Wiley, 2010.
[4] I. Ugi, A. Dömling, and W. Hörl, 'Multicomponent reactions in organic chemistry', *Endeavour*, vol. 18, no. 3, pp. 115–122, Jan. 1994, doi: 10.1016/S0160-9327(05)80086-9.
[5] S. Brauch, L. Gabriel, and B. Westermann, 'Seven-component reactions by sequential chemoselective Ugi–Mumm/Ugi–Smiles reactions', *Chemical Communications*, vol. 46, no. 19, p. 3387, 2010, doi: 10.1039/b927388c.
[6] M. Tandi, V. Sharma, B. Gopal, and S. Sundriyal, 'Multicomponent reactions (MCRs) yielding medicinally relevant rings: a recent update and chemical space analysis of the scaffolds', Jan. 16, 2025, *Royal Society of Chemistry*. doi: 10.1039/d4ra06681b.
[7] A. Dömling, W. Wang, and K. Wang, 'Chemistry and biology of multicomponent reactions', Jun. 13, 2012. doi: 10.1021/cr100233r.
[8] C. Zhu, N. W. J. Ang, T. H. Meyer, Y. Qiu, and L. Ackermann, 'Organic Electrochemistry: Molecular Syntheses with Potential', *ACS Cent Sci*, vol. 7, no. 3, pp. 415–431, Mar. 2021, doi: 10.1021/acscentsci.0c01532.
[9] S. S. Salim, L. B. Masram, Y. U. Gadkari, A. B. Barkule, and V. N. Telvekar, 'Tartaric Acid as an Expeditious and Green Catalyst for the Synthesis of 1,2,4-Triazolidine-3-thiones in an Aqueous Medium', *Org Prep Proced Int*, vol. 55, no. 6, pp. 584–590, 2023, doi: 10.1080/00304948.2023.2202107.
[10] C. Capello, U. Fischer, and K. Hungerbühler, 'What is a green solvent? A comprehensive framework for the environmental assessment of solvents', *Green Chemistry*, vol. 9, no. 9, pp. 927–93, Aug. 2007, doi: 10.1039/b617536h.

9th International Conference on Novel Materials Fundamentals and Applications
High Tatras, 12.10.-15.10.2025

Nanostructured Metallic Electrodes for Sensor Applications

F. Maerzweiler[a,*], G. Fafilek[a].
[a] Institute of Chemical Technologies and Analytics, TU Wien, Getreidemarkt 9/164ec, 1060 Vienna, Austria
* florian.maerzweiler@tuwien.ac.at

Introduction

Current enzymatic biosensors for glucose have in common, that the enzyme glucose oxidase is immobilized in the sensor to facilitate the oxidation of glucose. As biological molecules are used, those sensors benefit from high sensitivity, selectivity and fast response. However, the sensors are susceptible to high temperatures and changes in pH, suffer a low-shelf life and are mostly for single-use only [1, 2]. Therefore, research has lately been focusing on non-enzymatic biosensors that employ inorganic materials such as gold, platinum or TiO_2 that allow for direct oxidation of glucose and potentially better stability [3, 4, 5].
Even though the noble metals gold, platinum and palladium are especially promising electrode materials for direct glucose oxidation, these electrodes are negatively influenced by chloride. Chloride causes etching, resulting in electrode deterioration as well inhibition of active sites for the glucose oxidation by chemisorption [6-11]. Both these processes result in continuous changes in the oxidation current and render the results unreliable. In this work we work we present both a novel fabrication method of nanostructured metallic electrodes and the application of such as working electrodes in non-enzymatic biosensors, shown in the example of nanocubic nickel surfaces for a non-enzymatic glucose biosensor that is impervious to the described debilities.

Experimental

All electrochemical experiments were conducted in an H-Cell, in which platinum was used as a counter electrode and a $Hg/HgSO_4$ electrode as the reference. For the preparation of the nanostructured electrodes, polished metal wires or sheets of the studied metal were used as the working electrodes and modified using cyclic voltammetry. For evaluation of the performance of nanostructured nickel as a working electrode for glucose quantification, glucose concentrations of 5, 10, 20 and 40 mM solutions in PBS by Thermo Fischer were tested with cyclic voltammetry as well.

Results and discussion

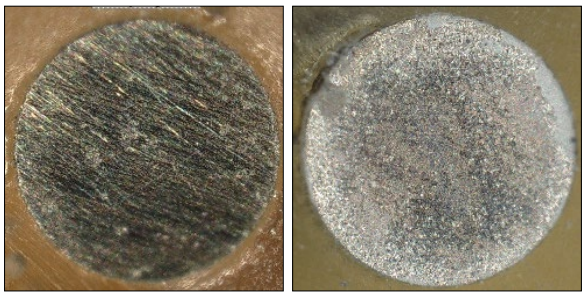

Figure 1 Microscope recording of untreated (left) and surface-treated (right) electrodes.

Figure 2 shows the sensor surface of a polished nickel electrode before the treatment procedure and after. As can be seen in the picture, an obvious change has taken place on the surface after the procedure. Further tests including solutions with the different concentrations of glucose also showed that untreated nickel shows little to no change to varying concentrations of glucose, as visualized in *Figure 2 A*. The pictures of the nickel working electrode in *Figure 1* suggest that the surface area of the electrode has increased after the surface treatment procedure. To test if the current increase is caused by a higher surface area, a nickel electrode was roughened by etching in PBS to yield a higher, non-specific surface area. Despite the higher surface area of the etched electrode, the resulting current is comparable to that of an untreated electrode, as shown in *Figure 2 B*. This allows the assumption that the glucose detection on nickel is surface-dependent and that this required surface is generated by the surface treatment procedure.

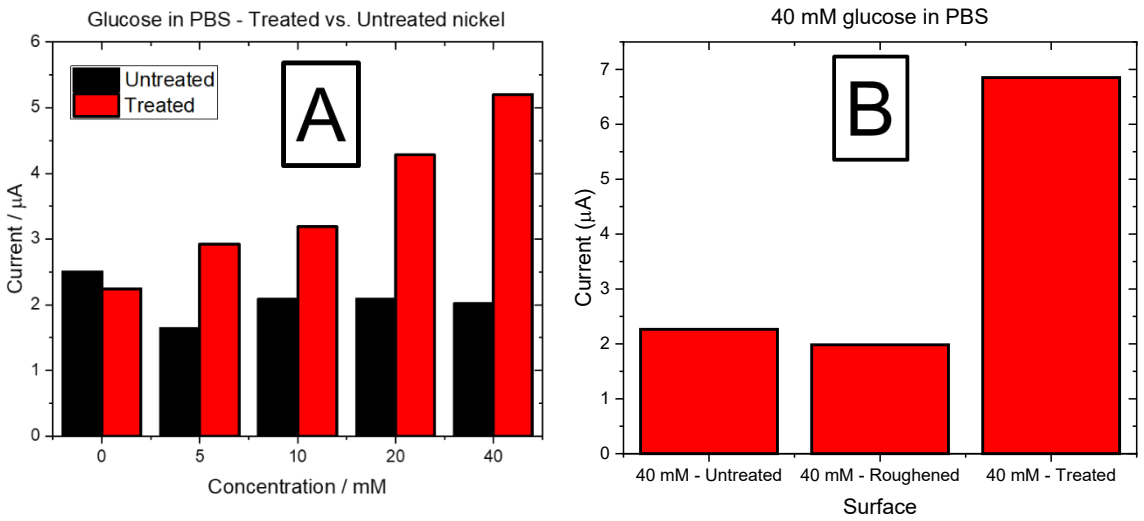

Figure 2 A) Response current (µA) of untreated (black) and surface-treated (red) nickel electrodes to varying glucose concentrations (mM); *B)* Comparison of three nickel electrode surfaces for a 40 mM solution of glucose in PBS. Left: Untreated nickel electrode, center: Nickel electrode roughened by etching, right: Surface-treated nickel electrode.

To test the chloride stability of the biosensor, nickel electrodes were cycled in PBS every 6 hours at a potential range of -0.6 V to -1.4 V with 50 V/s. The range is below the equilibrium voltage of -0.67 vs. Hg/HgSO4 in PBS, where no nickel dissolution is expected. However, if nickel dissolution by other processes were to happen, reductive deposition of nickel cations from solution should be observed. In between the cycles, a potential of -690 mV was applied on the nickel electrode. The cyclic voltammograms are shown in *Figure 3*. After 6 hours the capacitive charging current changed slightly, after which the voltammograms remain unaltered. The unchanged voltammograms and the absence of dissolution or reduction peaks suggest that in fact no dissolution of nickel, corrosion or other means of degradation of the electrode have taken place.

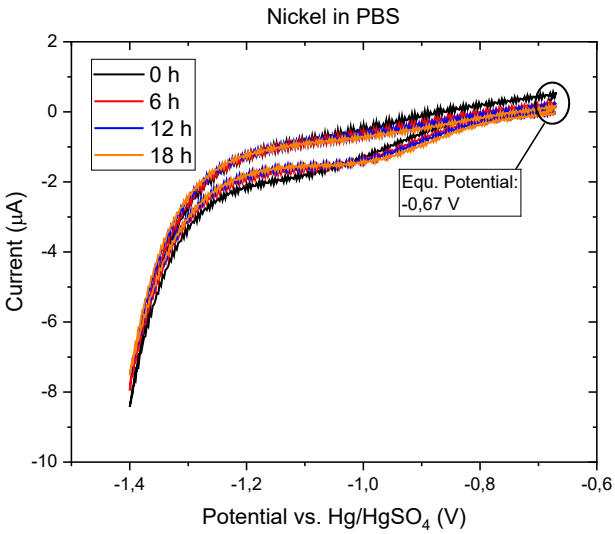

Figure 3 Cyclic voltammograms of a nickel electrode recorded every 6 hours in PBS.

Conclusion

Surface-treated nickel proves to be a viable electrode material for the non-enzymatic detection and quantification of glucose. The ability for glucose detection is enabled by the surface treatment procedure, which generates a favorable surface for glucose detection. The nickel electrodes also exhibited a long-term chloride stability, which can be ensured with little effort by applying a suitable potential in between measurements.

Outlook

Future experiments will be concerned with the characterization of the electrode surface and processes at the electrode-solution interface during measurements.
The surface before and after surface treatment as well as during chloride stability tests will be investigated using electrochemical impedance spectroscopy. Surface processes during measurement and the surface treatment procedure will be monitored using techniques from infrared spectroscopy as well as an in-situ XRD-cell [12].
Other analytes, e.g. environmentally harmful substances, will be tested for the nickel-based biosensor.

Acknowledgements

This research was sponsored by the NATO Science for Peace and Security Programme under grant id. G6106.

References

[1] W. Lee, K. Kim, N.G. Gurudatt, K. Hussain, C. Choi, D. Park et. al., "Comparison of enzymatic and non enzymatic Glucose Sensors based on hierarchical Au-Ni Alloy with conductive Polymer", Biosens. Bioelectron., vol. 130, pp. 48-54, January 2019
[2]M. Hassan, C. Vyas, B. Grieve, P. Bartolo, "Recent Advances in enzymatic and non-enzymatic electrochemical Glucose Sensing", Sensors, vol. 21, pp. 4672-4698, July 2021
[3]S. Kulveer, K. Maurya, M. Malviya, „Recent Progress on Nanomaterial-based electrochemical Sensors for Glucose Detection in Human Bodily Fluids", MCA, vol. 192, January 2025
[4]P. Bollela, K. Evgeny, "Biosensors – Recent Advances and future Challenges", Sensors, vol 20, November 2020
[5]Md. Harun-Or-Rashid, M. Nazmin Aktar, V. Preda, N. Nasiri, "Advances in electrochemical sensors for real-time Glucose Monitoring", Sens. Diagn., vol. 3, pp. 893-914, May 2024
[6]G. Horanyi, G. Inzelt, "Study of the Adsorption of Chloride Ions on Platinum Electrodes from concentrated Solutions of H2SO4, H3PO4, and HClO4", J. Electroanal. Chem., vol. 86, pp. 215-218, February 1977
[7]B. Ratna Shrestha, N. Tada Eiji, A. Nishikita, "Effect of Chloride on Platinum Dissolution", Electrochim. Acta, vol. 143, pp. 161-167, August 2014
[8]O. Kasian, N. Kulyk, A. Mingers, A.R. Zeradjanin, K J.J. Mayrhofer, S. Cherevko, "Electrochemical Dissolution of Gold in Presence of Chloride and Bromide Traces studied by on-line electrochemical inductively coupled plasma Mass Spectrometry", Electrochim. Acta, vol. 222, pp. 1056-1063, November 2016
[9]X. Xu, A. Makaraviciute, S. Petterson, S. Zhan, L. Nyholm, Z. Zhang, "Revising the Factors influencing gold electrodes prepared using cyclic voltammetry", Sens. Actuators B Chem., vol. 283, pp. 146-153, December 2018
[10]J. Schrattenecker, R. Heer, E. Melnik, T. Maier, G. Fafilek, Rainer Hainberger, "Hexaaminrhutnium (II)/(III) as alternative redox-Probe to Hexacyanoferrat (II)/(III) for stable impedimetric Biosensing with Gold Electrodes", Biosens. Bioelectron, vol. 127, pp 25-30, December 2018
[11]M. Gerstl, M. Joksch, G. Fafilek, "The dissolution of Palladium as a Function of Glucose Concentration in Chloride containing Solutions of acidic pH", vol. 741, pp. 1-7, January 2015
[12]F. Froech, S. Kubicek, W. Artner, M. Nelhiebel, S. Larisegger, G. Fafilek, "A versatile electrochemical Cell for in-situ GI-XRD Measurements on lab-scale XRD devices", J. Electroanal. Chem., vol. 971, October 2024

Multi-phase energy storage media for enhanced energy density of redox flow batteries

P. Mazur[a,*], M. Marek[a], A. Taccori[a], J. Krsek[a], M. Spurny[a], D. Graf[a], P. Richtr[a], M. Drnec[a], J. Charvat[b], J. Pocedic[b]
[a] Department of Chemical Engineering, University of Chemistry and Technology Prague, Technicka 5, 16628 Praha 6, Czechia
[b] Pinflow Energy Storage, s.r.o., Křižovnická 86/6, 110 00 Prague, Czechia
* mazurp@vscht.cz

With the unavoidable depletion of fossil fuels and a general shift towards more sustainable generation of energy, suitable technologies for reliable and economic energy storage at various scales are urgently needed. Redox flow batteries, prospective candidates for stationary energy storage, offer excellent scalability and safety, making them fit for a broad range of applications. On the other hand, generally low energy density, when compared to other competing technologies (such Li-ion), motivates the search for high-energy-density solutions with multi-phase storage media as a promising up-and-coming technology. Within our lecture the selected promising approaches investigated with various R&D projects will be introduced incl. flow batteries with metal deposition, micro-emulsion electrolytes and solid redox-mediated capacity boosters.

Flow batteries with metal deposition negative electrode enables multiple increase of the energy density and use of abundant and non-toxic electro-active metals such as Zn or Fe. The non-homogeneity of metal distribution during the battery operation, however, poses significant challenges in terms of cycling stability and safety due to risk of internal short circuit by growing Zn dendrites. in this part, we will summarize the selected experimental and modelling experiences with Zn-air and Zn-iodine flow batteries, primarily aimed to get better insight into the processes affecting Zn distribution and morphology deposited on both planar and 3D substrates as a function of battery operating conditions (electrolyte composition, flow rate, state of charge etc.). Complex combination of post mortem characterization techniques (SEM-EDS, micro-CT, laser confocal microscopy) and spatially distributed physical models enabled us to optimize performance and stability of the studied systems.

Micro-emulsions are thermodynamically stable electrolytes, which enable the dissolution of water insoluble compounds in the emulsion's non-aqueous phase, while maintaining suitable electrochemical and physical properties such as low viscosity, high ionic conductivity, safety and lower volatility. Via primary screening tests of redox active species found in literature we aim to identify satisfactory candidates for their use in micro-emulsion based flow batteries. Glassy carbon rotation disk electrode tests are employed to analyse the electrochemical properties of each substance with subsequent charge-discharge and EIS analysis in a laboratory flow battery single-cell. Possible promising systems are further optimized with respect to electrolyte composition, cell components and operating conditions to reach efficient and stable battery performance.

The principle of capacity booster is to immobilize insoluble redox-active species into a form of mechanically stable granules, which are in contact with flowing electrolyte. The electrolyte then functions as electron mediator between the electrode and the capacity booster [1]. When the booster is fully charged, the electrolyte itself stores capacity. This configuration enables to bypass the concentration limit of various redox-active species. The composition and character of the booster structure is closely tied to the kinetics of the electron transfer. Our goal is to identify optimal preparation methods for the solid boosters by combining different polymer binder, redox active and conductive materials to reach the desired electrochemical and physical properties. These in-house prepared boosters are then employed in battery tests to evaluate their performance.

Acknowledgements
This work was supported by the Slovak Research and Development Agency under the Contract no. DS-FR-24-0004. This publication was supported by the project "The Energy Conversion and Storage", funded as project No. CZ.02.01.01/00/22_008/0004617 by Programme Johannes Amos Comenius, call Excellent Research.
This work was supported by TAČR, program TREND, project no. FW06010097.

References
[1] Khor, A. et al., Review of zinc-based hybrid flow batteries: From fundamentals to applications. Materials Today Energy 2018, 8, 80-108.
[2] S. Gentil, D. Reynard and H. H. Girault, Current Opinion in Electrochemistry, 21, 7 (2020).

Modified UiO-66(Zr) Frameworks for Targeting Brain Tumours via pH-Responsive Drug Delivery

A. Migasova[a], L. Zauska[a], T. Zelenka[b], S. Tomkova[c], Z. Jurasekova[d], A. Unterhuber[e], M. Andreana[e], V. Huntosova[c], M. Almasi[a,*]

[a] Department of Inorganic Chemistry, Institute of Chemistry, Faculty of Science, P. J. Šafárik University in Košice, Moyzesova 11, SK-041 54 Košice, Slovak Republic

[b] Department of Chemistry, Faculty of Science, University of Ostrava, 30. dubna 22, CZ-702 00 Ostrava, Czech Republic

[c] Center for Interdisciplinary Biosciences, Technology and Innovation Park, Pavol Jozef Šafárik University in Košice, Jesenná 5, SK-041 54 Košice, Slovak Republic

[d] Department of Biophysics, Institute of Physics, Faculty of Science, P.J. Šafárik University in Košice, Jesenná 5, SK-041 54 Košice, Slovak Republic

[e] Center for Medical Physics and Biomedical Engineering is located at AKH Vienna, Leitsstelle 4L, Währinger Gürtel 18-20, AT-1090 Vienna, Austria

* miroslav.almasi@upjs.sk

Brain tumours, particularly glioblastoma multiforme (GBM), represent one of the most aggressive and lethal forms of cancer, with extremely poor prognosis and median survival rarely exceeding 15 months despite multimodal treatment. Conventional therapeutic strategies, including surgical resection, radiotherapy, and systemic chemotherapy, face severe limitations due to tumour heterogeneity, drug resistance, and the presence of the blood–brain barrier (BBB), which restricts penetration of therapeutic agents into brain tissue. One of the most widely used chemotherapeutics, 5-fluorouracil (5FU), is a pyrimidine analogue with potent antimetabolic activity that interferes with DNA and RNA synthesis, ultimately suppressing tumour cell proliferation. However, systemic administration of 5FU is plagued by rapid degradation, poor bioavailability, non-selective distribution, and serious systemic toxicity, all of which limit its therapeutic efficacy against brain malignancies. In this context, there is a pressing need for advanced nanocarriers that can encapsulate 5FU, protect it from premature degradation, and ensure controlled and site-specific release within the slightly acidic microenvironment of glioblastomas.

Metal–organic frameworks (MOFs) have recently emerged as highly promising platforms for biomedical applications, particularly drug delivery, due to their crystalline structure, tunable pore architecture, exceptionally high surface area, and potential for functional modification. Among these, UiO-66(Zr) and its aminated derivative UiO-66(Zr)-NH_2 stand out for their high stability, excellent biocompatibility, and structural versatility. The framework is composed of hexanuclear zirconium-oxo clusters $[Zr_6O_4(OH)_4]$ connected by 2-aminoterephthalate linkers, resulting in a robust *fcu* topology with octahedral and tetrahedral cages. The presence of amine groups further enhances the framework's reactivity, allowing post-synthetic modifications to introduce specific functionalities that can tailor drug loading and release behaviour. Previous reports have demonstrated successful encapsulation of anticancer drugs, such as doxorubicin and pemetrexed, into UiO-66(Zr)-NH_2 with clear evidence of *pH*-responsive release, confirming the suitability of this MOF for controlled delivery in tumour environments.

In the present work, we designed and evaluated a histidine-modified derivative of UiO-66(Zr)-NH_2 (UiO-66(Zr)-His) as a multifunctional nanocarrier for 5FU. Histidine, a natural amino acid bearing an imidazole moiety, was selected due to its amphoteric properties, capacity for π–π and cation–π interactions, and its ability to undergo protonation–deprotonation transitions around physiological *pH*. These features confer histidine with *pH*-sensitive behaviour that can be exploited for drug release in acidic tumour microenvironments (*pH* 5.9–6.9). Moreover, histidine is known to interact with overexpressed L-type amino acid transporters (LAT1) in glioblastoma cells, potentially improving tumour selectivity and uptake. Beyond targeting, histidine has been implicated in modulating cellular signalling, promoting autophagy, and enhancing cytotoxic responses in glioblastoma, all of which make it an ideal candidate for MOF functionalisation aimed at synergistic anticancer effects.

UiO-66(Zr)-NH_2 was synthesised via a solvothermal procedure, followed by post-synthetic functionalisation with protected histidine through amide bond formation, yielding UiO-66(Zr)-His with a functionalisation degree of approximately 62% of available amine sites. Both pristine and histidine-modified MOFs were impregnated with 5FU, and the resulting composites were extensively characterised. Infrared spectroscopy confirmed the successful incorporation of histidine through the disappearance of primary amine stretching bands and emergence of secondary amide features. Thermogravimetric analysis (TGA) allowed quantification of both histidine and 5FU loadings, revealing that UiO-66(Zr)-NH_2 achieved a higher encapsulation capacity (137.1 mg g^{-1}) compared to UiO-66(Zr)-His (45.0 mg g^{-1}). This difference highlights the trade-off between functionalisation and available pore volume, while simultaneously opening opportunities for controlled release through histidine-mediated interactions.

Powder X-ray diffraction (PXRD) confirmed that both UiO-66(Zr)-NH_2 and UiO-66(Zr)-His preserved their crystallinity after modification and drug loading, with lattice parameters consistent with the parent UiO-66 structure. Adsorption measurements using N_2 and Ar demonstrated typical microporous behaviour with S_{BET} values

around 930–1080 $m^2 g^{-1}$ for UiO-66(Zr)-NH_2 and 977–1045 $m^2 g^{-1}$ for UiO-66(Zr)-His. Upon 5FU loading, surface areas decreased significantly, consistent with pore occupation by drug molecules. Notably, interactions between nitrogen quadrupole moments and histidine residues yielded slightly higher BET values for the functionalised materials when measured with N_2, while Ar adsorption clarified that histidine was primarily anchored on external surfaces rather than within pores.

Drug release experiments were performed at 37 °C under three different *pH* conditions mimicking physiological (*pH* 7.4), tumoural (*pH* 5.5), and gastric (*pH* 2.0) environments. All systems exhibited an initial burst release within the first 30 minutes, corresponding to drug molecules loosely bound on particle surfaces. Subsequently, the release profiles diverged significantly depending on carrier type and *pH*. UiO-66(Zr)-NH_2 showed maximum releases of 68%, 71%, and 81% at *pH* 2.0, 5.5, and 7.4, respectively, whereas UiO-66(Zr)-His exhibited the highest release under mildly acidic conditions (88% at *pH* 5.5). This behaviour is attributed to the protonation state of the imidazole group, which optimally weakens drug–carrier interactions at *pH* close to its *pKa*, thus facilitating release in tumour-like environments. These findings confirm that histidine functionalisation enables fine-tuning of drug release towards pathologically relevant conditions, enhancing therapeutic selectivity.

Mathematical modelling of drug release kinetics further clarified the underlying mechanisms. The Weibull and Higuchi models provided the best fit ($R^2 > 0.9$), indicating diffusion-controlled release from the microporous frameworks. The superior fit of the Weibull model emphasises the complex interplay between diffusion, pore confinement, and surface interactions. Release rates were consistently higher for UiO-66(Zr)-His under acidic conditions, while being slower at neutral *pH*, further corroborating its *pH*-responsive behaviour. Compared to other reported carriers such as MIL-100, SBA-15, or polydopamine-coated MOFs, UiO-66(Zr)-His+5FU exhibited lower loading but far superior release efficiency (L/R ratio as low as 0.11 at *pH* 5.5), underscoring its potential as a highly efficient therapeutic platform.

The biological performance of the systems was investigated *in vitro* and *in vivo*. Cytocompatibility assays on dermal fibroblasts confirmed high biocompatibility of both UiO-66(Zr)-NH_2 and UiO-66(Zr)-His, with minimal toxicity at concentrations relevant for drug delivery. Uptake studies in U87MG glioblastoma cells using confocal fluorescence microscopy revealed efficient internalisation of both carriers, with histidine-modified nanoparticles showing enhanced colocalisation with lysosomes and partial crosstalk with mitochondria. This suggests that histidine not only improves cellular entry via LAT1 recognition but also facilitates trafficking into organelles critical for apoptotic signalling. Indeed, biochemical assays demonstrated increased lactate dehydrogenase (LDH) release and activation of caspase-3 in cells treated with UiO-66(Zr)-His+5FU compared to unmodified carriers. Western-Blot analyses further confirmed autophagy induction, providing a cytoprotective mechanism in healthy fibroblasts while simultaneously promoting cytotoxicity in tumour cells.

The enhanced therapeutic activity of UiO-66(Zr)-His+5FU was particularly evident in three-dimensional glioblastoma spheroid models, which more closely mimic *in vivo* tumour microenvironments (see *Figure 1*). Treatment with UiO-66(Zr)-His+5FU resulted in significant inhibition of spheroid growth and viability, demonstrating its superior efficacy compared to UiO-66(Zr)-NH_2+5FU and free drug controls. In addition, *in vivo* testing on the chorioallantoic membrane (CAM) model of Japanese quail embryos confirmed excellent biocompatibility, fluorescence-based bioimaging capability, and uniform biodistribution of nanoparticles within vascularised tissues. These findings highlight the theranostic potential of histidine-modified UiO-66(Zr), combining controlled drug release with intrinsic imaging properties for multimodal cancer therapy.

In conclusion, the histidine-modified UiO-66(Zr)-His developed in this study represents a highly promising nanocarrier for targeted brain tumour therapy. Compared to pristine UiO-66(Zr)-NH_2, the histidine functionalisation significantly alters drug loading and release behaviour, favouring efficient 5FU release under tumour-mimicking acidic conditions. The resulting nanoparticles exhibit high stability, excellent biocompatibility, efficient cellular uptake, lysosomal targeting, and enhanced cytotoxicity against glioblastoma cells in both 2D and 3D models. Moreover, the ability to visualise the carriers via fluorescence imaging and their favourable biodistribution *in vivo* open avenues for integrated theranostic applications. This work thus demonstrates that rational post-synthetic modification of MOFs with biologically relevant molecules such as histidine can substantially improve the therapeutic efficacy and selectivity of nanocarrier systems. Future research should address long-term pharmacokinetics, blood–brain barrier penetration, and combined therapeutic modalities, such as photodynamic therapy, to fully exploit the potential of UiO-66(Zr)-His for clinical translation in brain cancer treatment.

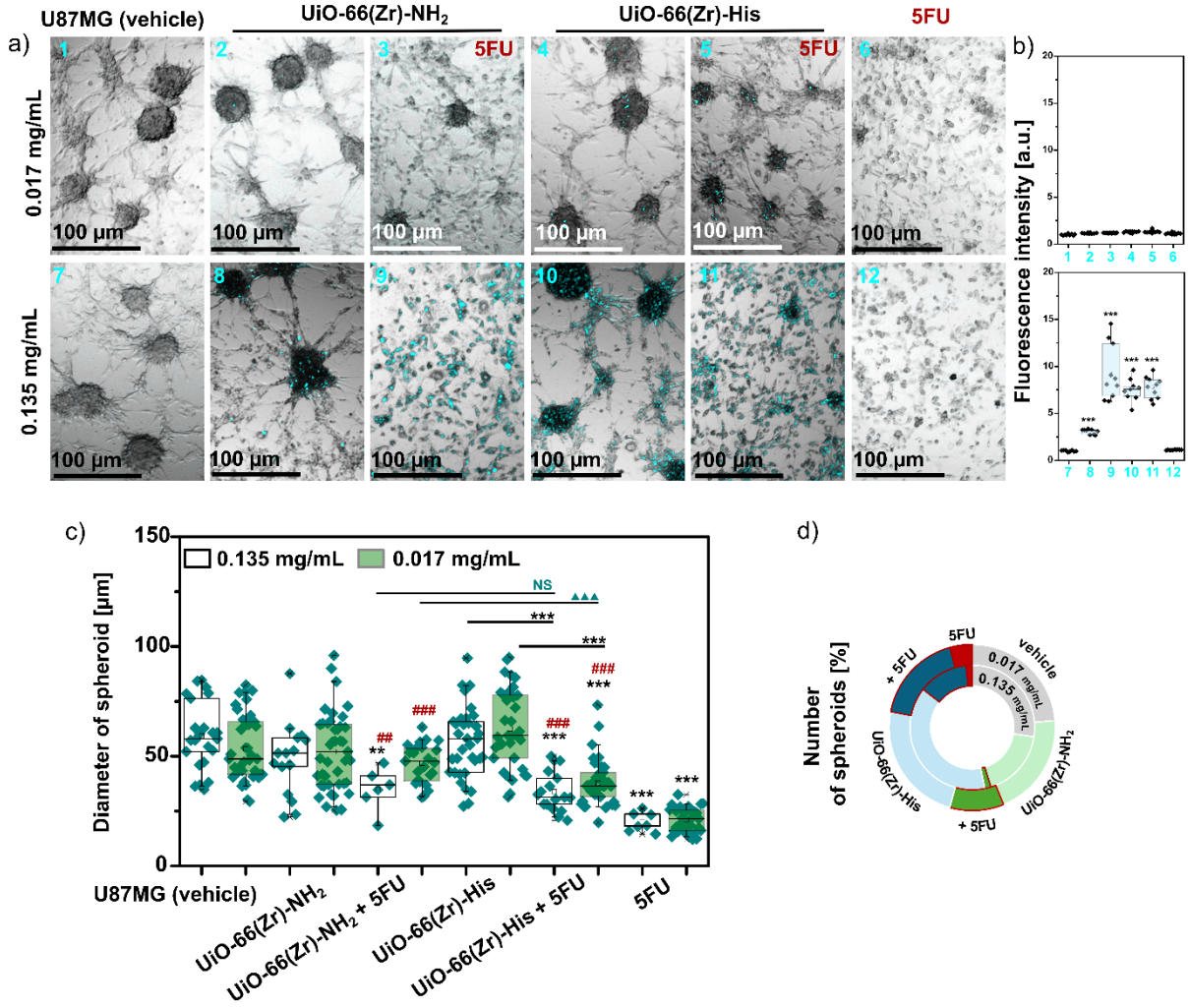

Figure 1 Inhibition of cancer spheroid formation. *a)* U87MG cells exposed to vehicle, nanoparticles and 5FU at different concentrations for 5 days. *b)* The fluorescence intensity of the nanoparticles (cyan) was recorded (treatments 1-10) and shown in box-plots (n = 10). *c)* Diameter of spheroids exposed to different treatments for 5 days ($n > 10$). An one-way ANOVA test was performed to determine significant differences between the samples and the control (vehicle): $^{**}p < 0.01$, $^{***}p < 0.001$, and 5FU-exposed cells: $^{\#\#}p < 0.01$, $^{\#\#\#}p < 0.001$. Blue triangles indicate the differences between exposure to His-modified and non-modified particles. *d)* Illustrative representation of the number of spheroids calculated for the different conditions.

Acknowledgements
This work was supported by APVV project no. SK-AT-23-0001 and by the EU NextGenerationEU through the Recovery and Resilience Plan for Slovakia under the project BCOrgFluorIDA No. 09I03-03-V04-00007.

Preliminary Study on Electrochemical Deposition of Hydroxyapatite on Ti-6Al-4V Substrates with Different 3D Patterns

I. Mojzisova[a,*], A Kemeny[b], B. Borbas[b], R. Orinakova[a]
[a] Department of Physical Chemistry, Faculty of Science, P. J. Šafárik University in Košice, Moyzesova 11, 041 54, Košice
[b] Department of Materials Science and Engineering, Faculty of Mechanical Engineering, Budapest University of Technology and Economics, Műegyetem Rkp. 3., H-1111, Budapest, Hungary
* ivana.mojzisova@student.upjs.sk

Introduction

Titanium alloys are the most frequently used materials in orthopaedics and dentistry due to their exceptional biocompatibility, chemical inertness, and favourable mechanical properties. Among them, the most used material in biomaterial applications is Ti-6Al-4V, which combines relatively low density with good biocompatibility. However, titanium-based prostheses still do not fully meet clinical requirements, particularly with respect to biological activity, as they do not allow interactions with surrounding bone tissue [1]. For the effective and successful performance of the long-term orthopaedic implants in the body, it is crucial to ensure appropriate interaction between the implant surface and osteogenic cells to achieve a stable fixation. The osteointegration of the implant is strongly influenced by its surface characteristics. Therefore, various surface modification strategies have been developed with the aim of increasing surface roughness and mimicking the natural bone structure. These approaches generally involve physical, chemical, or mechanical techniques [2].

One of the widely used physical techniques is additive manufacturing (AM), which provides an efficient and economical procedure to prepare porous structures with patient-specific geometries. An important advantage of AM is its ability to produce complex metallic implants with customised shape, sizes, and designs based on medical imaging data from patient injury analysis [3]. Porous structures produced by AM facilitate bone ingrowth and vascularisation, enhancing osseointegration, improving implant fixation, and reducing stress shielding around the implant [3, 4].

Chemical techniques include surface modification with various coatings. Among them, hydroxyapatite (HAp) coatings have received significant attention because HAp is the main mineral component of human bone and exhibits excellent osteoconductive and osteointegrative properties. Hydroxyapatite promotes direct chemical bonding with host bone, which improves biological performance. Furthermore, the long-term use of Ti-6Al-4V implants raises concerns about the release of potentially harmful aluminium and vanadium ions into surrounding body fluids, which can induce systemic toxicity. The application of a ceramic coating such as HAp on the implant surface can mitigate these risks.

The purpose of this study was to electrochemically deposit a hydroxyapatite coating on Ti-6Al-4V substrates fabricated by additive manufacturing. The work focused on initial attempts to achieve coating formation on the samples with different surface architectures and relative densities of the lattice structure. Specifically, the coating was deposited on the (i) planar Ti-6Al-4V samples with a dense surface, (ii) gyroid lattice structures, and (iii) diamond lattice structures with different densities.

Experiment

Prior to electrochemical deposition, the Ti-6Al-4V substrates were ultrasonically cleaned for 10 min in acetone and subsequently for 10 min in 96 % ethanol. The cleaned samples were dried at 60 °C for 10 min. The electrochemical deposition of ceramic coating was carried out in galvanostatic mode using a three-electrode setup, where the sample served as the working electrode, a Pt sheet as the counter electrode, and Ag/AgCl (3 M KCl) as the reference electrode. The electrolyte consisted of $4.2 \cdot 10^{-2}$ mol/dm^3 $Ca(NO_3)_2 \cdot 4\ H_2O$ and $2.5 \cdot 10^{-2}$ mol/dm^3 $NH_4H_2PO_4$, providing a Ca/P molar ratio of 1.67, which corresponds to stoichiometric hydroxyapatite. To promote coating formation, H_2O_2 was added to the electrolyte in a final concentration of approximately 12 mM. The deposition was performed at a constant current 5mA and temperature of 65°C. The deposition was carried out for 20 minutes. After the electrochemical deposition, the samples were subjected to thermal alkali treatment in 1 M NaOH at 60 °C for 60 min. This treatment aimed to convert the initially deposited brushite ($CaHPO_4 \cdot 2\ H_2O$), which preferentially precipitates under the given conditions, into hydroxyapatite, which is thermodynamically more stable in alkaline environments. After the alkali treatment, the substrates were thoroughly rinsed with distilled water and dried at 60 °C for 60 min. The surface morphology of coated and uncoated samples was examined using optical microscopy to assess the distribution and continuity of the coating. To evaluate deposition efficiency, samples of planar and diamond lattice architectures were weighed before and after electrodeposition, and the coating mass gain was analysed with respect to substrate structure and density.

Results and discussion

Figure 1 shows the planar and cellular Ti-6Al-4V samples before and after electrochemical deposition of the hydroxyapatite. Before deposition, the surface of the samples exhibited a uniformly roughened morphology with metallic lustre. After the deposition process, a white crystalline coating was observed that was evenly distributed and covered the entire surface of the samples. Only a small number of pores were present within the coating, most likely resulting from hydrogen gas evolution during the electrochemical deposition. The relatively low pores density can be attributed to the addition of H_2O_2 to the electrolyte. Hydrogen peroxide promotes coating formation by generating OH^- radicals during H_2O_2 electrolysis, thus enhancing the stability of apatite phases in alkaline environments [5].

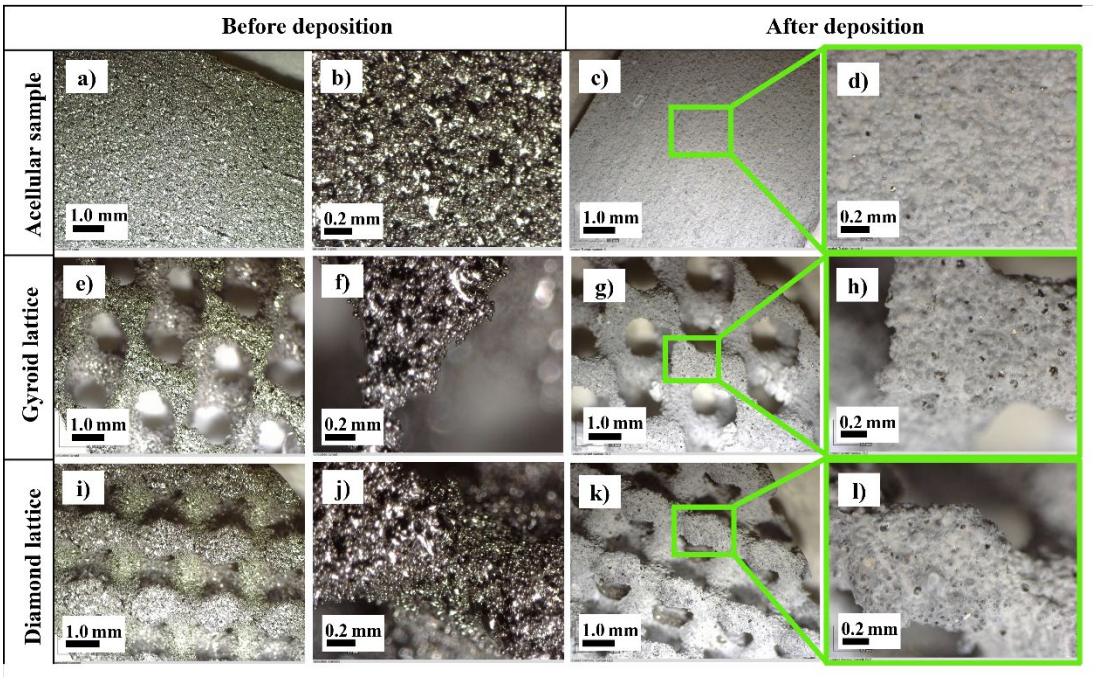

Figure 1 Optical microscopy images of acellular planar samples (*a, b, c, d*), gyroid lattice samples (*e, f, g, h*) and diamond lattice samples (*i, j, k, l*) before and after electrochemical deposition of hydroxyapatite.

The deposited hydroxyapatite mass depended on the substrate geometry and relative density (*Table 1*). The diamond lattice with low density showed the highest coating mass (5.33 mg), followed by the planar sample (4.42 mg), while the high-density lattice exhibited the lowest value (3.83 mg). The increased coating on the low-density lattice can be explained by its open architecture, which provides greater surface accessibility for electrolyte penetration and nucleation. In contrast, the compact geometry of the high-density lattice restricts electrolyte access and reduces the effective deposition area. Additionally, the accumulation of gas bubbles in pores and uneven current distribution may decrease the coating efficiency in the high-density samples.

Table 1 Average weights of planar samples (P) and diamond lattice samples with low (DL) and high density (DH) measured before deposition (m_0) and after hydroxyapatite coating (m), together with the calculated coating mass ($m_{coating}$).

Sample	m_0 [g]	m [g]	$m_{coating}$ [mg]
P	1.1512 ± 0.095	1.1556 ± 0.095	**4.42 ± 0.41**
DL	0.6805 ± 0.226	0.6859 ± 0.227	**5.33 ± 0.31**
DH	1.7191 ± 0.128	1.7229 ± 0.129	**3.83 ± 0.50**

The results indicate that porous materials with a relative lower density could more effectively support osteointegration due to the higher amount of deposited hydroxyapatite and the open porous structure favourable for cell penetration [6]. However, it is crucial to evaluate the compromise between biological function and mechanical stability during the final design of orthopaedic implants.

Acknowledgements

This work was supported by the Slovak Research and Development Agency under the projects APVV-24-0033 and APVV-20-0278. The work was supported by the EKÖP-25-2-BME-78 Program of the Ministry for Culture and Innovation from the source of the National Research, Development and Innovation Fund.

References

[1] A. Jain and V. Bajpai, "Alteration in Ti6Al4V implant surface properties with micro textures density," *Surface Engineering*, vol. 38, no. 2, pp. 174–182, 2022, doi: 10.1080/02670844.2022.2058163.
[2] Y. Liu, B. Rath, M. Tingart, and J. Eschweiler, "Role of implants surface modification in osseointegration: A systematic review," Mar. 01, 2020, *John Wiley and Sons Inc.* doi: 10.1002/jbm.a.36829.
[3] M. Javaid and A. Haleem, "Additive manufacturing applications in orthopaedics: A review," *J Clin Orthop Trauma*, vol. 9, no. 3, pp. 202–206, Jul. 2018, doi: 10.1016/J.JCOT.2018.04.008.
[4] J. Sharath Kumar, R. Kumar, and R. Verma, "Surface Modification Aspects for Improving Biomedical Properties in Implants: A Review," Feb. 01, 2024, *Springer*. doi: 10.1007/s40195-023-01631-7.
[5] L. Ling *et al.*, "Effect of hydrogen peroxide concentration on the nanostructure of hydroxyapatite coatings via ultrasonic-assisted electrodeposition," *Mater Lett*, vol. 261, p. 126989, Feb. 2020, doi: 10.1016/J.MATLET.2019.126989.
[6] T. Zhang, X. Zhang, M. Mao, J. Li, T. Wei, and H. Sun, "Chitosan/hydroxyapatite composite coatings on porous Ti6Al4V titanium implants: In vitro and in vivo studies," *J Periodontal Implant Sci*, vol. 50, 2020, doi: 10.5051/jpis.1905680284.

Graphite Functionalization of Glass Fiber Separator to Enhance Stability of Li–S Batteries

V. Niscakova[a,*], A. Strakova Fedorkova[a], J. Lescinsky[a]
[a] Pavol Jozef Safarik University of Kosice, Department of Physical chemistry, Šrobárová 2, 040 01, Kosice
* veronika.niscakova@upjs.sk

Introduction

Lithium-sulfur (Li-S) batteries are considered one of the most promising technologies for future energy storage systems due to their high theoretical specific capacity of 1675 mAh g^{-1} and energy density of approximately 2600 W kg^{-1} [1, 2]. Additionally, their use of abundant and low-cost sulfur makes them a highly attractive alternative to traditional lithium-ion batteries [3].

However, the widespread commercialization of Li-S batteries is hindered by several major challenges. The most significant issue is the "shuttle effect," in which soluble lithium polysulfides (LiPSs) migrate between the cathode and anode, leading to rapid capacity degradation and a shortened cycle life [2, 4, 5]. Other critical problems include the low electrical conductivity of sulfur, lithium dendrite growth, and poor thermal stability [1, 5].

To overcome these obstacles, research has increasingly focused on modifying the separator as an effective strategy to enhance the electrochemical performance of Li-S batteries [6]. To address the limitations, the use of carbon coatings is being explored for the development of multifunctional separators [1, 3, 4]. These coatings act as a physical barrier to polysulfide migration and dendrite growth while simultaneously improving electrical conductivity and promoting the efficient capture and catalysis of polysulfides [2, 4, 6]. Additionally, materials that increase thermal stability and overall battery safety are examined [3].

The results of this study demonstrate that a well-designed modified separator is crucial for achieving high performance and long-term stability in Li-S batteries.

Experimental part

Graphite-modified glass fiber separators (GF_Gr) were fabricated by coating a slurry composed of poly(vinylidene fluoride) (PVDF) binder, Super P, and graphite conductive additive (60 wt.% of the coating composition) dispersed in N-methyl-2-pyrrolidone (NMP). The slurry was applied onto commercial glass fiber (GF) separators using the doctor-blade technique to form an uniform coating layer. The coated separators were subsequently dried under ambient conditions for 24 h to remove residual solvent and consolidate the coating structure.

Electrodes for electrochemical testing were prepared from a mixture containing 60 wt.% sulfur, 30 wt.% carbon Super P, and 10 wt.% PVDF binder. The active material slurry was homogenized in NMP and cast onto aluminum foil current collectors, followed by drying to eliminate the solvent. Electrode disks were then punched from the coated foil.

Electrochemical measurements were performed in three-electrode El-cells, employing the sulfur-based electrodes as working electrodes (WE) and lithium metal as both counter (CE) and reference electrode (RE). The graphite-modified separator (GF_Gr) was positioned between the working electrode and lithium metal. Cyclic voltammetry (CV) and galvanostatic charge–discharge cycling were carried out within a potential window of 1.8–2.8 V.

Results and Discussion

The CV profiles (*Figure 1 A*) exhibited two characteristic cathodic peaks, associated with the multistep reduction of sulfur: the first peak at approximately 2.35 V corresponded to the reduction of elemental sulfur (S_8) to soluble polysulfides, while the second peak near 2.0 V was attributed to the further reduction of polysulfides to Li_2S_2 and Li_2S. Two corresponding anodic peaks were observed upon oxidation, reflecting the reversible conversion of polysulfides back to elemental sulfur. These electrochemical features confirm the typical redox mechanism of Li–S batteries. The positions and intensities of the peaks remain consistent across scan rates, indicating good electrochemical reversibility of the redox reactions. At a current rate of 0.1 C, the sulfur electrode with the GF_Gr separator delivered an initial discharge capacity of ~1416 mAh g^{-1}, representing 84% of the theoretical specific capacity of sulfur (1675 mAh g^{-1}). In contrast to the graphite-modified separator (GF_Gr), the unmodified glass fiber separator (GF) exhibited an initial discharge capacity of approximately 919 mAh g^{-1}.

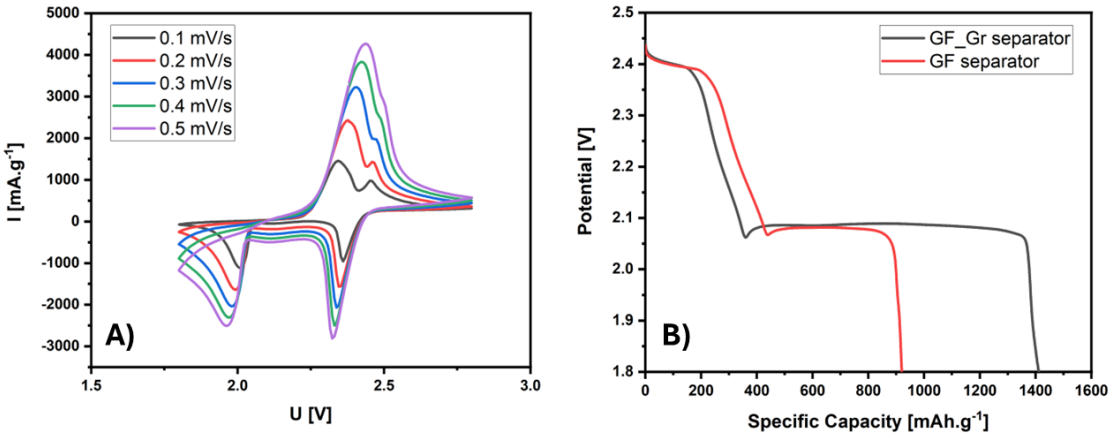

Figure 1 A) Cyclic voltammograms at different scane rates (0.1; 0.2; 0.3; 0.4 and 0.5 mV/s) and *B)* discharge curves of modified and not modified GF separator at 0.1 C.

These findings highlight the beneficial role of the graphite-modified glass fiber separator in improving sulfur utilization and overall electrochemical performance. The approach provides a straightforward and cost-effective strategy for separator modification, supporting the development of high-performance lithium–sulfur batteries.

Acknowledgements
Funded by the Slovak Research and Development Agency under the Contract no. DS-FR-24-0004, by the project KEGA 002UPJŠ-4/2024 and EU NextGenerationEU through the Recovery and Resilience Plan for Slovakia under the project SUNFLOWERS No. 09I02-03-V01-00022.

References
[1] Z. Huang, W. Sun, Z. Sun, R. Ding, and X. Wang, "Graphene-Based Materials for the Separator Functionalization of Lithium-Ion/Metal/Sulfur Batteries," Materials (Basel)., vol. 16, no. 12, 2023, doi: 10.3390/ma16124449.
[2] Y. Li et al., "Glass fiber separator coated by porous carbon nanofiber derived from immiscible PAN/PMMA for high-performance lithium-sulfur batteries," J. Memb. Sci., vol. 552, no. October 2017, pp. 31–42, 2018, doi: 10.1016/j.memsci.2018.01.062.
[3] J. Wang, M. Chen, W. Qin, and M. Zhou, "A novel flame-resistant separator for high performance lithium-sulfur batteries," Mater. Adv., vol. 3, no. 16, pp. 6628–6635, 2022, doi: 10.1039/d2ma00576j.
[4] S. A. Abbas et al., "Modified Separators with Ultrathin Graphite Coating Simultaneously Mitigate the Issues of Metal Dendrites and Lithium Polysulfides to Provide Stable Lithium-Sulfur Batteries," ACS Sustain. Chem. Eng., vol. 7, no. 19, pp. 16604–16611, 2019, doi: 10.1021/acssuschemeng.9b03751.
[5] S. Ponnada et al., "Insight into Lithium-Sulfur Batteries with Novel Modified Separators: Recent Progress and Perspectives," Energy and Fuels, vol. 35, no. 14, pp. 11089–11117, 2021, doi: 10.1021/acs.energyfuels.1c01509.
[6] B. Wei, Y. Xia, S. Chen, and H. L. Wang, "Modified Separator with Nitrogen-doped High-graphitized Carbon for Lithium-sulfur Batteries," Electroanalysis, vol. 34, no. 9, pp. 1472–1477, 2022, doi: 10.1002/elan.202200003.

9th International Conference on Novel Materials Fundamentals and Applications
High Tatras, 12.10.-15.10.2025

Regulatory Frameworks for Battery Recycling

A. Orinak[a,*]
[a] Department of Commercial Law and Business Law, Faculty of Law, P.J. Safarik University, Kováčska 26, 040 75 Košice, Slovakia
* andrej.orinak@student.upjs.sk

The increasing need to combat climate change has driven a worldwide transition towards renewable energy sources and electrification, especially within the transportation sector [1]. Electric vehicles (EVs) have emerged as a crucial solution for reducing greenhouse gas emissions and paving the way for a sustainable future [2].
The European Union (EU) has introduced a comprehensive regulatory framework for batteries with Regulation (EU) 2023/1542, which replaces Directive 2006/66/EC. This new regulation covers the entire life cycle of batteries, from material extraction and production to use and recycling, with the main aim of minimising environmental impact and promoting a sustainable battery industry. Key provisions include strict restrictions on substances, mandatory collection and recycling targets for Member States and extended producer responsibility. The framework also introduces requirements for the carbon footprint of batteries, sets minimum levels of recycled content for new batteries and mandates the use of a 'battery passport' for certain types. The regulation, which entered into force on 17 August 2023, is a key part of the EU's wider efforts to promote a circular economy, reduce dependence on imported raw materials and support the transition to a low-carbon economy. In Slovakia, the regulation is directly applicable without the need for national transposition and is based on the country's existing waste management framework.
In this new regulation, the European Commission (EC) has introduced recycling as a key element for the development of the electric vehicle (EV) sector, and particularly the battery sector [1]. It is intended to be a central part of the European Union's industrial strategy, which encompasses economic, social and environmental objectives. One of its main initiatives is the introduction of minimum thresholds for the recovery of recycled materials in new batteries. The feasibility of the proposed recycling thresholds is most sensitive to the lifetime of the batteries [3]. This suggests a potential conflict between the recycling objectives of the regulation and the desire to extend the lifetime of batteries through second-hand applications. However, the feasibility of the thresholds is not very sensitive to changes in material intensity, recycling efficiency or the pace of demand for electric vehicles [3].
Regulatory frameworks differ substantially across regions, influenced by economic objectives, technological capacities, and existing legal structures.
China has developed a comprehensive regulatory framework for battery recycling [4], moving from fragmented early efforts to a robust system [5]. Key milestones include the "Technical Guidelines for Pollution Prevention and Control of Waste Batteries" in 2003, which established the principle of Extended Producer Responsibility (EPR) and required manufacturers and sellers to set up recycling facilities. Subsequent five-year plans and laws further reinforced the EPR system and promoted the efficient use of resources.
Since 2015, the focus has shifted to practical implementation. This phase introduced specialized policies, pilot projects, and a battery coding system for traceability. The "Interim Measures for the Management of New Energy Vehicle Power Battery Recycling" in 2018 made EV manufacturers primarily responsible for recycling. The government has also accelerated policy development to create a comprehensive framework, with a 2023 draft regulation expected to be China's first legally binding law for battery recycling. This law reinforces EPR and establishes a full lifecycle management system for batteries. Despite these advances, challenges remain, including fragmented regulations, low public awareness, and unclear accountability.
The EU is a leader in battery recycling regulation, aiming to create a circular economy. The process began with directives like the "Battery Directive 91/157/EEC" and the "End-of-Life Vehicle Directive 2000/53/EC," which introduced EPR. The new "Regulation (EU) 2023/1542" is a binding law that replaces earlier directives. It sets ambitious targets for battery collection and recycling efficiency, as well as minimum recovery rates for materials like lithium, cobalt, and nickel.
The regulation also mandates the use of recycled content in new batteries, introduces digital battery passports for transparency and traceability, and requires manufacturers to report their carbon footprints. This framework is designed to reduce the EU's reliance on raw materials and meet its climate goals [6].
The US regulatory landscape for battery recycling is fragmented, with no single federal law specifically for EV batteries [7]. Existing laws like the "Resource Conservation and Recovery Act of 1976" and the "Mercury-Containing and Rechargeable Battery Management Act (1996)" provide a foundation but do not directly address the unique challenges of lithium-ion batteries.
More recent federal efforts have focused on funding and research. The "Infrastructure Investment and Jobs Act (2021)" and the "Inflation Reduction Act (2022)" provide grants and tax incentives to support battery recycling and the development of a domestic supply chain for critical minerals. State-level policies vary widely, with

California adopting an EPR framework and other states exploring different approaches [8]. The absence of a unified national policy remains a significant challenge to the scalability and efficiency of recycling infrastructure. Other countries, such as Japan and South Korea, are also actively developing battery recycling systems [1]. Japan's framework is built on the principle of EPR, with laws like the "Act on the Promotion of Effective Utilization of Resources" (1991) and the "Law for the Recycling of End-of-Life Vehicles" (2001). While it has a clear system for consumer engagement and hazardous substance management, it still lacks specific, comprehensive regulations for EV battery recycling. The need for consensus among various ministries and advisory councils has contributed to delays in establishing targeted laws.

Although many countries are introducing regulations, they are often ineffective and fragmented across regions [4]. There is a need for a single global framework to ensure sustainable and efficient battery recycling, and the lack of standardized regulations complicates compliance and hinders international cooperation. Low public awareness and economic/security challenges are significant barriers to the development of a robust and sustainable recycling ecosystem.

Acknowledgements

This work was funded by the EU NextGenerationEU through the Recovery and Resilience Plan for Slovakia under the project SUNFLOWERS No. 09I02-03-V01-00022.

References

[1] D. Su, Y. Mei, T. Liu, and K. Amine, “Global Regulations for Sustainable Battery Recycling: Challenges and Opportunities”, Sustainability, vol. 17, no. 7, p. 3045, 2025, doi: 10.3390/su1707304523R1542.

[2] M. Muratori, M. Alexander, D. Arent, M. Bazilian, P. Cazzola, E.M. Dede, J. Farrell, C. Gearhart, D. Greene, and A. Jenn, “The rise of electric vehicles—2020 status and future expectations”, Prog. Energy, vol. 3, no. 2, p. 022002, 2021, doi: 10.1088/2516-1083/abe0ad.

[3] Q. Hoarau, and E. Lorang, “An assessment of the European regulation on battery recycling for electric vehicles”, Energy Policy, vol. 162, no. March, p. 112770, 2022, doi: 10.1016/j.enpol.2021.112770.

[4] S. Sun, C. Jin, W. He, G. Li, H. Zhu, and J. Huang, “Management status of waste lithium-ion batteries in China and a complete closed-circuit recycling process”, Sci. Total Environ., vol. 776, no. 1 July, p. 145913, 2021, doi: 10.1016/j.scitotenv.2021.145913.

[5] J. Li, Z. Wang, H. Li, and J. Jiao, “Which policy can effectively promote the formal recycling of power batteries in China?”, Energy, vol. 299, no. 15 July, p. 131445, 2024, doi: 10.1016/j.energy.2024.131445.

[6] H.E. Melin, M.A. Rajaeifar, A.Y. Ku, A. Kendall, G. Harper, and O. Heidrich, “Global implications of the EU battery regulation”, Science, vol. 373, no. 6553, pp. 384–387, 2021, doi: 10.1126/science.abh1416.

[7] J.M. Turner, and L.M. Nugent, “Charging up battery recycling policies: Extended producer responsibility for single-use batteries in the European union, Canada, and the United States”, J. Ind. Ecol., vol. 20, no. 5, pp. 1148–1158, 2016, doi: 10.1111/jiec.12351.

[8] A. Lovelady, and D.W. Owens, “2019 North Carolina Legislation Related to Planning and Development Regulation. Plan”, Zoning Law Bull., vol. 2019, no. 28, pp. 1–29, 2019.

Simple Sensors for Gentamicin Detection

R. Orinakova[a,*], J. Demeterova[a], I. Sisolakova[a], J. Shepa[a]
[a] Department of Physical Chemistry, Pavol Jozef Šafárik University in Košice, Moyzesova 11, 040 01 Košice, Slovak Republic
* orinakova.renata@upjs.sk

Introduction

Antibiotics represent one of humanity's foremost medical achievements, functioning as secondary metabolites derived from various microorganisms and biological sources to interfere with the development of living cells. While indispensable for treating diseases, alleviating pain, and saving lives, the widespread use of these compounds carries significant dual consequences. In food production, antibiotic use enhances animal and plant morphology and growth cycles, yet their overuse compromises nutritional quality and palatability [1]. Crucially, the long-term ingestion of food containing antibiotic residues leads to bioaccumulation in human tissues, increasing the risk of tissue and organ diseases, and potentially contributing to oncogenesis. Furthermore, the burgeoning annual consumption of the major antibiotic groups—cephalosporins, macrolides, quinolones, and penicillins—is the primary driver for the alarming global spread of antimicrobial resistance (AMR), necessitating stringent monitoring in pharmaceutical dosage forms, food products, and, critically, drinking water supplies [2]. Among them gentamicin (*Figure 1*) is a potent, broad-spectrum aminoglycoside antibiotic primarily administered for the treatment of severe systemic infections, particularly those caused by susceptible Gram-negative bacteria, by irreversibly binding to the 30S ribosomal subunit and inhibiting microbial protein synthesis [3], [4].

To effectively address the imperative for continuous, highly sensitive monitoring of antibiotic levels, this paper investigates the application of electrochemical sensors as an interdisciplinary field. Specifically, electrochemical biosensors are highlighted for their distinct advantages, including strong specificity, fast response, low sample consumption, ease of portability, and suitability for continuous on-line monitoring, thereby combining the high selectivity of biometric systems with the high sensitivity of electrochemical transducers [1].

To overcome the inherent limitations of traditional electrode materials and dramatically improve analytical performance, the integration of nanomaterials is explored. Owing to their unique physical and chemical properties, nanomaterials are exceptionally effective "functional" transducers within biosensing systems. Among these, Carbon Nanotubes (CNTs) are particularly significant. CNTs provide robust scaffolds for efficient biomolecule immobilization and possess a unique combination of electrical and physicochemical properties, making them highly suitable for antibiotic detection. Functionalization strategies further enhance CNTs' potential by improving properties like solubility, making functionalized CNTs (CNT-composites) a prerequisite for advanced nano-device fabrication. Numerous studies confirm that electrodes nanostructured with CNT-composites lead to a remarkable enhancement in electrochemical performance, achieving wider detection ranges and significantly lower limits of detection (LODs) for commonly used antibiotics [5].

The fabrication of electrochemical sensors, particularly those optimized through the incorporation of nanomaterials like CNTs, offers a high-automation, cost-effective, and highly selective analytical methodology. These advancements are pivotal in ensuring consumer safety through vigilant antibiotic residue monitoring and in global efforts to mitigate the critical public health threat posed by antimicrobial resistance.

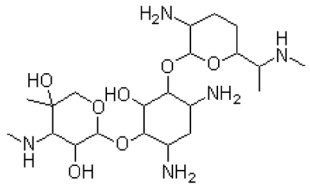

Figure 1 Structure of gentamicin [4].

Experimental part

Multi-walled carbon nanotubes (MWCNTs) were used to prepare a suspension for electrode modification. Specifically, 0.0050 g of MWCNTs were dispersed in 1.25 mL of a Nafion–ethanol solution and homogenised by ultrasonication for 45 min. Subsequently, 0.75 µL of the suspension was drop-cast onto the working surface of a screen-printed carbon electrode (SPCE) and dried under ambient conditions. Electrochemical measurements were performed in phosphate-buffered saline (PBS, pH 7.4) with successive additions of gentamicin, using cyclic voltammetry (CV) as the detection technique within the potential window from 0.8 V to 1.5 V, with scan rate 100 mV/s.

Results and discussion

Figure 2 provides a comparative electrochemical characterization of gentamicin detection using two distinct configurations: an unmodified SPCE (*Figure 2 A*) and modified SPCE (MWCNT/SPCE, *Figure 2 B*). The data is presented as cyclic voltammograms (CVs) obtained across gentamicin concentrations ranging from 200µM to 1000µM, with corresponding calibration curves shown in the respective insets.

Figure 2 A illustrates the CVs recorded at the bare SPCE, which exhibits an irreversible oxidation peak in the positive potential region, typically observed between 1.3V. The inset calibration plot, detailing the oxidation peak current (*Ip*) versus concentration (*c*), suggests a limited linear range and moderate sensitivity, indicative of the sluggish electron transfer kinetics inherent to the unmodified carbon surface.

In distinct contrast, *Figure 2 B* displays the CV response of the MWCNT/SPCE under identical experimental conditions. The MWCNT modification resulted in a dramatic and pronounced amplification of the electrochemical signal. The maximum current observed in this setup reaches approximately 1.0 µA at the highest concentration, representing a multiple-fold increase in signal intensity compared to the bare SPCE. This substantial enhancement is primarily attributed to the MWCNTs' superior conductivity, high effective surface area, and potent electrocatalytic properties, which collectively facilitate faster electron transfer kinetics and increased analyte accumulation at the electrode interface. Consequently, the inset calibration curve in *Figure 2 B* exhibits a significantly improved linearity and a steeper slope, confirming that the MWCNT incorporation effectively increases the analytical sensitivity and expands the dynamic detection range for the quantitative determination of gentamicin. The sensitivity of modified electrode was 0.88 µA/µM and limit of detection 220 µM.

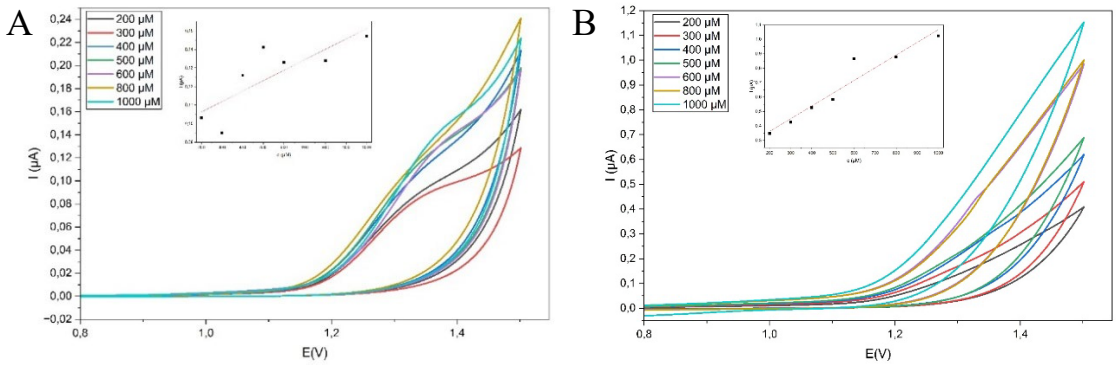

Figure 2 Cyclic voltammograms for SPCE (*A*) and MWCNTs/SPCE (*B*) samples for various concentrations of gentamicin from 200 µM to 1 mM. Insets: Calibration curve.

These parameters made the proposed sensor as a suitable adept for gentamicin detection in real samples.

Acknowledgements

This work was funded by the EU NextGenerationEU through the Recovery and Resilience Plan of the Slovak Republic under project no. 09-I05-03-V02-00047.

References

[1] Y. Pang, “Recent development and progress of electrochemical sensors for antibiotic detection,” 2020, *Electrochemical Science Group*. doi: 10.20964/2020.06.40.

[2] O. I. Guliy and L. A. Dykman, “Prospects for the use of nanozyme-based electrochemical and colorimetric sensors for antibiotic detection,” May 01, 2025, *Elsevier B.V.* doi: 10.1016/j.talanta.2025.127524.

[3] I. T. Somé *et al.*, “Validation of gentamicin congeners using HPLC with electrochemical detection: Comparison with fluorimetric detection,” *Comptes Rendus Chimie*, vol. 7, no. 10–11, pp. 1087–1093, Oct. 2004, doi: 10.1016/j.crci.2003.12.037.

[4] S. Naveed *et al.*, “Manufacturing of new formulation of gentamicin capsule,” 2014. [Online]. Available: https://www.irjps.in

[5] A. Joshi and K. H. Kim, “Recent advances in nanomaterial-based electrochemical detection of antibiotics: Challenges and future perspectives,” Apr. 01, 2020, *Elsevier Ltd*. doi: 10.1016/j.bios.2020.112046.

Plasma-Modified PANI/PLA Composites as Biodegradable and Flexible Platforms for Biosensor applications

K. Ozaltin[a], I. Sisolakova[b], J. Shepa[b], R. Orinakova[a,b], P. Saha[a,*],

[a] Centre of Polymer Systems, University Institute, Tomas Bata University in Zlín, Třída Tomáše Bati 5678, 76001 Zlín, Czech Republic

[b] Department of Physical Chemistry, Faculty of Science, P.J. Šafarik University in Košice, Moyzesova 11, 041 54, Košice

* saha@utb.cz

Abstract

Conductive polymers (CPs) have attracted significant attention in biosensing applications owing to their intrinsic conductivity and structural tunability, therefore often used in sensors for glucose monitoringt in medical diagnostics and wearable technologies [1,2]. Yet, their sensing performance is frequently limited by surface inertness and the scarcity of functional groups that facilitate biomolecule immobilization and electron transfer. To address this limitation, surface modification through plasma treatment provides an effective strategy, as it introduces hydroxyl (–OH) functionalities that enhance hydrophilicity and create active sites for bio-interfacing. In parallel with this approach, the mechanical rigidity and non-degradable nature of polyaniline (PANI) restrict its practical deployment in flexible sensor platforms. To overcome these drawbacks, we incorporated poly(lactic acid) (PLA) into PANI matrices, yielding composite films that retain conductivity while gaining enhanced ductility and controlled degradability under physiological conditions. The synergistic effect of plasma-induced hydroxylation and PLA blending resulted in improved surface wettability, flexibility, and biodegradability, collectively advancing the suitability of the material for wearable and transient glucose biosensors. This strategy complements existing surface engineering methods and broadens the design space for next-generation conductive polymer-based sensing platforms.

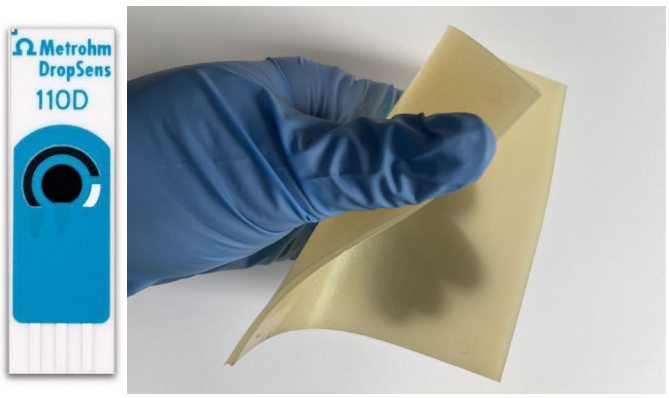

Figure 1 The sensor and flexible-degradable polymeric substrate.

Acknowledgements

This research was sponsored by the NATO Science for Peace and Security Programme under grant id. G6106.

References

[1] I. Šišolaková, R. Gorejová, F. Chovancová, J. Shepa, F. A. Ngwabebhoh, A. S. Fedorková, P. Sáha, R. Oriňaková, " Polymer-based Electrochemical Sensor: Fast, Accurate, and Simple Insulin Diagnostics Tool," Electrocatalysis., Apr. 2023, doi.org/10.1007/s12678-023-00827-w.

[2] J. Hovancová, I. Šišoláková, R. Oriňaková, and A. Oriňak, "Nanomaterial-based electrochemical sensors for detection of glucose and insulin," Journal of Solid State Electrochemistry, vol. 21, no. 8, pp. 2147–2166, 2017, doi: 10.1007/s10008-017-3544-0.

Surface Engineering of Polymer Films by Plasma Treatment for Improved Biosensing Applications

K. Ozaltin[a,*], I. Sisolakova[b], J. Shepa[b], R. Orinakova[a,b], P. Saha[a]
[a] Centre of Polymer Systems, University Institute, Tomas Bata University in Zlín, Třída Tomáše Bati 5678, 76001 Zlín, Czech Republic
[b] Department of Physical Chemistry, Faculty of Science, P.J. Šafarik University in Košice, Moyzesova 11, 041 54, Košice
* ozaltin@utb.cz

Abstract
Conductive polymers (CPs) have emerged as highly promising materials for electrochemical due to their tunable electrical properties and ability to undergo doping processes in response to analyte interactions [1]. Their intrinsic conductivity combined with structural versatility allows the development of sensitive, selective, and flexible sensor platforms. Among various applications, CP-based sensors for glucose monitoring have gained significant interest in medical diagnostics and wearable technologies [2]. However, the sensing performance of CPs is often limited by surface inertness and insufficient functional groups that facilitate biomolecule attachment or electron transfer.
To overcome these limitations, we report a surface modification strategy involving plasma treatment to introduce hydroxyl (-OH) functionalities onto the polymer surface, thereby enhancing hydrophilicity and providing active sites for further functionalization or direct analyte interaction. In this study, polyaniline (PANI) films were subjected to air plasma treatment under controlled conditions of 50W in vacuum used DC plasma source. The treated surfaces were characterized by surface energy revealed a significant decrease in surface hydrophobicity, indicating enhanced wettability post-treatment, increased surface area and functional –OH groups.
The findings suggest that plasma-induced hydroxylation may serve as a facile and effective method to augment the sensing properties of CP-based glucose sensors, and can be generalized for other biosensing platforms. This approach aligns with recent advancements in surface engineering of polymeric materials to enhance their biointerfacing capabilities [3][4].

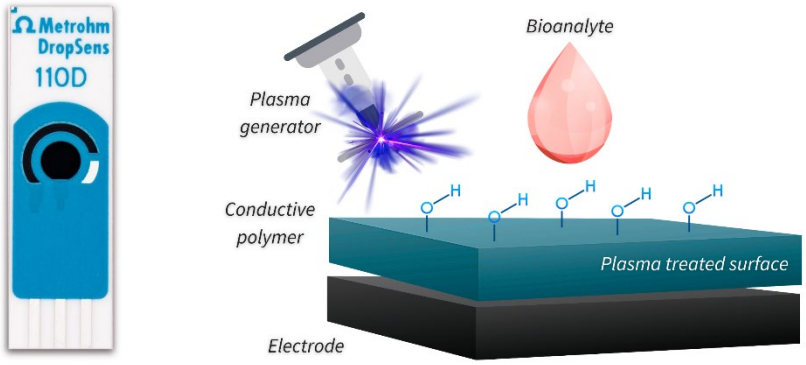

Figure 1 Schematic diagram of the plasma process on the polymeric substrate of the sensor.

Acknowledgements
This research was sponsored by the NATO Science for Peace and Security Programme under grant id. G6106.

References
[1] I. Šišolaková, R. Gorejová, F. Chovancová, J. Shepa, F. A. Ngwabebhoh, A. S. Fedorková, P. Sáha, R. Oriňaková, " Polymer-based Electrochemical Sensor: Fast, Accurate, and Simple Insulin Diagnostics Tool," Electrocatalysis., Apr. 2023, doi.org/10.1007/s12678-023-00827-w.
[2] J. Hovancová, I. Šišoláková, R. Oriňaková, and A. Oriňak, "Nanomaterial-based electrochemical sensors for detection of glucose and insulin," Journal of Solid State Electrochemistry, vol. 21, no. 8, pp. 2147–2166, 2017, doi: 10.1007/s10008-017-3544-0.
[3] S. Madhu, S. Ramasamy and J. Choi, "Recent Developments in Electrochemical Sensors for the Detection of Antibiotic-Resistant Bacteria," Pharmaceuticals., vol. 15, Nov. 2022, doi.org/10.3390/ph15121488.

Materials Challenges in Water Electrolysis Technologies

M. Paidar[a,*], J. Hnat[a]
[a]University of Chemistry and Technology, Prague, Technicka 5,166 28 PRAHA 6, Czech Republic
* paidarm@vscht.cz

Water electrolysis represents efficient way for conversion of electric energy to valuable chemical with multipurpose use. If the used electric energy is generated by renewable or low emission power sources, it can serve to decarbonisation of transportation or energetics. The main drawback is the dependence of electrolysis operation in connection to the actual production of power source. Fluctuating performance with frequent stops impact significantly durability of cells. For practical application it is necessary to guarantee more than 10 000 operating hours. Thus, materials for cell constructions are crucial to fulfil this request. It is not only electrochemical cell itself but also whole circulating loop with gas separators, pumps etc. Currently three different technologies are used for water electrolysis: Proton exchange membrane water electrolysis (PEMWE), alkaline water electrolysis (AWE) and high temperature solid oxide cell (SOWE). Each of them has different operating environment and face different degradation mechanisms. Challenges of each electrolysis type were analysed.

PEMWE is today most used type of electrolysis for combination with intermittent power supply. High flexibility and high intensity of process are compensated by need of platinum metals for catalysts and PFAS based ion exchange membrane.

Catalysts in PEMWE is composed of noble metals such as IrO_2 and Pt for the anode, experience efficiency losses over time due to electrochemical erosion and dissolution. The anode is especially vulnerable since it operates at high potentials above 1.5 V, with iridium mass activity degrading more rapidly when the voltage exceeds 1.8 V. In addition to chemical processes, physical degradation mechanisms such as Ostwald ripening and sintering reduce the active surface area of catalysts, leading to diminished efficiency as nanoparticles agglomerate and coarsen during prolonged operation. Catalyst poisoning is another challenge, arising from contamination by impurities such as sodium (Na^+) and calcium (Ca^{2+}) ions originating from feed water or iron (Fe^{2+}) from corrosion products. These cations migrate into the membrane or catalyst layer, where they occupy ion exchange sites, increase charge transfer resistance and overpotential, and block platinum active sites at the cathode. It indicates importance of water purity and corrosion resistance of all components in contact to circulating water.

The proton exchange membrane (PEM) is often considered as the weakest component of a PEMWE electrolyzer due to its susceptibility to both mechanical and chemical stresses. Mechanical failures can arise from pinholes, cracks, and wrinkles caused by improper compression or localized stress introduced by sharp edges and rough surfaces of the gas diffusion layer (GDL) and bipolar plates (BPPs). Under high-pressure conditions, membranes may creep, leading to increased gas crossover. Chemical degradation is primarily driven by radicals, which attack polymer backbones, strip functional groups, and cause dissolution of the membrane structure. Localized hot spots can accelerate polymer chain breaks and shortening membrane life.

Beside the core of cell represented by membrane with catalytic layers recent interest is focused on Bipolar plates (BPPs) and separator plates. BPPs are most expensive components in a PEMWE stack, require exceptional corrosion resistance under harsh electrochemical conditions. Titanium, the most commonly used material, exhibits high corrosion resistance on the anodic side in acidic and oxidizing environments. But at high potentials, titanium passivates by forming a non-conductive oxide layer, which increases interfacial contact resistance. On the cathode side, titanium is vulnerable to hydrogen embrittlement, as absorbed hydrogen decreases mechanical strength and can induce cracking under operational loads. Although cheaper materials like stainless steel offer a cost advantage, they are prone to generalized corrosion at high potentials or localized pitting under corrosive conditions near the membrane. Protective coatings are often applied to metallic BPPs to mitigate these issues.

Alkaline water electrolysis is the most robust technology based on non-precious metal materials. Although it is a mature technology, face significant performance limitations due to the corrosive nature of the electrolyte and inherent operational constraints. The liquid electrolytes, typically hot KOH, are highly corrosive and can accelerate component degradation. In addition, AWEs are sensitive to CO_2 contamination, which can lead to carbonate deposition on electrodes and severely reduce performance. The porous diaphragms used for electrode separation do not provide strict gas isolation, making gas crossover a persistent issue that reduces efficiency and raises safety risks, particularly at high current densities. Finally, AWEs suffer from slow start-up procedure and limited load variability. It reduces their ability to integrate effectively with variable renewable energy sources.

Due to the focus on efficiency nowadays inert porous separator (diaphragm) is replaced by anion selective membrane. Anion exchange membrane (AEM) membranes and ionomers face significant challenges compared to proton exchange membranes (PEMs), as they exhibit lower intrinsic ionic conductivity and suffer from limited chemical and mechanical stability under highly basic conditions at elevated temperatures. Electrode instability also poses a concern, since non-precious metal catalysts are commonly used, yet their long-term stability remains uncertain due to susceptibility to degradation influenced by temperature, and electrolyte composition. Inefficient bubble management adds to performance losses, as bubble accumulation near the catalyst layer causes ohmic

resistance by obstructing the electrode surface and results in uneven water distribution and local overheating. Finally, hydrogen embrittlement, much like in PEMWE components, presents a durability issue, as hydrogen absorption in catalysts weakens the material mechanically, leading to particle separation and subsequent performance reduction.

Solid oxide water electrolyzers (SOWEs) significantly differs to the previous types. SOWE operate at very high temperatures, typically in the range of 700–850 °C. While this improves overall efficiency, it also places extreme demands on component stability. One of the primary challenges lies in the limited durability of ceramic materials, as such high operating temperatures intensify requirements for both thermal and chemical stability. The system is particularly vulnerable to thermo-mechanical deterioration of electrolyte/electrodes interfaces, which can result from thermal cycling and the presence of large temperature gradients. Elevated operating conditions and changing of atmosphere may also cause sintering of catalyst particles, such as the NiO cathode, reducing active surface area and three phase boundary. In addition, cation migration within catalyst structures can alter phases and lower activity. Finally, the formation of secondary phases by undesired interaction at electrolyte/electrode interface reduce conductivity and catalytic activity. All these factors make SOWE the most sensitive system to the intermittent operation.

Acknowledgements

This work was supported by the OPST Project Green Energy Technologies Centre of UJEP, reg. No: CZ.10.02.01/00/24_061/0000462 co-financed by EU.

9th International Conference on Novel Materials Fundamentals and Applications
High Tatras, 12.10.-15.10.2025

Evaluation of a Non-Precious-Metal-Based High-Entropy Catalyst for Alkaline Oxygen Evolution Reaction

M. Parackova[a,*], R. Orinakova[a], M. Streckova[b], M. Ivanisko[a]
[a] Department of Physical Chemistry, Faculty of Science, P.J. Šafárik University in Košice, Moyzesova 11, 040 01 Košice, Slovakia
[b] Institute of Materials Research, Slovak Academy of Sciences, Watsonova 47, 040 01 Košice, Slovakia
* maria.parackova@student.upjs.sk

Introduction

The rise in atmospheric concentrations of greenhouse gases (GHG), primarily driven by anthropogenic activities such as fossil fuel combustion, deforestation, industrial processes, and agriculture, represents a severe global challenge [1, 2]. These gases absorb infrared radiation re-emitted from Earth's surface after the absorption of solar radiation, and subsequently re-emit part of this energy back into the atmosphere, thereby increasing the temperature of both the air and the Earth's surface [3]. While this process is essential for regulating Earth's temperature, its intensification due to rising concentrations of GHG has led to global warming. As a result, Earth's climate is undergoing changes, the consequences of which pose significant risks to human societies, biodiversity, and the stability of ecosystems worldwide [2, 3].

To mitigate these threats, global efforts are underway to reduce GHG emissions. One key strategy involves replacing fossil fuels with more sustainable alternatives [2, 3]. In recent years, significant efforts have been made toward the implementation of renewable energy technologies. However, because of the wide-ranging uses of fossil fuels, many sectors remain challenging to decarbonize through electrification alone. This limitation can be addressed through the use of hydrogen, which can function both as a chemical feedstock and as a clean energy carrier [2-5]. To enable its widespread use in decarbonization, the efficiency of water electrolysis must be improved. While the theoretical voltage for water splitting is 1.229 V under standard conditions and decreases with temperature, practical operation is hindered by energy barriers primarily related to mass transport and kinetics. As a result, the typical operating potential of commercial electrolyzers remains substantially higher even at elevated operating temperatures, ranging from 1.8 to 2.4 V. Minimizing this additional voltage relies on the development of efficient and stable catalysts for both half reactions of water splitting, and high-entropy materials have recently emerged as promising candidates [4, 6-9].

Among the two half reactions of water splitting, the oxygen evolution reaction (OER) is thermodynamically more challenging [6]. Moreover, acidic conditions pose significant difficulties in developing stable OER catalysts [7], and commercial electrolyzers typically operate at elevated temperatures [8]. The aim of this work was therefore to evaluate the catalytic activity of a novel non-precious-metal-based high-entropy material for alkaline OER under varying temperatures.

Experimental

The high-entropy material (HEM) was synthesized from Cu, Fe, Ni, Mo, and Zn precursors via a citrate sol-gel method followed by heat treatment. A catalytic ink was then prepared from HEM and drop-cast onto glassy carbon rotating disk electrode (GC-RDE) with an approximate catalyst loading of 1 $mg \cdot cm^{-2}$. The prepared sample was subsequently evaluated for electrocatalytic activity toward OER in 1 M KOH using linear sweep voltammetry at five different temperatures (298.15–333.15 K). A silver/silver chloride electrode (Ag/AgCl, 3 M KCl) and a large-area platinum electrode were employed as the reference and counter electrodes, respectively. All potentials were 100 % corrected for uncompensated electrolyte resistance and converted to the reversible hydrogen electrode (RHE) scale.

Results and discussion

As shown in *Figure 1 A*, increasing the electrolyte temperature from 298.15 K to 333.15 K led to a decrease in the potential required to reach a current density of 10 $mA.cm^{-2}$ from 1.73 V to 1.59 V. Considering the temperature dependence of the theoretical OER thermodynamic potential provided in [10], the corresponding overpotentials decreased from 506 mV at 298.15 K to 388 mV at 333.15 K (*Figure 1 B*).

The apparent activation energy of OER was determined from this temperature-dependent analysis using Equation 1, where j_0 represents the exchange current density, A is the pre-exponential factor, T is the absolute temperature and R is the universal gas constant [11]. The Arrhenius plot of the temperature-dependent exchange current density, used to estimate the apparent activation energy, is shown in *Figure 2*. The calculated activation energy (61.4 $kJ \cdot mol^{-1}$) is lower than those reported for NiOOH (76 $kJ \cdot mol^{-1}$) and FeOOH (66 $kJ \cdot mol^{-1}$), but higher than that of $Fe_xNi_{1-x}OOH$ [12], indicating that the synthesized high-entropy material exhibits moderate activity toward OER.

$$log\ j_0 = log\ A - \frac{E_A}{2{,}303RT} \quad (1)$$

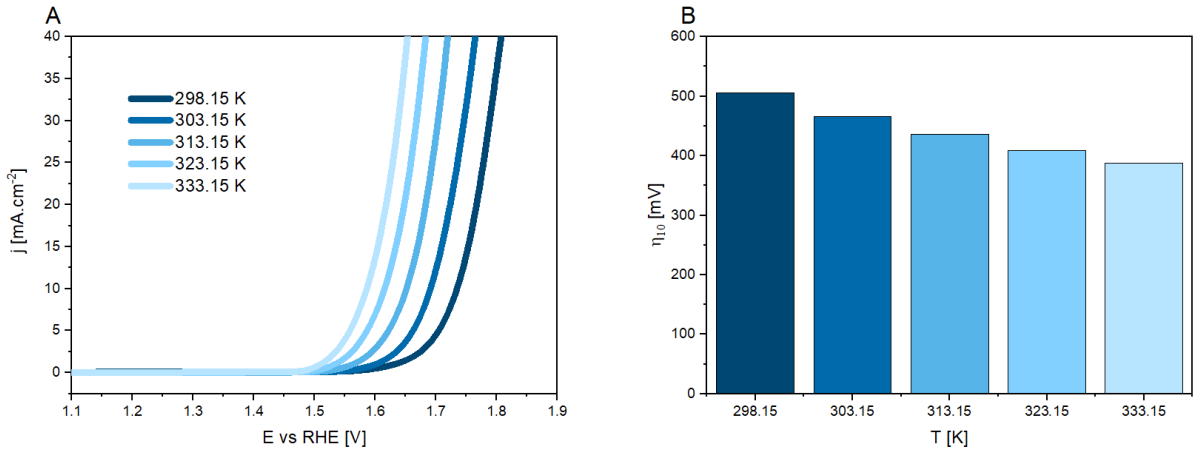

Figure 1 A) Current-potential curves of the prepared material for the oxygen evolution reaction in 1 M KOH at different temperatures; *B)* bar chart for corresponding overpotentials required to achieve a current density of 10 mA·cm^{-2}.

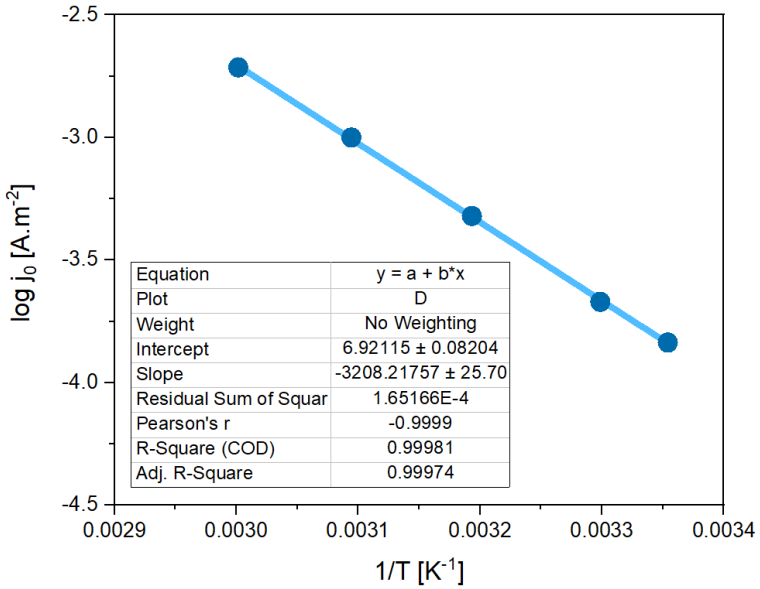

Figure 2 Arrhenius plot for the oxygen evolution reaction on the prepared material in 1 M KOH.

Acknowledgements
This research was supported by Internal Scientific Grant System - ESGD Program of Pavol Jozef Šafárik University in Košice (vvgs-2023-2957) funded by the EU NextGenerationEU through the Recovery and Resilience Plan for Slovakia under the project No. 09I03-03-V05-00008.

References
[1] G. Rothenberg, "A realistic look at CO2 emissions, climate change and the role of sustainable chemistry," *Sustainable Chemistry for Climate Action*, vol. 2, p. 100012, Jan. 2023, doi: 10.1016/J.SCCA.2023.100012.
[2] U. A. Bhatti *et al.*, "Global production patterns: Understanding the relationship between greenhouse gas emissions, agriculture greening and climate variability," *Environ Res*, vol. 245, p. 118049, Mar. 2024, doi: 10.1016/J.ENVRES.2023.118049.
[3] M. Filonchyk, M. P. Peterson, L. Zhang, V. Hurynovich, and Y. He, "Greenhouse gases emissions and global climate change: Examining the influence of CO2, CH4, and N2O," *Science of The Total Environment*, vol. 935, p. 173359, Jul. 2024, doi: 10.1016/J.SCITOTENV.2024.173359.
[4] A. M. Oliveira, R. R. Beswick, and Y. Yan, "A green hydrogen economy for a renewable energy society," *Curr Opin Chem Eng*, vol. 33, p. 100701, Sep. 2021, doi: 10.1016/J.COCHE.2021.100701.
[5] R. Jayabal, "Towards a carbon-free society: Innovations in green energy for a sustainable future," *Results in Engineering*, vol. 24, p. 103121, Dec. 2024, doi: 10.1016/J.RINENG.2024.103121.

[6] M. Yu, E. Budiyanto, and H. Tüysüz, "Principles of Water Electrolysis and Recent Progress in Cobalt-, Nickel-, and Iron-Based Oxides for the Oxygen Evolution Reaction," *Angewandte Chemie International Edition*, vol. 61, no. 1, Jan. 2022, doi: 10.1002/anie.202103824.
[7] W. Li, H. Tian, L. Ma, Y. Wang, X. Liu, and X. Gao, "Low-temperature water electrolysis: fundamentals, progress, and new strategies," *Mater Adv*, vol. 3, no. 14, pp. 5598–5644, 2022, doi: 10.1039/D2MA00185C.
[8] C. Xiang, K. M. Papadantonakis, and N. S. Lewis, "Principles and implementations of electrolysis systems for water splitting," *Mater Horiz*, vol. 3, no. 3, pp. 169–173, 2016, doi: 10.1039/C6MH00016A.
[9] Z. J. Zhang *et al.*, "High entropy catalysts in electrolytic water splitting: A review from properties to applications," *Chemical Engineering Journal*, vol. 498, p. 155736, Oct. 2024, doi: 10.1016/J.CEJ.2024.155736.
[10] Y. Du *et al.*, "Continuous strain tuning of oxygen evolution catalysts with anisotropic thermal expansion," *Nat Commun*, vol. 15, no. 1, p. 1780, Feb. 2024, doi: 10.1038/s41467-024-46216-9.
[11] A. R. Zeradjanin, P. Narangoda, J. Masa, and R. Schlögl, "What Controls Activity Trends of Electrocatalytic Hydrogen Evolution Reaction?─Activation Energy *Versus* Frequency Factor," *ACS Catal*, vol. 12, no. 19, pp. 11597–11605, Oct. 2022, doi: 10.1021/acscatal.2c02964.
[12] J. R. Swierk, S. Klaus, L. Trotochaud, A. T. Bell, and T. D. Tilley, "Electrochemical Study of the Energetics of the Oxygen Evolution Reaction at Nickel Iron (Oxy)Hydroxide Catalysts," *The Journal of Physical Chemistry C*, vol. 119, no. 33, pp. 19022–19029, Aug. 2015, doi: 10.1021/acs.jpcc.5b05861.

Conductive Composites Based on Thermoplastic Starch: Electrical Conductivity Behavior during Cyclic Mechanical Deformation

H. Peidayesh[a,]*, M. Micusik[a], I. Chodak[a]
[a] Polymer Institute of the Slovak Academy of Sciences, Dúbravská cesta 9, 845 41 Bratislava, Slovakia
* hamed.peidayesh@savba.sk

Conductive polymer composites (CPCs) are fabricated by mixing an insulating polymeric matrix with conductive fillers. Substantial effort has been devoted in the past decade to understanding the features of CPCs with respect to conductivity changes under external stimuli, such as thermal, electrical, mechanical, or chemical stresses [1]. Mechanical deformation is likely the most important factor that affects the structure of the conductive pathways. In this regard, investigation of the dependence of electrical conductivity on mechanical deformation is of particular interest, especially if measured for conductive two-phase systems consisting of an insulating polymeric matrix filled with a conductive filler. On the other hand, polymers from renewable resources as matrices for solid conducting composites have been considered. Starch has been considered as one of the most promising candidates in the biopolymer industry since it is abundant in nature, cost-effective, available from renewable resources, and biodegradable. Thermoplastic starch (TPS) is a plasticized version of starch that can be obtained by the destruction of starch granules in the presence of plasticizers under heat and shear conditions [2]. To the best of our knowledge, the dependence of electrical conductivity on mechanical deformation for TPS-based composite has not yet been investigated in similar experiments using online measurements.

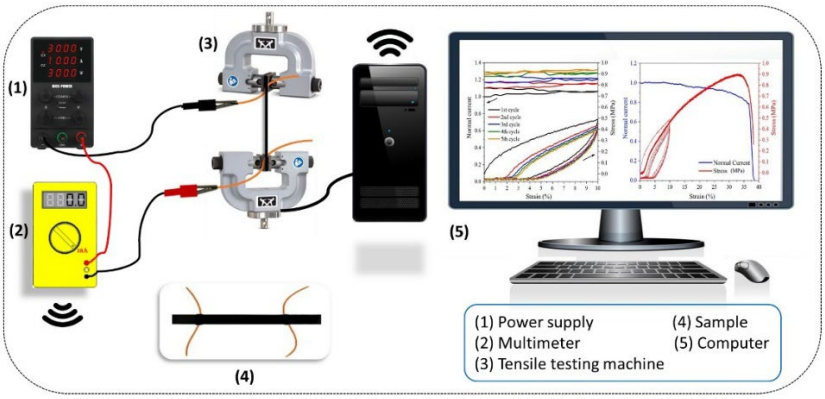

Figure 1 Online measurement of conductivity changes during cycling deformation [3].

Herein, this contribution is focused on investigating the changes in electroconductive paths during cyclic deformation of electroconductive TPS-based composites. TPS-based composites filled with various carbon black (CB) contents were prepared through melt processing. The physical and mechanical properties and static conductivity were evaluated. Furthermore, both the electrical conductivity and stress-strain curves were recorded in parallel using online measurements (*Figure 1*). With increasing CB content, the tensile strength and Young's modulus were found to increase substantially. We found a percolation threshold for the CB loading of approximately 5.5 wt% based on the rheology and electrical conductivity. Both the electrical conductivity and mechanical properties were recorded in parallel using online measurements. The standard shapes of stress-strain cycles with typical hysteresis were seen for composites, where the stress is considerably higher than the stress values during the decrease in deformation. The electrical conductivity increased or at least remained constant during five runs of repeated cyclic mechanical deformations to constant deformation below strain at break, indicating more perfect recovery of conductive paths and their new formation.

Acknowledgements
This study was supported by projects APVV-23-0224 and VEGA 2/0109/23.

References
[1] M. Omastova, I. Chodak, and J. Pionteck, "Electrical and mechanical properties of conducting polymer composites," *Synth. Met.,* vol. 102, no. 1-3, pp. 1251–1252, 1999, doi: 10.1016/S0379-6779(98)01453-2.
[2] H. Peidayesh, A. Heydari, K. Mosnáčková, and I. Chodák, "In situ dual crosslinking strategy to improve the physico-chemical properties of thermoplastic starch," *Carbohydr. Polym.,* vol. 269, p. 118250, 2021, doi: 10.1016/j.carbpol.2021.118250.
[3] H. Peidayesh, Z. Špitalský, and I. Chodák, "Electrical conductivity of rubber composites with varying crosslink density under cyclic deformation," *Polymers,* vol. 14, no. 17, p. 3640, 2022, doi: 10.3390/polym14173640.

Preparation of NiFe LDH Catalyst for the Oxygen Evolution Reaction by Electrodeposition on Nickel Foam

M. Plevova[a,*], J. Hnat[b], K. Bouzek[b]
[a] Institute of Materials Research, Watsonova 47, 040 01 Košice, Slovak Republic
[b] University of Chemistry and Technology, Prague, Department of Inorganic Technology, Technická 5, 166 28 Prague 6, Czech Republic
* mplevova@saske.sk

The transition towards sustainable energy requires reducing CO_2 emissions and dependence on fossil fuels, which has intensified interest in hydrogen as an energy carrier for power generation, industry, and transportation. Hydrogen can be produced without CO_2 emissions via electrochemical water splitting powered by renewable electricity. However, the widespread adoption of water electrolysis relies on the development of efficient and cost-effective catalysts capable of reducing the associated energy demands. While noble metal-based materials such as Pt and IrO_2 exhibit the highest activity and are indispensable in systems operating with demineralized water, transition metal compounds, particularly those based on nickel and iron, have shown comparable activity and stability in alkaline environments.

In this work, a nickel–iron layered double hydroxide (NiFe LDH) catalyst was synthesized directly on a three-dimensional nickel foam (NF) support by a simple one-step electrodeposition method. The resulting NiFe LDH/NF electrode demonstrated a low overpotential for oxygen evolution (180 mV at 10 mA cm^{-2}) and showed a very good performance in an alkaline membrane water electrolyzer (1 mol dm^{-3} KOH, 50 °C, loading ~2 mg cm^{-2}). Owing to its excellent activity and stability, NiFe LDH/NF represents a highly promising catalyst for practical application in alkaline water electrolysis.

Acknowledgements
This work was funded by the EU Next Generation EU through the Recovery and Resilience Plan for Slovakia under the project No 09I04-03-V02-00006.

Computational Insights into Graphite Surface Doping in Vanadium Redox Flow Battery Systems

N. Podrojkova[a,*], A. Strakova Fedorkova[a]
[a] Department of Physical Chemistry, Pavol Jozef Šafárik University in Košice, Dr. Kostlivého 1, 040 01, Košice, Slovakia
* natalia.podrojkova@upjs.sk

Maximizing the efficiency of renewable energy utilization critically depends on the development of advanced energy storage technologies [1]. While lithium-ion batteries currently dominate the market owing to their high energy density, low self-discharge, and versatile chemistry, their limited power capability and inherent safety concerns restrict their application in large-scale stationary storage [1-3]. Achieving grid-level performance requires extensive cell stacking in series or parallel, which inevitably increases both cost and system complexity [1].
Redox flow batteries (RFBs) represent a promising alternative, as they store active redox species in external electrolyte tanks, allowing independent scaling of power and energy. Over the past decades, several flow-battery chemistries have been investigated, among which the all-vanadium redox flow battery (VRFB) has emerged as the most mature and commercially viable. VRFBs offer long cycle life, flexible operation, high energy efficiency, and low capital cost, while avoiding electrolyte cross-contamination by employing vanadium in multiple oxidation states [3]. The operation of the VRFB relies on two well-defined redox couples dissolved in sulfuric acid electrolytes. At the negative electrode, the V^{3+}/V^{2+} couple undergoes the reaction:

$$V^{3+} + e^- \rightleftharpoons V^{2+}$$

At the positive electrode, the VO_2^+/VO^{2+} couple is involved, following:

$$VO_2^+ + 2H^+ + e^- \rightleftharpoons VO^{2+} + H_2O$$

The overall cell reaction during discharge can therefore be expressed as:

$$VO_2^+ + 2H^+ + V^{2+} \rightarrow VO^{2+} + V^{3+} + H_2O,$$

yielding a theoretical cell voltage of approximately 1.26 V. This value is in close agreement with the experimentally observed open-circuit voltage of ~1.25 V, which enables safe and stable battery operation [1, 4].
Despite these advantages, the performance of VRFBs remains constrained by sluggish electrode kinetics and the insufficient catalytic activity of pristine graphite felt electrodes [5]. Graphite is chemically stable and electrically conductive, yet its inert basal planes and limited surface functionalization result in slow redox reaction rates. Considerable effort has therefore been directed toward surface modifications and heteroatom doping of graphite to enhance electrochemical activity. Incorporation of non-metallic dopants such as nitrogen, boron, phosphorus, or sulfur has been shown to alter the local electronic environment, increase defect density, and introduce active sites that facilitate vanadium redox reactions [5]. Such approaches significantly improve electrode kinetics and stability; however, they are often accompanied by challenges related to synthesis complexity, dopant distribution, and long-term durability [5].

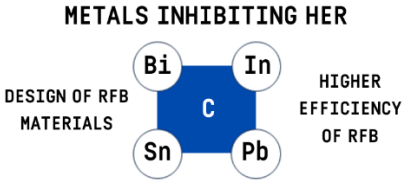

Figure 1 Schematic representation of carbon-based materials doped with Bi, In, Sn, and Pb as HER-inhibiting elements, enabling improved RFB material design and higher efficiency.

Beyond non-metallic dopants, recent research has highlighted the potential of incorporating metallic and semi-metallic elements into graphite frameworks [6]. Heavy p-block elements such as bismuth (Bi), indium (In), tin (Sn), and lead (Pb) are of interest due to their ability to modify surface adsorption properties and to suppress competing parasitic processes, most notably the hydrogen evolution reaction (HER) [6] – *Figure 1*. This side reaction, which occurs predominantly at the negative electrode during V(II)/V(III) cycling, reduces Coulombic efficiency, accelerates electrolyte imbalance, and diminishes overall battery performance. The presence of suitable

dopants can lower the overpotential for vanadium redox reactions while simultaneously increasing the overpotential for HER, thus selectively favoring the desired electrochemical processes.
Accordingly, this work focuses on the theoretical investigation of graphite surface doping with Bi, In, Sn, and Pb as a means of improving VRFB electrode performance. By elucidating how these dopants influence the electronic structure, adsorption behavior, and reaction energetics of vanadium species, this study aims to provide fundamental insights into rational strategies for suppressing hydrogen evolution while enhancing the kinetics of vanadium redox couples.

Acknowledgements
This work was supported by the EU NextGenerationEU through the Recovery and Resilience Plan for Slovakia under the project No. 09I03-03-V04-00109.

References
[1] W. Sharmoukh, "Redox flow batteries as energy storage systems: materials, viability, and industrial applications," *RSC Adv.*, vol. 15, pp 10106-10143, 2025, doi: 10.1039/D5RA00296F.
[2] Toshiba, "Toshiba Develops World's First Aqueous Lithium-ion Battery with Nonflammable Electrolyte," *Toshiba Global*, Nov. 19, 2020. https://www.global.toshiba/ww/technology/corporate/rdc/rd/topics/20/2011-01.html#:~:text=systems%20are%20lithium,a%20long%20period%20of%20time.
[3] A. L. Akman, M. Z. Arslan, M. Farsak, "The rise of vanadium redox flow batteries: A game-changer in energy storage," *J. Alloys Compd.*, vol 1038, 182869, Aug. 2025, doi: 10.1016/j.jallcom.2025.182869.
[4] H. Sun et al., "Vanadium Redox Flow Batteries Fabricated by 3D Printing and Employing Recycled Vanadium Collected from Ammonia Slag," J. Electrochem. Soc., vol. 166, no. 9, B3125, Apr. 2019, doi: 10.1149/2.0251909jes.
[5] Z. Jialin et al., "Nitrogen, Phosphorus Co-Doped Graphite Felt as Highly Efficient Electrode for VO^{2+}/VO_2^{+} Reaction," *Batteries*, vol. 9, no. 40, Jan. 2023, doi: 10.3390/batteries9010040.
[6] A. W. Bayeh et al., "Carbon and metal-based catalysts for vanadium redox flow batteries: a perspective and review of recent progress," *Sustain. Energy Fuels*, vol. 5, no. 6, pp. 1668–1707, Feb. 2021, doi: 10.1039/d0se01723j.

High Entropy Metal Oxide/TiO_2 Based Heterostructures for Selective CO_2 Detection

J. Shaikh[a,*], J. Matyas[a], R. Olejnik[a], N. Joseph[a], R. Orinakova[a,b], P. Saha[a]
[a] Centre of Polymer Systems, University Institute, Tomas Bata University in Zlín, Třída Tomáše Bati 5678, 76001 Zlín, Czech Republic
[b] Department of Physical Chemistry, Faculty of Science, P.J. Šafarik University in Košice, Moyzesova 11, 041 54, Košice
* jshaikh@utb.cz

Examining the air quality in the environment, particularly in closed spaces, via the detection of different types of gases like acetone, formaldehyde, carbon monoxide, methane, carbon dioxide, etc., is a fundamental requirement. Different metal oxides have been employed for the detection of gases. TiO2 is preferred due to its high temperature, chemical and mechanical stabilities. However, TiO2-based sensors required high operating temperatures (200-400 °C) to reach good sensitivity. Hence, currently it is important to explore other novel materials to selectively detect CO2 gas with a wide range of concentrations at low working temperatures with enhanced response/ recovery time and sensitivity. The making of a heterostructure with different types of materials is an effective strategy to enhance the gas sensor response and selectivity. Recently emerged high entropy metal oxide (HEMO) can be used as effective gas sensor for the detection of CO2 because of it has large surface-to-volume ration, more surface-active sites, and intrinsic oxygen vacancies. Also, HEMO has high electrical conductivity at room temperature, and it can be useful for the sensor to reduce power consumption. In this work, we synthesized five elements based HEMO by the auto-combustion method. Here, HEMO-TiO2 heterostructure was synthesized by ultrasonic treatment of HEMO-TiO2 mixture in water. Commercial TiO2 powder has been used for this heterostructure preparation. Consequently, gas sensing properties of the above-mentioned heterostructure can exhibit improved sensing performance at low temperature. Polyaniline (PANI) is a widely investigated conducting polymer in CO2 gas sensors owing to its high electric conductivity, unique redox and doping properties, which lead to high conductivity tuning upon exposure to CO2 gas molecules. PANI is useful for sensing at room temperature, making it a good candidate for real-time sensing. In future work, we will prepare HEMO-TiO2-PANI-based heterostructure for CO2 sensing at room temperature with high sensitivity.

Acknowledgements

This research was supported by the NATO Science for Peace and Security Programme, grant No. G6106 and also by the Ministry of Education, Youth and Sports of the Czech Republic - DKRVO (RP/CPS/2024-28/005).

References

[1] S. C. Pathan, J. S. Shaikh, M. Rittiruam, T. Saelee, V. Márquez, P. Khajondetchairit, S. S. Mali, J. V. Patil, C. K. Hong, P. Praserthdam and S. Praserthdam,. (2024). High entropy metal oxide/TiO2 nanocomposite for electrocatalytic overall water splitting. Journal of Alloys and Compounds, 176811. https://doi.org/10.1016/j.jallcom.2024.176811 [4] J. Sambrook and D. W. Russell, *Molecular cloning: a laboratory manual*, 3rd ed. Cold Spring Harbor, NY: CSHL Press, 2001.

Screen-Printed Electrode Modified by Gold Nanoparticles for Glucose and Ascorbic Acid Detection

J. Shepa[a,]*, N. Jasnakova[a], I. Sisolakova[a], R. Orinakova[a]
[a] Department of Physical Chemistry, Pavol Jozef Šafárik University in Košice, Moyzesova 11, 040 01 Košice, Slovak Republic
* jana.shepa@upjs.sk

Introduction

Diabetes mellitus is a critical global health challenge, often leading to severe complications such as cardiovascular disease, stroke, and chronic kidney failure. Consequently, the development of reliable, sensitive, and inexpensive glucose sensing devices has attracted widespread attention from the clinical and pharmaceutical industries [1]. Simultaneously, the accurate detection of ascorbic acid (AA), commonly known as vitamin C, is also crucial for both healthcare and food quality control. As a vital nutrient and potent antioxidant, AA plays a significant role in metabolic processes and is used to prevent and treat various diseases. Its unstable nature in food also necessitates a fast, simple, and sensitive detection strategy to ensure nutritional quality [2].

Traditional glucose and AA sensing technologies, particularly those based on enzymes, have long been utilized due to their high specificity. However, their practical application is limited by several significant drawbacks, including poor stability, susceptibility to environmental factors such as humidity and pH, high manufacturing costs, and a lack of reproducibility. These limitations have motivated researchers to focus on developing non-enzymatic electrochemical sensing electrodes, which offer a compelling alternative [3]. This approach effectively overcomes the shortcomings of enzyme-based sensors by providing increased stability, ease of manufacture, and excellent repeatability, making them an ideal platform for glucose and AA detection.

The performance of these electrochemical sensors is largely determined by the catalytic materials used. Over recent years, significant efforts have been dedicated to synthesizing nanomaterials with precisely controlled morphologies and sizes. Nanomaterials possess unique chemical and physical features, such as a high surface-area-to-volume ratio, exceptional electrical conductivity, and enhanced catalytic activity, which are ideal for improving sensor performance [4], [5], [6]. The introduction of nano-metals, heterogeneous structures, and nanostructured composites into biosensors has been shown to significantly improve sensing capabilities. For example, noble metals like gold nanoparticles (AuNPs) are highly stable and have a strong affinity for specific biomolecules, which can be leveraged to create highly efficient sensing surfaces [4], [7], [8]. When combined with other materials, such as graphene oxide, these nanostructured composites offer synergistic effects that enhance both electron transfer and the density of binding sites.

This work explores the use of AuNPs decorated screen-printed carbon electrodes (SPCE) to develop a highly effective non-enzymatic electrochemical sensor. By leveraging the unique properties of these materials, our aim is to create a robust and sensitive platform that can accurately and simultaneously detect glucose and ascorbic acid. This advancement not only addresses the critical need for improved diabetes management tools but also provides a versatile method for quality control in the food and pharmaceutical industries, paving the way for more reliable and accessible diagnostic and analytical technologies.

Experimental part

Glucose and PBS were purchased from Sigma Aldrich and NaOH was obtained from CentralChem. All chemicals were used without further purification. Screen-printed carbon electrodes were obtained from Dropsens, Metrohm. Morphology of modified electrodes was studied via confocal microscopy (PLuneox3D Optical Profiler – SENSOFAR). All electrochemical measurements were performed using Solartron ModuLab XM ECS. A calibration curve was made based on the cyclic voltammetry measurements within the potential window -1 V – +1.5 V, at scan rate 100 mV/s, concentration range from 0.1 mM to 10 mM for both glucose and ascorbic acid in 0.1 M NaOH in PBS.

Results and discussion

SPCE were modified with the AuNPs during 5 (5AuNPs/SPCE), 10 (10AuNPs/SPCE), and 15 cycles (15AuNPs/SPCE) of electrodeposition (Figure 1). Morphology of modified electrodes was studied via confocal microscopy and analysis of images was realised by using Gwyddion software.

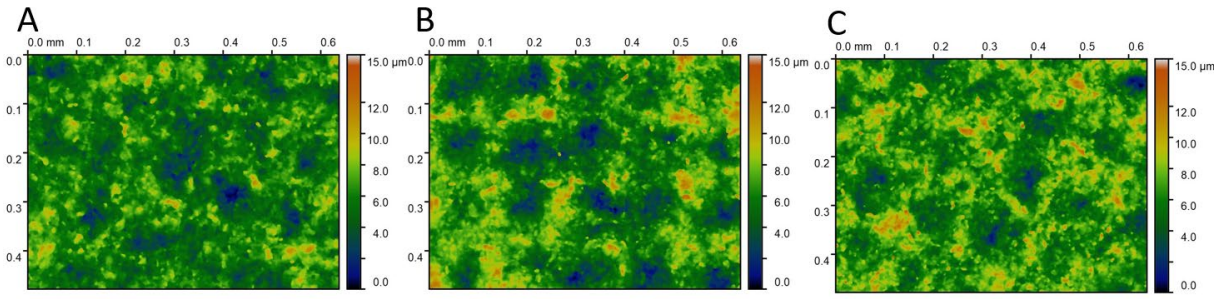

Figure 1 Confocal microscopy images of SPCE decorated by gold nanoparticles during 5 *(A)*, 10 *(B)*, and 15 *(C)* cycles of deposition.

The analysis of surface roughness revealed a non-linear relationship with number of electrodeposition cycles of gold nanoparticles. The 10AuNPs/SPCE sample exhibited the highest roughness value at 1.526 µm, a notable increase compared to the 5AuNPs/SPCE (1.185 µm). This suggests that more cycles of electrodeposition effectively enhance surface irregularities, likely due to the random deposition and clustering of the nanoparticles. However, the roughness decreased to 1.285 µm for the 15AuNPs/SPCE sample. This reduction could be attributed to the onset of nanoparticle agglomeration or a more densely packed.
The maximum height parameter, which represents the highest vertical point of the deposited material, showed a clear positive correlation with the number of cycles. The values increased progressively from 5AuNPs/SPCE (11.57 µm) to 10AuNPs/SPCE (13.5 µm), culminating in the highest value of 14.24 µm for 15AuNPs/SPCE. This trend indicates that higher amount of AuNPs results in a thicker overall film on the electrode surface, consistent with the increased amount of material being deposited.
The calculated values of surface area ranged from a low of 0.3202 mm^2 for the 5AuNPs/SPCE to a high of 0.3256 mm^2 for the 15AuNPs/SPCE. The minimal variation suggests that the electrodeposition of gold nanoparticles, within this number of cycles, does not substantially increase the total geometrical or electrochemically active surface area. This finding is crucial, as it implies that the enhanced performance often associated with AuNPs is more likely due to their unique catalytic properties and improved mass transport rather than a simple increase in available surface area.

Table 1 Table of modified AuNPs/SPCE characteristics – roughness, maximum high, and surface area.

	Roughness	**Maximum high**	**Surface area**
5AuNPs/SPCE	1,185 µm	11,57 µm	0,3202 mm^2
10AuNPs/SPCE	1,526 µm	13,5 µm	0,3216 mm^2
15AuNPs/SPCE	1,285 µm	14,24 µm	0,3256 mm^2

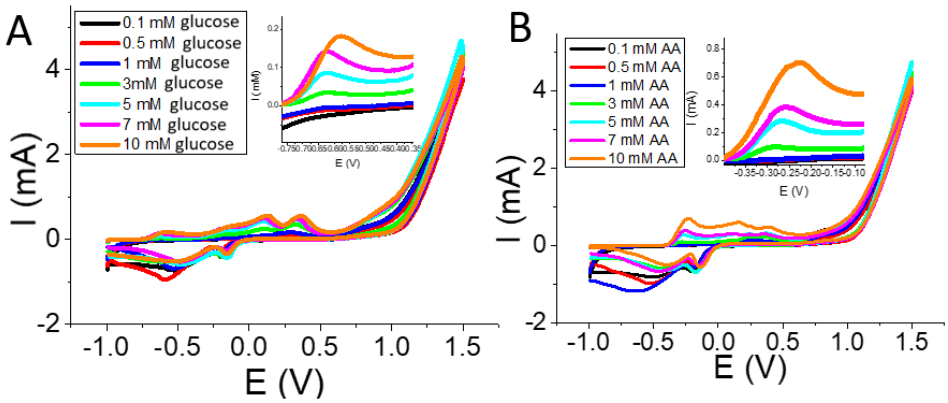

Figure 2 Cyclic voltammograms for 15AuNPs/SPCE for various concentration of glucose (0.1, 0.5, 1, 3, 5, 7, and 10 mM) and for ascorbic acid (0.1, 0.5, 1, 3, 5, 7, and 10 mM) in 0.1 M NaOH in PBS from the potential -1 V to 1.5 V at the scan rate 100 mV/s.

The electrochemical behaviour of the sensor was characterized by cyclic voltammetry (CV) in a solution containing varying concentrations of glucose and ascorbic acid (AA) in 0.1 M NaOH dissolved in PBS, as shown in the *Figure 2*. The recorded cyclic voltammograms reveal the distinct electrochemical signatures of both analytes,

confirming the sensor's ability to differentiate between them. A clear and well-defined oxidation peak for ascorbic acid is observed at approximately -0.25 V, a potential significantly higher than that of glucose. At a more negative potential, around -0.65 V, a second, separate oxidation peak corresponding to glucose is evident. The distinct separation of these two peaks is a crucial indicator of the electrode's high selectivity, which is essential for accurately detecting glucose in complex biological matrices where electroactive interferents like AA are present. Upon the successive addition of increasing concentrations of either glucose or AA, a proportional increase in the respective anodic peak current is consistently observed. This direct relationship demonstrates the concentration-dependent response of the electrode, a fundamental requirement for quantitative sensing. The peak current for both analytes increases linearly with concentration over a wide range from 0.1 mM to 10 mM for both analytes, indicating a robust and predictable performance (*Figure 3*). The linearity of this response allows for the construction of calibration curves, from which the sensor's sensitivity was 0.07 mA/mM and 0.2 mA/mM for ascorbic acid and glucose, respectively. Limit of detection was for ascorbic acid 1.48 mM and for glucose 0.8 mM. The consistent and well-resolved CV signals, combined with the linear correlation between peak current and concentration, confirm the excellent quantitative capability and reliability of the developed sensor for the simultaneous detection of both glucose and ascorbic acid.

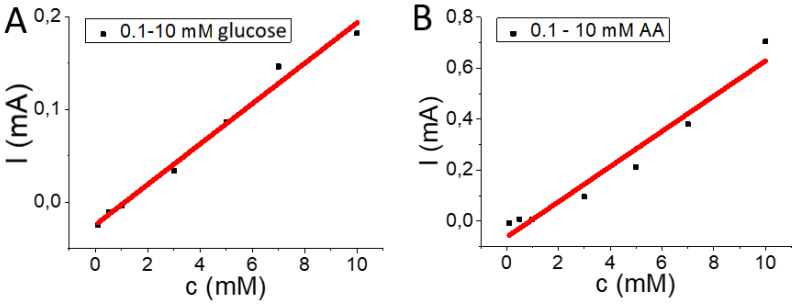

Figure 3 Calibration curve for various concentration of glucose *(A)* and ascorbic acid *(B)* in 0.1 M NaOH in PBS.

Above mention results make developed sensor promising candidate for glucose and ascorbic acid detection in real samples.

Acknowledgements
Funded by the EU NextGenerationEU through the Recovery and Resilience Plan for Slovakia under the project No. 09I03-03-V05-00008.

References
[1] K. N. Fatema and W. C. Oh, “A comparative electrochemical study of non-enzymatic glucose, ascorbic acid, and albumin detection by using a ternary mesoporous metal oxide (ZrO2, SiO2and In2O3) modified graphene composite based biosensor,” RSC Adv, vol. 11, no. 7, pp. 4256–4269, Jan. 2021, doi: 10.1039/d0ra09886h.
[2] H. Li, Y. Sun, T. Xian, J. Bao, W. Liu, and X. Lu, “Construction of Cu2O/PANI-GO/SS flexible electrode with three-dimensional network structure towards electrochemical sensing of glucose and ascorbic acid,” J Alloys Compd, vol. 1015, Feb. 2025, doi: 10.1016/j.jallcom.2025.178919.
[3] J. Hovancová, I. Šišoláková, R. Oriňaková, and A. Oriňak, “Nanomaterial-based electrochemical sensors for detection of glucose and insulin,” Aug. 01, 2017, Springer New York LLC. doi: 10.1007/s10008-017-3544-0.
[4] H. C. Chen, Y. S. Lin, M. H. Yen, and J. Y. Lin, “Gold nanoparticles modified Cu2O/ZnO nanorod arrays synthesized with anodic aluminum oxide template for high performance non-enzymatic glucose sensor,” Mater Chem Phys, vol. 341, Sep. 2025, doi: 10.1016/j.matchemphys.2025.130886.
[5] F. Zhou et al., “Synergistic effect of gold nanoparticles/ZnO nanorods heterojunctions and ultraviolet irradiation for enhanced electro-catalytic capacity of flexible non-enzymatic electrochemical glucose sensor,” Microchemical Journal, vol. 209, Feb. 2025, doi: 10.1016/j.microc.2025.112798.
[6] M. Y. A. Khan et al., “Visible light photocatalytic degradation of crystal violet dye and electrochemical detection of ascorbic acid & glucose using BaWO4 nanorods,” Mater Res Bull, vol. 104, pp. 38–43, Aug. 2018, doi: 10.1016/j.materresbull.2018.03.049.
[7] J. Hovancová et al., “Nanostructured Gold Microelectrodes for Non-enzymatic Glucose Sensor,” Electroanalysis, vol. 31, no. 9, pp. 1680–1689, Sep. 2019, doi: 10.1002/elan.201900163.
[8] J. Hovancová et al., “Gold Microelectrodes Decorated by Spike-Like Nanostructures as a Promising Non-Enzymatic Glucose Sensor,” Electroanalysis, vol. 33, no. 2, pp. 347–354, Feb. 2021, doi: 10.1002/elan.202060207.

Morphology-Controlled Copper Pulsed Deposition on Carbon Electrodes for Insulin Sensing

I. Sisolakova[a,*], S. Vanchak[a], R. Filip[a], P. Hviscova[b], I. Shepa[b], F. Talarovic[c], J. Shepa[a]
[a] Department of Physical Chemistry, Pavol Jozef Šafárik University in Košice, Moyzesova 11, 040 01, Košice, Slovak republic
[b] Institute of Material Research, Slovak Academy of Sciences, Watsonova 47, 040 01, Košice, Slovak republic
[c] FECUPRAL, spol s.r.o, Jilemnického 3578, 080 01, Prešov, Slovak republic
* ivana.sisolakova@upjs.sk

Pulsed electrodeposition has emerged as an effective method for controlling nucleation and growth of metal particles, preventing dendritic or uncontrolled formation, and regulating the distribution of oxidation states [1, 2]. In this study, we focused on carbon paste electrodes (CPEs) modified via pulsed copper deposition, analyzing their morphology, electrochemical properties, and performance in insulin detection.
The CPEs were prepared using carbon powder derived from waste materials, with coconut oil serving as a natural binder (*Figure 1*). Copper was deposited onto the electrode surface using a pulsed potentiostatic approach: a potential of – 0.40 V was applied in alternating on/off pulses, with varying pulse numbers (5, 10, 15, 20, 25). This method allowed controlled growth of copper and partially oxidized copper species on the carbon surface

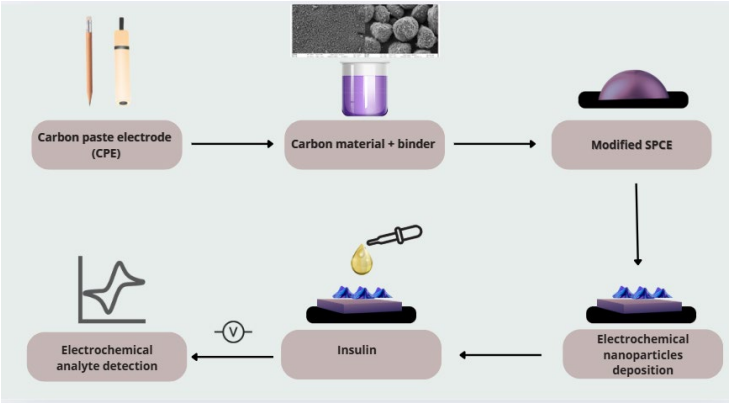

Figure 1 Fabrication process of Cu modified CPE.

Scanning electron microscopy revealed that 5 to 10 pulses produced relatively uniform, discrete copper nanoparticles (~1.4 –1.5 µm). At 15 pulses, particles began to merge, forming larger agglomerates (~2.7 µm).Further increases to 20 to 25 pulses caused overlapping of copper domains, reducing particle definition and decreasing surface roughness. Quantitative surface roughness measurements (e.g., maximum height, RMS deviation) also declined beyond 15 pulses due to cluster overlap. Raman spectroscopy confirmed increasing copper oxide formation (e.g., Cu_2O) in the 15 and 25 pulse samples, while lower pulse counts showed weaker oxide signals.
Cyclic voltammetry (CV) in phosphate buffer (pH 9) containing insulin showed clear redox peaks for all pulsed electrodes, confirming electroactive incorporation of copper species. Peak currents strongly depended on pulse number. The 15-pulse electrode (15 pCu/CPE) exhibited the highest oxidation currents, suggesting an optimal balance between active surface area and particle connectivity. Higher pulse counts reduced electrochemical accessibility due to overlapping agglomerates, while lower pulse counts limited copper coverage and current response.
Pulsed copper deposition on CPEs provides a tunable platform for insulin sensing but has notable limitations. The 15-pulse modification gave the best electrochemical response due to favorable morphology, yet the redox process is limited by slow charge-transfer kinetics. Compared to CV-modified electrodes, pulsed electrodes show lower reproducibility. These findings provide insights into how pulse parameters affect morphology, oxidation state, and electroanalytical behavior, informing future optimization or hybrid deposition strategies.

Acknowledgements
This work was funded by the EU NextGenerationEU through the Recovery and Resilience Plan for Slovakia under the project No. 09I03-03-V04-00180.

References

[1] A. Hassan, A. E. Radi, and K. A. El-Shaikh, "Electrochemical sensing of antibiotics in complex biological matrices: challenges and prospects," *Biosens. Bioelectron.*, vol. 176, p. 112925, 2021, doi: 10.1016/j.bios.2020.112925.

[2] J. Smith, L. Wang, and M. Brown, "Pulsed electrodeposition of metals: kinetics and morphology control," *Electrochim. Acta*, vol. 210, pp. 456–467, 2016, doi: 10.1016/j.electacta.2016.05.032.

A Sensitive and Selective Electrochemical Sensor for Gentamicin Based on Modified Screen-Printed Carbon Electrodes

I. Sisolakova[a,*], J. Demeterova[a], J. Shepa[a], N. Kiraly[b], M. Almasi[b], I. Mojzisova[a], R. Orinakova[a]

[a] Department of Physical Chemistry, Pavol Jozef Šafárik University in Košice, Moyzesova 11, 040 01, Košice, Slovak republic

[b] Department of Inorganic Chemistry, Pavol Jozef Šafárik University in Košice, Moyzesova 11, 040 01, Košice, Slovak republic

* ivana.sisolakova@upjs.sk

Electrochemical sensors are widely recognized as promising analytical tools due to their high sensitivity, low cost, and suitability for real-time monitoring. Their application is particularly important for the detection of antibiotics, whose residues and release kinetics are of significant biomedical and pharmaceutical concern. Gentamicin, a widely used aminoglycoside antibiotic, plays a key role in the treatment of severe infections; however, its detection at low concentrations remains analytically challenging. Therefore, the development of highly sensitive, selective, and reliable sensors for gentamicin monitoring is essential [1, 2].

In this study, we present the development of an electrochemical sensor for the detection of gentamicin sulfate based on the modification of screen-printed carbon electrodes (SPCEs). The SPCEs consisted of a three-electrode system (carbon working electrode, Ag/AgCl reference electrode, and carbon counter electrode) printed on a ceramic substrate. The working electrode surface was modified by drop-casting chromium-based metal–organic frameworks (Cr-MOFs), multi-walled carbon nanotubes (MWCNTs), and Nafion, either individually or in combination. The electrochemical behavior of the unmodified and modified electrodes was investigated by cyclic voltammetry (CV) in 5 mM $K_3[Fe(CN)_6]/K_4[Fe(CN)_6]$ and in 300 µM gentamicin solution in PBS. While the highest electroactive surface area was observed for unmodified SPCEs, the best current response for gentamicin oxidation (0.2–0.5 V) was achieved with electrodes modified by the combination of Cr-MOF, MWCNTs, and Nafion. This synergistic effect is attributed to the adsorption capacity of Cr-MOF and the efficient electron transfer of MWCNTs [3, 4].

Performance characteristics, including sensitivity and detection limit, were evaluated using CV, chronoamperometry (CHA), and differential pulse voltammetry (DPV). The most sensitive method was CV, with a sensitivity of 1.37×10^{-4} mA/µM, a detection limit of 230.60 µM, and a linear detection range of 200–1000 µM. No significant current response was observed in PBS alone, confirming the selectivity of the sensor toward gentamicin [5].

In conclusion, the SPCE electrode modified with Cr-MOF/MWCNTs/Nafion demonstrated the best analytical performance, combining ease of preparation with reliable detection of gentamicin in the range of 0.1–1 mM. These results highlight the potential of such electrochemical sensors for antibiotic monitoring in biomedical and pharmaceutical applications [6].

Acknowledgements

This research was sponsored by the NATO Science for Peace and Security Programme under grant id. G6106.

References

[1] L. Zhao, Z. Wang, and W. Zhang, "Electrochemical sensors for the detection of antibiotics in environmental and biological samples," *Analytica Chimica Acta*, vol. 1134, pp. 83–96, 2020, doi: 10.1016/j.aca.2020.01.017.

[2] J. Zhou, L. Liao, and Q. Wei, "Recent advances in electrochemical sensors for the determination of aminoglycoside antibiotics: Gentamicin as a case study," *J. Electroanal. Chem.*, vol. 815, pp. 105–113, 2018, doi: 10.1016/j.jelechem.2018.02.014.

[3] M. López-Moreno and M. Martínez-Díaz, "A review of electrochemical sensors for the analysis of antibiotics," *TrAC Trends Anal. Chem.*, vol. 92, pp. 15–27, 2017, doi: 10.1016/j.trac.2017.05.016.

[4] Q. Liu, X. Zhang, and Z. Li, "Development of an electrochemical sensor for gentamicin detection using a multi-walled carbon nanotube modified electrode," *Sens. Actuators B Chem.*, vol. 289, pp. 567–574, 2019, doi: 10.1016/j.snb.2019.03.016.

[5] G. Tóth and O. Arogundade, "Cr-MOFs-based electrochemical sensors for biomedical applications," *Electroanalysis*, vol. 32, no. 12, pp. 2598–2610, 2020, doi: 10.1002/elan.202000441.

[6] Z. Zhang, L. Lu, and H. Chen, "Electrochemical sensors for the detection of antibiotics: From electrode materials to sensing strategies," *Electrochim. Acta*, vol. 271, pp. 495–512, 2018, doi: 10.1016/j.electacta.2018.03.022.

Phytochemical Profiling and Antimicrobial Properties of Selected Slovak Medicinal Herbs

J. Skolka[a,b], E. Ivanisova[c,d,*], J. Lakatosova[e], M. Kacaniova[f], A. Kolesarova[a,e]
[a] Institute of Applied Biology, Slovak University of Agriculture in Nitra, Tr. A. Hlinku 2, 949 76 Nitra, Slovak Republic
[b] BIOTATRY H&B, s.r.o., Východná 465, 032 32 Východná, Slovak republic
[c] Institute of Food Sciences, Slovak University of Agriculture in Nitra, Tr. A. Hlinku 2, 949 76 Nitra, Slovak Republic
[d] Food Incubator, AgroBioTech Research Centre, Slovak University of Agriculture in Nitra, Tr. A. Hlinku 2, 949 76 Nitra, Slovak Republic
[e] AgroBioTech Research Centre, Slovak University of Agriculture in Nitra, Tr. A. Hlinku 2, 949 76 Nitra, Slovak Republic
[f] Institute of Horticulture, Slovak University of Agriculture in Nitra, Tr. A. Hlinku 2, 949 76 Nitra, Slovak Republic
* eva.ivanisova@uniag.sk

Introduction

Currently, there is growing interest in exploring the effectiveness of plants in traditional medicine due to their affordability and minimal side effects. In contrast, synthetic preservatives, commonly used in food products for many years, have been linked to various health risks [1]. People in ancient times and today value traditional folk medicine, which is widely used to treat different diseases. However, there remains a lack of detailed information about the specific plants common to traditional medicine in certain countries, on their usage, and their effects [2]. This research focused on antioxidant activity, total polyphenols, flavonoids, phenolic acids, HPLC analysis of specific phenolic compounds and antimicrobial activity of some medicinal herbs from Slovak republic – goat's rue, Lady's Mantle, plantain, hyssop and golden marguerite.

Material and Methods

Medicinal herbs – goat's rue (Galega officinalis L.) – flowering plant, Lady's Mantle (Alchemilla xanthochlora L.) – leaves, plantain (Plantago lanceolata L.) – leaves, hyssop (Hyssopus officinalis L.) – flowering plant and golden marguerite (Anthemis tinctoria L.) – flowers were obtained directly from Slovak company Biotatry in dry form and bio quality, year 2023 (760 m.a.s.l.). Material were ground to an average particle size (20 mesh), suitable for preparation of extracts. All the chemicals used were of analytical grade and were purchased from Sigma-Aldrich (USA) and CentralChem (Slovak republic). Antioxidant activity was determined by DPPH method according to the method of Sanchéz-Moreno (1998) [3] with slight modifications. Trolox was used as a standard, and the results were expressed in mg/g of Trolox equivalent. Total polyphenol content was measured in accordance with Singleton and Rossi (1965) [4] using Folin-Ciocalteu reagent. Gallic acid was used as a standard and the results were expressed in mg GAE/g. Total flavonoid content was measured in accordance with Willet (2002) [5] using aluminium – chloride method. Quercetin was used as a standard and the results were expressed in mg QE/g. Total phenolic acid content was detected using Arnova reagent with modified method from Jain (2017). Caffeic acid was used as the standard and the results were expressed in mg/g caffeic acid equivalents [6]. Polyphenols composition was determined using separation gradient method RP-HPLC/DAD by Agilent 1260 Infinity high performance liquid chromatograph (Agilent Technologies, Waldbronn, Germany). Separation was achieved on a Accucore C18 column (4.6 mm × 100 mm × 2.6 μm) (Fisher Scientific, New Hampshire, USA). The mobile phase for polyphenols consisted of phosphoric acid in HPLC grade water (A) (1 ml/1000 ml); acetonitrile (B). Results were expressed in μg/g [7]. Antimicrobial activity was tested with the disc diffusion method. Altogether eleven strains of microorganisms were used, including five yeasts from genus Candida (C. glabrata CCM 8270, C. albicans CCM 8186, C. krusei CCM 8271, C. parapsylosis CCM 8260 and C. tropicalis CCM 8223), three Gram-negative bacteria (Salmonella enterica subsp. enterica CCM 3807, Escherichia coli CCM 3954 and Yersinia enterocolitica CCM 56714) and three Gram-positive bacteria (Listeria monocytogenes CCM 4699, Enterococcus faecalis CCM 4224 and Staphylococcus aureus subsp. aureus CCM 3953). All the tested strains were from the Czech Collection of Microorganisms. Results were expressed in mm.

Results and Discussion

Goat's rue showed the lowest antioxidant activity (0.95 ± 0.01 mg TEAC/g), correlating with its low levels of polyphenols (9.36 ± 0.15 mg GAE/g) and flavonoids (5.92 ± 0.09 mg QE/g), and minimal phenolic acids content (2.36 ± 0.25 mg CAE/g) (*Table 1*). In contrast, Lady's Mantle exhibited the highest antioxidant capacity (7.28 ± 0.05 mg TEAC/g), attributed to its high polyphenols (59.97 ± 4.72 mg GAE/g) and phenolic acids (10.32 ± 0.59 mg CAE/g), supporting previous research linking polyphenols to strong antioxidant activity (*Table 1*). Plantain also showed good antioxidant potential (5.01 ± 0.63 mg TEAC/g), driven by its high phenolic acids content (14.44

± 2.55 mg CAE/g), while hyssop had a moderate activity (3.87 ± 0.36 mg TEAC/g) due to a balanced presence of flavonoids (4.43 ± 0.48 mg QE/g) and phenolic acids (12.42 ± 0.95 mg CAE/g). Golden marguerite displayed a DPPH value of 5.99 ± 0.05 mg TEAC/g, where flavonoids and polyphenols likely played a more significant role than phenolic acids [8].

Table 1 Antioxidant activity, total polyphenols, flavonoids and phenolic acids in samples.

Sample	DPPH [mg TEAC/g]	Polyphenols [mg GAE/g]	Flavonoids [mg QE/g]	Phenolic acids [mg CAEg]
Goat's rue	0.95 ±0.01	9.36 ±0.15	5.92 ±0.09	2.36 ±0.25
Lady's Mantle	7.28 ±0.05	59.97 ±4.72	3.64 ±0.03	10.32 ±0.59
Plantain	5.01 ±0.63	37.63 ±0.22	2.29 ±0.12	14.44±2.55
Hyssop	3.87 ±0.36	16.08 ±0.06	4.43 ±0.48	12.42 ±0.95
Golden marguerite	5.99 ±0.05	45.13 ±0.24	12.21 ±0.46	1.77 ±0.18

DPPH – 2,2-diphenyl-1-picrylhydrazyl; TEAC – Trolox equivalent antioxidant capacity; GAE – gallic acid equivalent; QE – quercetin equivalent; CAE – caffeic acid equivalent; ± standard deviation

This study examined the variation in phenolic compounds across five plant species, revealing distinct profiles in antioxidant-related compounds. Goat's rue exhibited relatively low concentrations of most phenolics, with notable levels of 4-hydroxybenzoic acid (12.41 ± 0.51 μg/g) and sinapic acid (29.01 ± 0.03 μg/g), but generally low antioxidant potential (*Table 2*). In contrast, Lady's Mantle was rich in gallic acid (467.2 ± 5.52 μg/g) and quercetin (95.72 ± 0.41 μg/g), suggesting its strong antioxidant capacity. The absence of rosmarinic acid may reduce its overall potential, but its phenolic profile is still robust (*Table 2*). Plantain contained substantial amounts of rosmarinic acid (105.90 ± 2.86 μg/g) and gallic acid (317.81 ± 8.15 μg/g), contributing to moderate antioxidant activity. Hyssop stood out with a high concentration of rosmarinic acid (1598.71 ± 42.01 μg/g), aligning with its strong antioxidant properties (*Table 2*). Golden marguerite showed an abundance of quercetin (3237.01 ± 0.63 μg/g) and gallic acid (751.12 ± 0.05 μg/g), positioning it as a potent source of antioxidants. The relatively high levels of trans-p-coumaric acid (53.61 ± 0.01 μg/g) and sinapic acid (5.13 ± 0.63 μg/g) further support its antioxidant potential.

Table 2 Concentrations of selected phenolics in samples determined by HPLC-DAD

Sample / Compounds [μg/g]	Goat's rue	Lady's Mantle	Plantain	Hyssop	Golden marguerite
4-hydroxybenzoic acid	12.41 ±0.51	195.51 ±2.74	17.71 ±1.12	53.71 ±0.11	7.33 ±0.01
Rosmarinic acid	97.82 ±0.01	n. d.	105.90 ±2.86	1598.71 ±42.01	11.91 ±0.05
Sinapic acid	29.01 ±0.03	128.65 ±0.98	27.11 ±0.02	28.11 ±0.54	5.13 ±0.63
***trans*-cinnamic acid**	7.91 ±0.22	1.32 ±0.05	2.21 ±0.01	8.63 ±0.19	16.71 ±0.36
Gallic acid	37.32 ±0.58	467.2 ±5.52	317.81 ±8.15	50.13 ±7.76	751.12 ±0.05
***trans*-caffeic acid**	6.22 ±0.11	9.12 ±0.29	13.32±2.61	38.31 ±0.88	4.73 ±0.05
***trans-p*-coumaric acid**	13.52 ±0.14	49.5 ±0.27	9.41 ±0.18	3.22 ±0.02	53.61 ±0.01
Kaempferol	9.93 ±0.13	n. d.	8.11 ±0.04	3.95 ±0.12	4.22 ±0.05
Quercetin	13.61 ±0.02	95.72 ±0.41	14.32 ±0.26	38.21 ±0.78	3237.01 ±0.63
Resveratrol	3.22 ±0.01	1.52 ±0.14	1.22 ±0.03	4.91 ±0.05	12.84 ±0.36
Rutin	56.11 ±0.25	n. d.	20.21 ±0.32	25.82 ±0.49	31.97 ±0.36

n.d. – not detected; ± standard deviation

Among the bacterial strains tested, L. monocytogenes was the most susceptible, particularly to Lady's Mantle and goat's rue, both showing inhibition zones around 10.3 mm (*Table 3*). This aligns with previous findings that L. monocytogenes is highly sensitive to phenolic compounds commonly found in herbal extracts [9]. Plantain also demonstrated strong antibacterial activity against S. enterica and C. parapsilosis, with inhibition zones of 10.33 mm and 10.67 mm respectively, suggesting broad-spectrum efficacy. Interestingly, golden marguerite although less effective against most bacterial strains, showed the highest antifungal activity against C. albicans and C. glabrata (10.33 mm) (*Table 3*). This supports earlier findings on the antifungal potential of flavonoid-rich extracts from the Asteraceae family [10]. Conversely, hyssop generally exhibited the weakest antimicrobial activity, with inhibition zones consistently under 6 mm, except against Y. enterocolitica (8.33 mm), indicating limited but selective action (*Table 3*).

Table 3 Antimicrobial activity of tested samples

Sample Inhibition zone [mm]	Goat's rue	Lady's Mantle	Plantain	Hyssop	Golden marguerite
E. faecalis	8.33 ±0.11	5.33 ±0.51	8.33 ±0.11	4.67 ±0.11	5.67 ±0.11
S. aureus	7.67 ±0.23	6.67 ±0.52	7.67 ±0.52	5.67 ±0.03	5.67 ±0.12
L. monocytogenes	10.30 ±0.58	10.33 ±0.58	7.67 ±0.23	5.67 ±0.11	5.33 ±0.14
S. enterica	7.67 ±0.25	8.67 ±0.52	10.33 ±0.11	5.67 ±0.19	2.67 ±0.51
E. coli	5.67 ±0.11	8.67 ±0.33	7.67 ±0.23	7.62 ±0.13	8.67 ±0.05
Y. enterocolitica	5.82 ±0.12	8,68 ±0.11	5.67 ±0.13	8.33 ±0.58	5.67 ±0.05
C. albicans	2.33 ±0.12	8.33 ±0.51	8.33 ±0.18	4.33 ±0.02	10.33 ±0.58
C. glabrata	7.61 ±0.13	7.68 ±0.22	9.67 ±0.04	5.67 ±0.12	10.33 ±0.21
Candida krusei	3.33 ±0.02	7.33 ±0.11	7.33 ±0.26	n. d.	7.67 ±0.22
C. parapsylosis	5.67 ±0.21	8.67 ±0.14	10.67 ±0.12	5.33 ±0.13	n. d.
C. tropicalis	3.67 ±0.25	7.33 ±0.23	8.67 ±0.11	6.67 ±0.58	2.33 ±0.21

mm - millimetre; n.d. – not detected; ± standard deviation

Conclusion

The obtained results highlight the significant variation in antioxidant and antimicrobial properties among the five investigated plant species, closely linked to their distinct phenolic profiles. Lady's Mantle demonstrated the highest antioxidant and broad antimicrobial activities, attributed to its rich content of polyphenols, gallic acid, and quercetin. In contrast, goat's rue showed the lowest antioxidant potential, correlating with its minimal phenolic content, though it exhibited moderate antibacterial activity against Listeria monocytogenes. Plantain and golden marguerite emerged as promising sources of specific phenolics, contributing to their moderate antioxidant and notable antimicrobial effects, particularly against fungal strains. Hyssop, despite high levels of rosmarinic acid, displayed only moderate antioxidant capacity and weak antimicrobial activity. The findings reinforce the role of phenolic composition in determining the biological activity of medicinal plants and support their potential application in natural antioxidant and antimicrobial formulations.

Acknowledgements

The work was supported by The Ministry of Education, Research, Development and Youth of the Slovak Republic projects VEGA 1/0620/24 and the Operational Program Integrated Infrastructure funded this research within the project titled "Demand-driven research for sustainable and innovative food, Drive4SIFood 313011V336," cofinanced by the European Regional Development Fund.

References

[1] Karpavičienė, B. 2022. Traditional Uses of Medicinal Plants in South-Western Part of Lithuania. *Plants*, vol. 11, pp. 2093-2108. https://doi.org/ 10.3390/plants11162093.

[2] Obakiro, S.B., Kiprop, A., Kowino, I., Kigondu, E., Odero, M.P., Omara, T. and Bunalema, L. 2020. Ethnobotany, ethnopharmacology, and phytochemistry of traditional medicinal plants used in the management of symptoms of tuberculosis in East Africa: a systematic review. *Tropical Medicine and Health*, vol. 48, pp. 68-76. https://doi.org/10.1186/s41182-020-00256-1.

[3] Sánchés-Moreno, C., Larrauri, A. and Saura-Calixto, F. 1998. A procedure to measure the antioxidant efficiency of polyphenols. *Journal of Science and Food Agriculture*, vol. 76, pp. 270–276.

[4] Singleton, V.L. and Rossi, J.A. 1965. Colorimetry of total phenolics with phosphomolybdic-phosphotungstic acid reagents. *American Journal of Enology and Viticulture*, vol. 16, pp.144–158.

[5] Willett, W.C. 2002. Balancing life-style and genomics research for disease prevention. *Science*, vol. 80, pp. 695–698.

[6] Jain, R., Rao, B. and Tare, A.B. 2017. Comparative analysis of the spectrophotometry based total phenolic acid estimation methods. *Journal of Analytical Chemistry*, vol. 72, pp. 972–976. https://doi.org/ 10.1134/S106193481709009X.

[7] Kulig, D., Matysiak, M., Baldovska, S., Stefanikova, J., Maruniakova, N., Mnahoncakova, E., Arvay, J., Galbavy, D. and Kolesarova, A. 2019. Screening of polyphenolic compounds from traditional medicinal herbs. *Journal of Microbiology, Biotechnology and Food Sciences*, vol. 9(Special issue), pp. 487–491.

[8] Sulman, I., Hussain, H., Khan, G.A. and Marwat, I. 2025. Antioxidant properties of selected medicinal plants. *Journal of Medicinal Plants*, vol. 45, no. 3, pp. 321-329.

[9] Burt, S. 2004. Essential oils: their antibacterial properties and potential applications in foods—a review. *International Journal of Food Microbiology*, vol. 94, pp. 223–253. https://doi.org/10.1016/j.ijfoodmicro.2004.03.022

[10] Cowan, M.M. 1999. Plant products as antimicrobial agents. *Clinical Microbiology Reviews*, vol. 12, pp. 564–582. https://doi.org/10.1128/CMR.12.4.564

Comparative Analysis of CuO 550 and CuO 600 Fiber-Based Electrochemical Sensors for Insulin Detection

L. Slabejova[a,*], I. Sisolakova[a], E. Mudra[b], J. Shepa[a]
[a] Department of Physical Chemistry, Pavol Jozef Šafárik Slovak Republic University in Košice, Moyzesova 11, 040 01 Košice,
[b] Institute of Materials Research, Slovak Academy of Sciences, Watsonova 47, 040 01 Košice, Slovak Republic
* laura.slabejova@upjs.sk

Introduction

Insulin is a small polypeptide hormone very important for the human body as it regulates concentration of glucose in blood [1, 2]. The protein´s structure is divided into two chains and it contains together 51 amino acids [3]. The normal concentration of insulin in blood is 25 mlU/L. Low blood level of insulin is considered as very dangerous as it causes very common disease, diabetes mellitus [4]. Measuring its concentration in the blood provides a crucial tool for diagnosing this disease, but also insulinomas, and a range of metabolic disorders.
For insulin determination, carbon electrodes are often used with different types of modification [5]. These modifications are supposed to improve sensor´s properties and it is often achieved by metal or oxide nanoparticles. Metal ions such as Cu (II) or Mn (II) interact with amino acids in insulin, such as tyrosine or tryptophane. This interaction can cause changes in electrochemical behaviour of the sensors, which can be profiting for enhancing signal determination.
This work focuses on comparison of electrochemical sensors based on copper oxide fibers, CuO 550 and CuO 600, to find the best sensor modification for insulin detection.

Experiment and measurements

For all experiments in this work, were used carbon electrodes manufactured using screen printing (SPCE 11L, DropSens, Metrohm), which surfaces were modified with a CuO 550 and CuO 600.
Preparation of CuO 550 and CuO 600 (*Figure 1*) was performed in collaboration with colleagues from SAS. They prepared this material from waste contacts of a dual in-line RAM module using a multi-stage hydrometallurgical recycling process. Morphology of prepared CuO fibers was then characterized by scanning electron microscopy (SEM).
Modification of both types of electrodes was the same and it includes a few steps. First, the CuO fibers were dispersed in 10 ml of ethanol diluted with water in a 1:1 ratio and then treated with ultrasound for 20 minutes to achieve their homogeneous dispersion. From the obtained suspension, 1 µl was applied to the surface of each SPCE in four separate steps, with room-temperature drying following every application. Electrodes prepared this way were used to study mechanism of insulin oxidation using cyclic voltammetry (CV) (*Figure 1*).

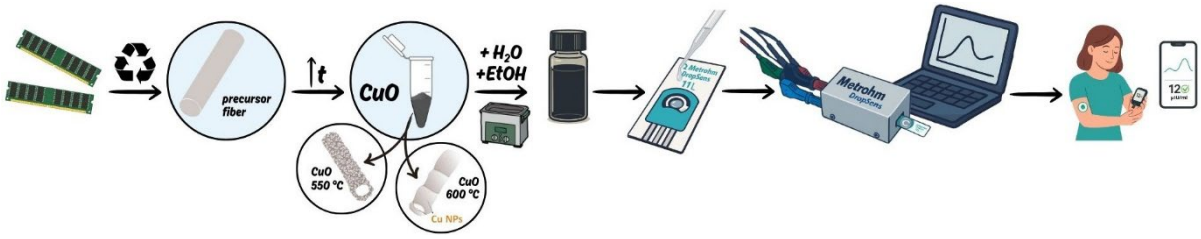

Figure 1 Scheme of experiment course.

Results and discussion

First, the morphology of the prepared CuO fibers was studied by SEM analysis (*Figure 2* and *3*). The results show a significant difference between fibers CuO 550 and CuO 600. Both materials consist of grains aggregated into tunnel-like structures. Grains of CuO 600 were 1 µm, but grains of CuO 550 were just 120 nm.

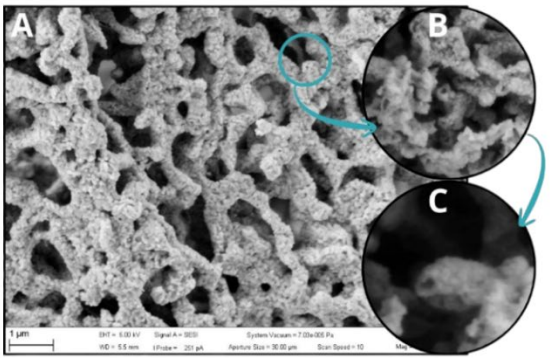

Figure 2 SEM images of CuO 550 fibers (magnification: A – 30 000x, B – 60 000x, C – 120 000x).

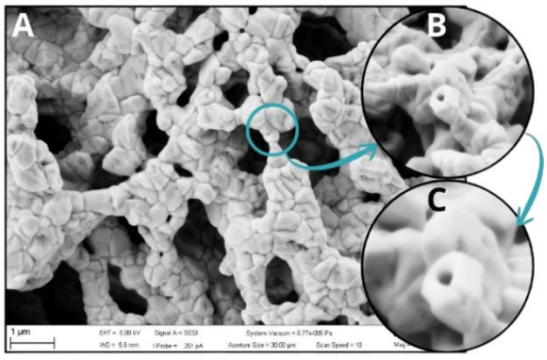

Figure 3 SEM images of CuO 600 fibers (magnification: A – 30 000x, B – 60 000x, C – 120 000.

To study the difference of these fibers, a series of measurements was conducted. Very important for the prepared sensors is its electrochemical response. This measurement was carried out using CV at a scan rate of 100 $mV.s^{-1}$. For each measurement, 60 µl of electrolyte (PBS solution (pH = 7) and PBS solution (pH = 7) containing 10 µM insulin) were used. The results are shown in *Figure 4*. In both cases on the SPCE/CuO-Cu voltametric curve in the presence of insulin, an oxidation peak appears at a potential of 0,46 V, which is attributed to the oxidation of insulin. In the case of CuO 550, the electrochemical response was much weaker.

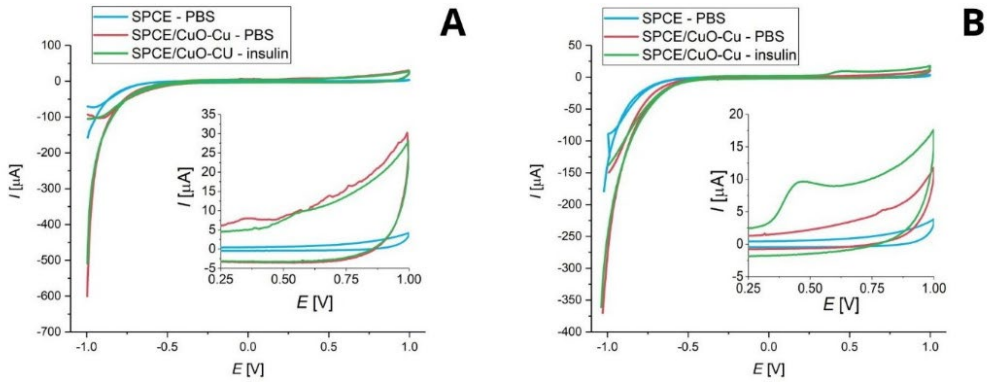

Figure 4 Cyclic voltammetry in PBS (pH=7) and 10 µM insulin in PBS (pH=7) on clean electrodes and CuO-modified electrodes at a scan rate of 100 $mV.s^{-1}$ (A - CuO 550 fibers; B - CuO 600 fibers).

After confirming that prepared sensors can detect insulin, further measurements were conducted in order to improve the sensitivity and stability of the system. Influence of acidic, neutral and alkalic environments, as well as different scan rates, was studied using CV.

The influence of pH on the electrochemical oxidation of insulin was investigated across a range of 1 – 12. Desired pH levels were adjusted by controlled addition of HCl or NaOH. CV measurements were performed at a scan rate of 100 $mV.s^{-1}$, using 60 µl of electrolyte per experiment. As shown in *Figure 5*, acidic conditions reduced stability of insulin, while in alkaline environments voltametric responses remained consistent and reproducible. These results indicate that higher pH values are more suitable for electrochemical studies, offering greater stability and reduced interference from chloride ions [6].

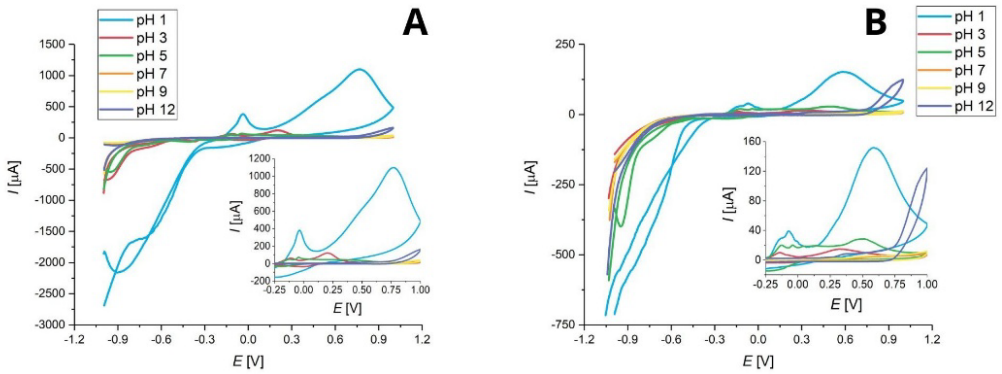

Figure 5 Cyclic voltammetry for 10 µM insulin in PBS with different pH values at a scan rate of 100 mV.s^{-1} (A - CuO 550 fibers, B - CuO 600 fibers).

The effect of scan rate (25 – 300 mV.s^{-1}) on the shape and intensity of voltametric peaks was examined. As illustrated in *Figure 6*, the current response increased with higher polarization rates. However, the most well-defined and reproducible signals were obtained at the lowest scan rate of 25 mV.s^{-1}.

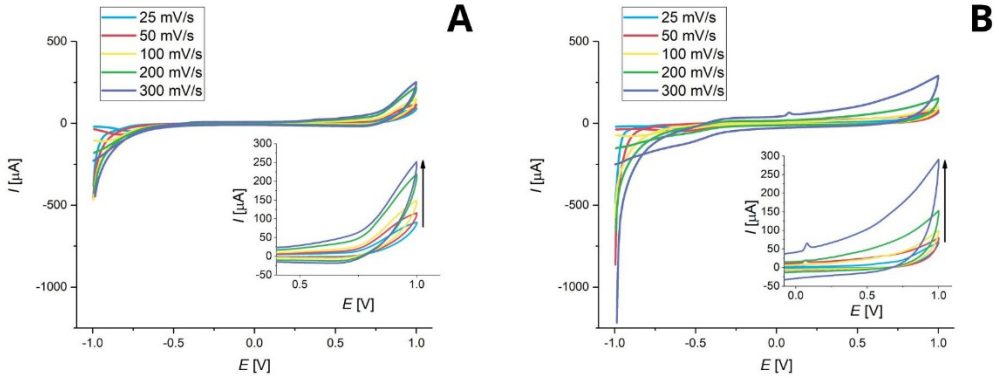

Figure 6 Cyclic voltammogram of 10 µM insulin in PBS on SPCE/CuO-Cu at different scan rates from 25 mV.s^{-1} to 300 mV.s^{-1} (A – CuO 550 fibers, B – CuO 600 fibers).

Conclusions

Screen-printed carbon electrodes were successfully modified with CuO 550 and CuO 600 fibers obtained from recycled dual in-line RAM module contacts. The electrochemical characterization revealed that the CuO modification significantly improves the electrodes ´responsiveness to insulin. Observed changes in voltametric signals upon insulin addition indicate interactions between copper and the insulin molecules [7], affecting the electrochemical behaviour of the system. This method offers a direct, eco-friendly, and effective approach for insulin detection, with potential applicability in practical sensor devices.

Acknowledgements

This work was funded by the EU NextGenerationEU through the Recovery and Resilience Plan of the Slovak Republic under project no. 09-I05-03-V02-00047.

References

[1] S. Ebrahimiasl, E. Fathi, and M. Ahmad, "Electrochemical Detection of Insulin in Blood serum using Ppy/GF Nanocomposite Modified Pencil Graphite Electrode," *Nanomedicine Research Journal,* vol. 3, no. 4, pp. 219-228, 2018, doi: 10.22034/nmrj.2018.04.006.

[2] R. Orinakova, F. Chovancová, I. Šišoláková, and J. Shepa, "Study of Insulin Electrochemical Reaction Mechanism on Modified Ni-Chit/SPCE Electrode," *ECS Meeting Abstracts,* vol. MA2024-02, no. 64, pp. 4288-4288, 2024, doi: 10.1149/MA2024-02644288mtgabs.

[3] I. Šišoláková *et al.*, "Comparison of Insulin Determination on NiNPs/chitosan- MWCNTs and NiONPs/chitosan-MWCNTs Modified Pencil Graphite Electrode," *Electroanalysis,* vol. 31, no. 1, pp. 103-112, 2018, doi: 10.1002/elan.201800483.
[4] J. Shepa *et al.*, "NiO Nanoparticles for Electrochemical Insulin Detection," *Sensors (Basel),* vol. 21, no. 15, Jul 26 2021, doi: 10.3390/s21155063.
[5] I. Šišoláková *et al.*, "Electrochemical determination of insulin at CuNPs/chitosan-MWCNTs and CoNPs/chitosan-MWCNTs modified screen printed carbon electrodes," *Journal of Electroanalytical Chemistry,* vol. 860, 2020, doi: 10.1016/j.jelechem.2020.113881.
[6] J. Hovancová *et al.*, "Nanostructured Gold Microelectrodes for Non-enzymatic Glucose Sensor," *Electroanalysis,* vol. 31, no. 9, pp. 1680-1689, 2019, doi: 10.1002/elan.201900163.
[7] Z. Rong *et al.*, "Electrochemical investigation on the complexes of Cu(II), Mn(II), Ca(II), and Mg(II) with insulin," *Journal of Molecular Structure,* vol. 1335, 2025, doi: 10.1016/j.molstruc.2025.141992.

Development and Characterization of Glycerol–Citrate Polyesters Modified with Bioactive Crosslinkers and Composite Strategies

T. Sopcak[a,*], L. Medvecky[a], T. Csanadi[a], J. Brus[b], M. Urbanova[b], M. Giretova[a], R. Stulajterova[a], F. Kromka[a], M. Faberova[a]

[a] Institute of Materials Research of SAS, Watsonova 47, 04001 Kosice, Slovak Republic

[b] Institute of Macromolecular Chemistry of the Czech Academy of Sciences, Heyrovskeho nam. 2, 162 06, Prague 6, Czech Republic

* tsopcak@saske.sk

Bioinspired and biodegradable polymers have attracted enormous interest in biomedical science and engineering due to their desirable properties, such as biocompatibility, tunable mechanical and biological performance, and structural versatility associated with suitable degradation. However, the development of an ideal material that fully meets clinical demands still remains a significant challenge. Polyester-type scaffolds are particularly attractive in tissue engineering, since their ester bonds undergo controlled hydrolytic cleavage, allowing gradual resorption in vivo, while their mechanical and degradation behavior can be tuned through composition and network design [1].

Citric acid-based polyesters have recently gained increasing interest, as citric acid is a naturally occurring metabolite involved in human biochemical pathways, including the Krebs cycle. When combined with other essential polyols, such as glycerol, it forms a biodegradable macromolecular glycerol–citrate (GCA) polyester with certain biofunctional properties [2]. However, despite their many favorable properties, several drawbacks remain associated with the use of pure glycerol–citrate polyesters. The most critical issues arise from their relatively rapid degradation, which leads to a local decrease in pH that may trigger undesirable tissue–material responses. To overcome these shortcomings, a variety of modification strategies have been investigated within the family of polyol–citrate polyesters. These include the incorporation of multifunctional additives, blending with other biodegradable polymers, and surface functionalization. Such approaches are designed to stabilize the polyester network and tailor its degradation profile, while other modifications target enhanced mechanical strength, improved antioxidant or anti-inflammatory activity, and increased bioactivity to better support tissue regeneration [3,4]. Among this family, poly(1,8-octanediol citrate) (POC) is the most extensively studied representative, and its structure has traditionally been modified with various molecules, such as urethane linkages, silica grafts, or bioactive compounds including vitamin C and curcumin, to improve its mechanical strength, biodegradability, and biological functionality. In contrast, glycerol–citrate polyesters remain less explored, despite their promising hydrophilic character and structural versatility, offering ample opportunities for novel functionalization approaches.

In this context, our research group has focused on GCA polyesters, aiming to exploit their hydrophilic and structurally versatile network for further functionalization. In particular, we have investigated dual crosslinking of GCA with tannic acid (TA) and boric acid (B) as a potential strategy to enhance stability, mechanical performance, and biological functionality (*Figure 1*). Both crosslinkers may bring complementary functionalities into the GCA network. Tannic acid, a natural polyphenol rich in hydroxyl groups, provides multiple binding sites and is well known for its antioxidant, anti-inflammatory, and antimicrobial properties. Boric acid, on the other hand, is able to form dynamic ester bonds with polyols, introducing additional crosslinking points that contribute to structural stability and tunable degradation behavior. When combined, these two additives are expected to synergistically enhance the physicochemical and biological performance of GCA, offering improved mechanical resilience together with bioactive functionality. The influence of both additives was systematically evaluated using a comprehensive set of characterization techniques. Structural and chemical features were analyzed by solid-state NMR, FTIR spectroscopy, and XRD, while thermal stability was examined by DSC/TGA technique. Morphological aspects were investigated by SEM. Mechanical performance was assessed through complementary methods, including macroscopic tensile testing, nanoindentation, and ultrasonic measurements. In addition, biological evaluation involved in vitro tests with osteoblastic cells to examine cytocompatibility and antibacterial assays against *Staphylococcus aureus* and *Escherichia coli* to assess antimicrobial activity.

The presentation will provide an overview of existing modification approaches, summarize our recent functionalization strategies, and discuss preliminary characterization of the modified GCA networks, highlighting how these modifications influence their overall performance and potential for biomedical applications.

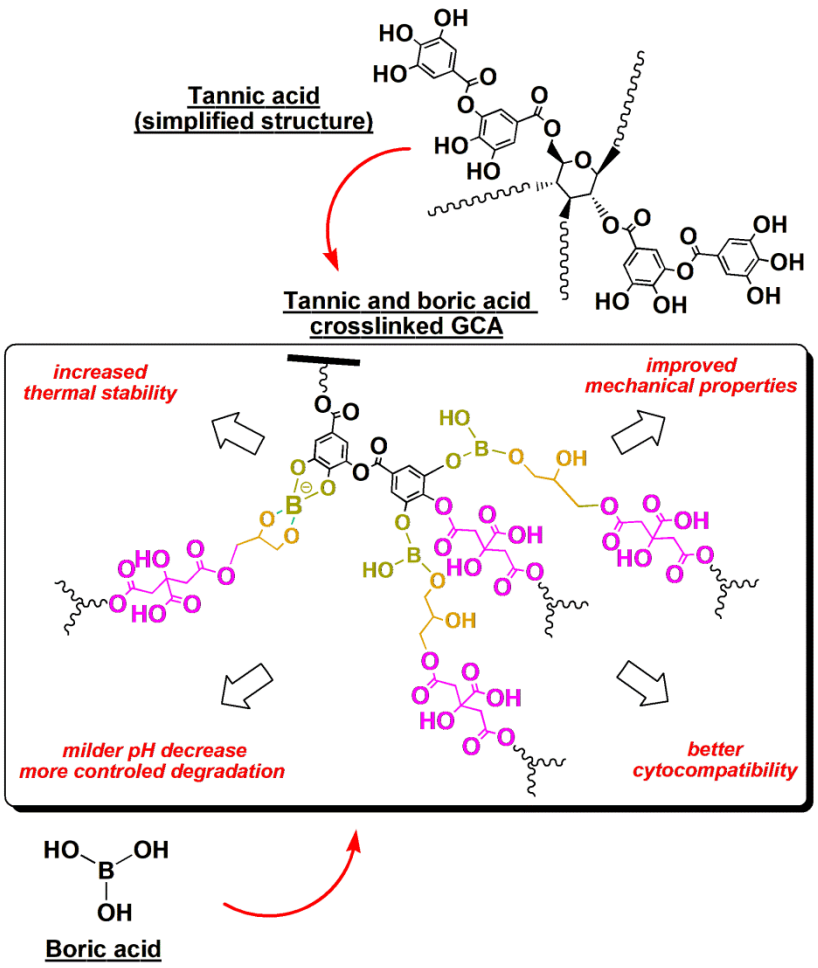

Figure 1 Schematic illustration of the tannic and boric acid crosslinked GCA and its improved properties.

Acknowledgements
This work was funded by the EU NextGenerationEU through the Recovery and Resilience Plan for Slovakia under the project No. 09I03-03-V04-00133.

References
[1] V. Fakhri, C.-H. Su, M. Tavakoli Dare, M. Bazmi, A. Jafari, V. Pirouzfar, "Harnessing the power of polyol-based polyesters for biomedical innovations: synthesis, properties, and biodegradation" *J. Mater. Chem. B*, vol. 11, pp. 9597–9629, 2023, doi:10.1039/D3TB01186K.
[2] B. Tisserat, G.W. Selling, J.A. Byars, A. Stuff, "Instrumental Physical Analysis of Microwaved Glycerol Citrate Foams,"*J. Polym. Environ*., vol. 20, pp. 291–298, 2012, doi:10.1007/s10924-011-0376-3.
[3] R. van Lith, E.K. Gregory, J. Yang, M.R. Kibbe, G.A. Ameer, "Engineering biodegradable polyester elastomers with antioxidant properties to attenuate oxidative stress in tissues,"*Biomaterials*, vol. 35, pp. 8113–8122, 2014, doi:10.1016/j.biomaterials.2014.06.004.
[4] T. Leng, L. Zhang, J. Ma, X. Qu, B. Lei, "Intrinsically bioactive multifunctional Poly(citrate-curcumin) for rapid lung injury and MRSA infection therapy," *Bioact. Mater.*, vol. 41, pp. 158–173, 2024, doi:10.1016/j.bioactmat.2024.07.002.

[5] A.-K. Koopmann, C. Schuster, J. Torres-Rodríguez, S. Kain, H. Pertl-Obermayer, A. Petutschnigg, N. Hüsing, "Tannin-Based Hybrid Materials and Their Applications: A Review," *Molecules*, vol. 25, 4910, 2020, doi:10.3390/molecules25214910.
[6] D. Efhamisisi, M.-F. Thevenon, Y. Hamzeh, A.-N. Karimi, A. Pizzi, K. Pourtahmasi, "Induced Tannin Adhesive by Boric Acid Addition and Its Effect on Bonding Quality and Biological Performance of Poplar Plywood,"*ACS Sustain. Chem. Eng.,* vol. 4, pp. 2734–2740, 2016, doi:10.1021/acssuschemeng.6b00230.

9th International Conference on Novel Materials Fundamentals and Applications
High Tatras, 12.10.-15.10.2025

Engineering High-Entropy Oxides to Conquer Polysulfide Shuttling in Li-S Batteries

A. Strakova Fedorkova[a,*], M. Asim[b], V. Niscakova[a]
[a] Department of Physical Chemistry, Faculty of Sciences, Pavol Jozef Safarik University in Košice, Moyzesova 11, 04154, Kosice, Slovak Republic
[b] Department of Chemistry, Quaid-i-Azam University, Islamabad 45320, Pakistan
* andrea.fedorkova@upjs.sk

Abstract
Lithium-sulfur batteries (LSBs) are highly promising candidates for next-generation energy storage, offering significantly higher theoretical specific capacity (1675 mAh/g) and energy density (up to 2800 Wh/L) - nearly five times that of conventional lithium-ion batteries (LIBs). Furthermore, the use of low-cost and environmentally friendly sulfur cathodes positions LSBs as a viable long-term alternative to LIBs [1]. However, the practical application of LSBs is hindered by challenges primarily related to the complex multi-electron redox process. During operation, the conversion of sulfur into soluble lithium polysulfides (LPSs) leads to their dissolution and diffusion (the "shuttle effect"), resulting in the loss of active material, the formation of insulating layers on electrodes, and progressive capacity degradation. To address these issues, extensive research has focused on incorporating functional catalysts into LSB cathodes to immobilize LPSs and enhance electrochemical performance. While initial efforts utilized porous carbon hosts, a more effective strategy involves polar transition metal oxides (TMOs), which chemically immobilize LPSs through the formation of metal-sulfur (M-S) bonds. Building upon this, multi-metal oxides, including emerging high-entropy oxides (HEOs), have garnered attention. HEOs, which feature five or more cationic species, offer exceptional compositional diversity and synergistic interactions that create abundant active sites for the effective anchoring and catalytic conversion of LPSs, thereby overcoming the limitations of single-metal and carbon-based materials.

Discussion
Scanning Electron Microscopy (SEM) analysis of both High-Entropy Oxide (HEO) compositions (*Figure 1*) revealed distinct, multi-scale microstructural characteristics. At low magnification (100 µm scale), both materials appeared as irregularly shaped particles, suggesting either particle agglomeration or a lack of well-defined crystalline facets. At higher magnification (nanoscale), the microstructure displayed uniformly distributed spherical nanoparticles with an average size of 30 to 40 nm. This spherical shape at higher resolution suggests that the particles nucleated and grew under conditions, specifically high-temperature calcination, that favored the isotropic minimization of surface energy. The irregular geometry observed at lower magnifications is likely the result of this more homogeneous spherical phase becoming agglomerated or incompletely sintered into larger clusters. Energy-Dispersive X-ray Spectroscopy (EDS) was performed on a selected region of the HEO-F material (*Figure 1 a*) to confirm its elemental composition. The resulting EDS spectrum (*Figure 1 b*), along with the pie chart showing the concentration percentages (*Figure 1 c*), verified the successful incorporation and presence of all constituent metal elements in the final HEO-F composition.

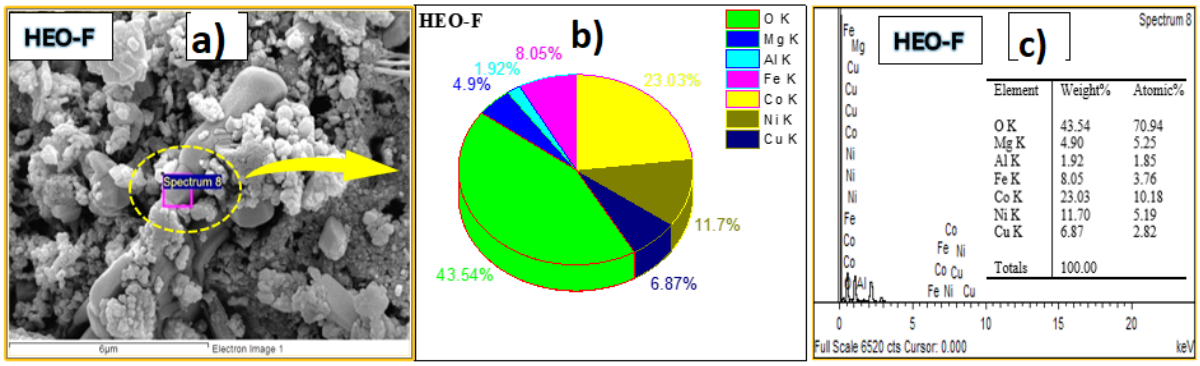

Figure 1 SEM image of HEO-F (a) selected region from SEM image of HEO-F for elemental analysis, (b) pie chart representing the % composition of all constituents in HEO-F composition, and (c) EDS mapping of HEO-F.

The CV profile recorded at 0.1 mV/s confirmed the characteristic Li-S redox behavior, displaying two clear reduction peaks and one broad, overlapping oxidation peak. The first reduction peak, located at ~2.36 V (vs. Li^+/Li), corresponds to the conversion of solid elemental sulfur (S_8) into soluble long-chain lithium polysulfides (Li_2S_n, $4 \leq n \leq 8$), marking a solid-to-liquid phase transition. The second reduction peak, at ~2.05 V, signifies the further reduction of these polysulfides into insoluble short-chain Li_2S_2/Li_2S, completing the liquid-to-solid transformation. Conversely, the merged oxidation peak during the charging sweep indicates the reverse process: the sequential oxidation of solid Li_2S back to liquid polysulfides, followed by their final conversion to solid sulfur. These sequential solid-liquid-solid phase transitions are intrinsic to the Li-S system, confirming the synthesized HEO/carbon-sulfur cathodes successfully facilitate the characteristic redox reactions with excellent electrochemical reversibility and no detectable side reactions [2,3]. To quantitatively assess the reaction kinetics and electrocatalytic activity, Tafel analysis was performed using the slopes derived from the two reduction peaks and the main oxidation peak in the CV profiles. A lower Tafel slope indicates faster reaction kinetics. The uniformly low Tafel slopes for both reduction and oxidation confirm HEO's exceptional bidirectional electrocatalytic activity, which effectively accelerates the reversible conversion between lithium polysulfides (LiPSs) and lithium sulfide (Li_2S) during battery cycling.

Conclusion

We successfully synthesized novel High-Entropy Oxides (HEOs) containing multiple cations (Al, Mg, Fe, Cu, Ni, Co) using a sol-gel approach. These HEOs, which featured cubic (rock-salt/spinel) structures with confirmed uniform composition, exhibited exceptional bidirectional electrocatalytic activity for the sulfur redox reactions essential to Lithium-Sulfur (Li-S) batteries. The unique multi-cation composition of the HEOs generated high configurational entropy and abundant oxygen vacancies. This design created numerous adsorption sites that effectively anchored soluble lithium polysulfides (LPSs) through strong Li-O and M-S chemical bonding. Electrochemical studies confirmed that the HEO cathodes played a dual catalytic role, accelerating the crucial interconversion processes among solid S_8, soluble LPSs, and solid Li_2S. This catalytic action resulted in superior electrochemical performance:

- High Initial Specific Capacity: ~1062 mAh/g for HEO-A and ~997 mAh/g for HEO-F at 0.1C.
- Excellent Cycling Stability: After 200 cycles at 0.5C, HEO-A maintained 648 mAh/g, and HEO-F maintained 416.8 mAh/g with an ultralow decay rate of just 0.095% per cycle.

Both cathodes also demonstrated excellent rate capability across a wide range (0.1–2C), highlighting their potential as high-performance sulfur hosts. This work establishes HEOs as promising materials for leveraging unique charge compensation and catalytic mechanisms in advanced energy storage [4].

Acknowledgements

This work was funded by the EU NextGenerationEU through the Recovery and Resilience Plan for Slovakia under the project SUNFLOWERS No. 09I02-03-V01-00022.

References

[1] D. Zalka, A. Vizintin, A. Maximenko, Z. Pászti, Z. Dankházi, K. Hegedüs, L. S. Shankar, R. Kun, K. Saksl, A. Straková Fedorková, and P. Jóvári, "Binder makes it run—how carrageenan boosts the performance of Li-S batteries," *Commun. Mater.*, vol. 6, no. 1, p. 17, 2025

[2] B. Liang, Y. Ai, Y. Wang, C. Liu, S. Ouyang, and M. Liu, "Spinel-type (FeCoCrMnZn)3O4 high-entropy oxide: Facile preparation and supercapacitor performance," *Materials*, vol. 13, no. 24, p. 5798, 2020.

[3] J. Sushil, A. Kumar, A. Gautam, and M. I. Ahmad, "High entropy phase evolution and fine structure of five component oxide (Mg, Co, Ni, Cu, Zn) O by citrate gel method," *Mater. Chem. Phys.*, vol. 259, p. 124014, 2021.

[4] M. Asim, A. Hussain, V. Niščáková, A. S. Fedorková, N. Király, and N. K. Janjua, "Unlocking the potential of rock salt and spinel high entropy oxides as cathode material for high-energy lithium-sulfur batteries," *J. Energy Storage*, vol. 133, p. 118083, 2025.

9th International Conference on Novel Materials Fundamentals and Applications
High Tatras, 12.10.-15.10.2025

Hydrogen Evolution on Transition Metal Phosphides: Electrochemical Performance and Activation Energy Study

M. Streckova[a,*], A Guboova[a], A. Fedorockova[b], C. Bera[a]
[a] Institute of Materials Research, Slovak Academy of Sciences, Watsonova 47, 040 01, Kosice, Slovak Republic.
[b] Faculty of Materials, Metallurgy and Recycling, Technical University of Kosice, Letna 9, 042 00 Kosice, Slovakia.
* mstreckova@saske.sk

Abstract
The future competitiveness of hydrogen as a fuel depends on the development of efficient, low-cost, and widely available catalysts. Transition metal phosphides, especially in multimetallic forms, have emerged as promising alternatives to platinum-based catalysts for use in electrolyzers and fuel cells. In this study, we report for the first time the use of the Spray Drying Method (SDM) as a scalable and user-friendly approach for producing transition metal phosphides as catalysts for the hydrogen evolution reaction (HER). Three MoFeP-based catalysts, modified with Co and Ni as third elements, were synthesized and evaluated electrochemically in 1 M KOH. Among them, MoFeCoP showed the best performance, with a low overpotential (η_{10}) of -285 mV and a Tafel slope of 83 mV dec^{-1}, along with strong long-term stability. Additionally, both MoFeNiP and MoFeCoP exhibited high double-layer capacitance values, indicating large surface areas and low activation energy for HER key attributes for efficient hydrogen production and practical application.
An exceptionally low activation energy, comparable to that of commercial noble-metal-based catalysts, was observed, emphasizing the high intrinsic activity of the synthesized trimetallic phosphides. This outstanding characteristic highlights their potential as cost-effective alternatives to noble-metal electrocatalysts for large-scale water electrolysis. The schematic illustration of the experimental procedure and results is provided in *Figure 1*.

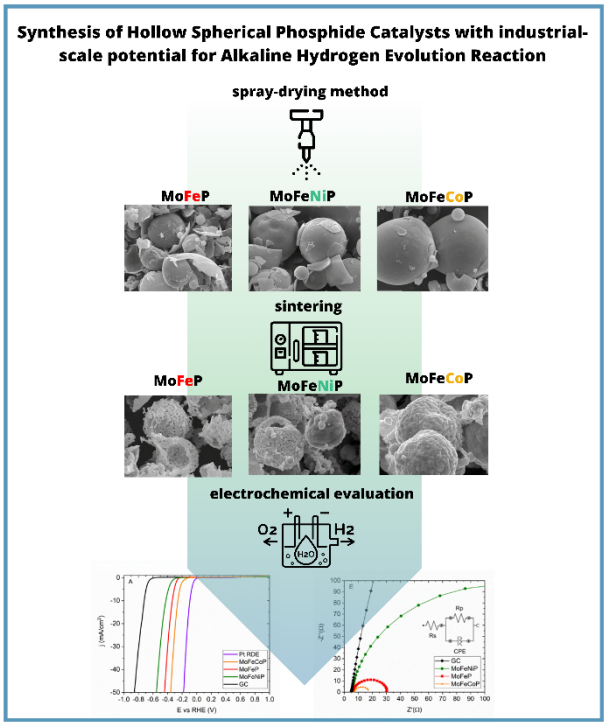

Figure 1 Scheme or MoFeP, MoFeNiP and MoFeCoP hollow sphere preparation.

Experimental

Material Preparation

Phosphide precursors were prepared using ammonium phosphate dibasic, iron(III) nitrate, cobalt(II) nitrate, nickel(II) nitrate, ammonium molybdate, and citric acid (all Centralchem, ≥98%). For electrochemical testing, 1 M KOH (Centralchem, 85%) was used as the electrolyte, with Pt/C and IrO_2 (Sigma-Aldrich) as reference catalysts. MoFeP, MoFeCoP, and MoFeNiP hollow spheres were synthesized via spray drying of aqueous solutions containing metal salts and citric acid (CA) at a molar ratio of CA:Fe:Mo:(Ni):(Co):P = 2:0.5:0.5:(0.5):(0.5):0.5, dissolved in 250 mL of 0.4 M CA.

The solution was spray-dried using a TEFIC TFS-2L system at 300 °C inlet temperature. Drying conditions were optimized for minimal residual water, with a cyclone fan speed of 70% and a suction flow rate of 30% (0.83 mL·min^{-1}). The resulting powders were heat-treated at 650 °C in a reducing H_2 atmosphere (66 mL·min^{-1}).

Electrochemical Characterization

Electrochemical tests were conducted in 1 M KOH using a three-electrode setup with a Vionic potentiostat and Autolab Intello software. A glassy carbon rotating disk electrode (5 mm, 500 RPM) coated with catalyst ink served as the working electrode. Ag/AgCl (3 M KCl) and Pt foil were used as reference and counter electrodes, respectively, while a 3 mm Pt RDE was used as a HER standard. Catalyst ink was prepared by mixing 750 µL isopropanol, 250 µL water, 20 µL Nafion (5 wt.%), and 50 mg catalyst. A 20 µL drop was applied to the GC electrode. Potentials were converted to RHE and corrected for 80% iR drop. Electrochemical techniques included LSV, CV, EIS, and chronoamperometry. Current densities were normalized to the GC electrode area (0.196 cm²). EIS was conducted from 10 kHz to 0.1 Hz at -285 mV vs. RHE with 5 mV amplitude; data were fitted using equivalent circuits. Electrochemical surface area was estimated via CV (±50 mV vs. OCP) at various scan rates, and double-layer capacitance (Cdl) was derived from Δj vs. scan rate plots. Catalyst stability was assessed via 22 h chronopotentiometry at -385 mV vs. RHE. Temperature-dependent HER performance was evaluated from 298.15 K to 338.15 K in 5 K increments, and apparent activation energies were calculated.

Activation energy evolution

The influence of temperature on HER activity for MoFeCoP and MoFeNiP was evaluated using LSV. Electrode potentials were converted to the RHE scale, accounting for temperature-induced shifts in the Ag/AgCl reference (Eq. $E^T{}_{vs\ RHE} = E^T{}_{vs\ Ag/AgCl} + E^T{}_{Ag/AgCl} + \frac{RT}{F} ln\ (10)\ pH$). Both catalysts showed enhanced performance with increasing temperature. At an overpotential of –500 mV, MoFeCoP's current density rose from –145 to –340 mA·cm^{-2} (Δ = 195 mA·cm^{-2}), outperforming MoFeNiP, which increased from –58 to –145 mA·cm^{-2} (Δ = 87 mA·cm^{-2}). Tafel plots were used to extract exchange current densities (j_0), and ln j_0 vs. 1/T followed Arrhenius behavior. Apparent activation energies (Ea) were calculated from the slopes: 21 kJ·mol^{-1} for MoFeCoP and 24 kJ·mol^{-1} for MoFeNiP at zero overpotential, with similar values at –0.5 V (19 and 23 kJ·mol^{-1}, respectively). These low Ea values are significantly below the ~50 kJ·mol^{-1} typical for transition metal phosphides (TMPs) and comparable to Pt (~20 kJ·mol^{-1}), suggesting efficient HER kinetics. These examples highlight the role of multimetallic synergy in enhancing HER performance by reducing activation energy.

Conclusion

This study presents a scalable, low-cost method for producing spherical transition metal phosphides MoFeP, MoFeNiP, and MoFeCoP using a spray-drying process followed by heat treatment at 650 °C in a reducing atmosphere. The resulting hollow 3D spheres were tested as electrocatalysts for the hydrogen evolution reaction (HER) in alkaline water electrolysis. Among the catalysts, MoFeCoP showed the best HER performance, with a low overpotential of –285 mV at –10 mA cm^{-2}, outperforming MoFeP (–337 mV) and MoFeNiP (–421 mV). Tafel slope analysis confirmed a Volmer–Heyrovsky mechanism with MoFeCoP exhibiting the most favorable kinetics. Its superior activity was linked to higher electroactive surface area and lower charge transfer resistance, as shown by double-layer capacitance and EIS. It also maintained good stability during 22 h of continuous operation at –385 mV vs RHE. These results highlight Co-doped phosphides as efficient, non-noble electrocatalysts for alkaline water splitting. The simplicity and scalability of this approach open new possibilities for the commercial production of TMP-based catalysts for clean hydrogen generation.

Acknowledgements

This work was funded by the EU Next Generation EU through the Recovery and Resilience Plan for Slovakia under the project No. 09I03-03-V04-00109.

Electrochemical Determination of Gentamicin for Potential Clinical Applications

O. Zahornacky[a,*], J. Demeterova[b], J. Shepa[b], I. Sisolakova[b], P. Jarcuska[a], R. Orinakova[b]

[a] Department of Infectology and Travel Medicine at the L. Pasteur University Hospital Košice, Slovakia, Pavol Jozef Šafárik University in Košice, Rastislavova 43, 040 01, Košice, Slovak republic

[b] Department of Physical Chemistry, Pavol Jozef Šafárik University in Košice, Moyzesova 11, 040 01, Košice, Slovak republic

* ondrej.zahornacky@upjs.sk

Introduction

Since their discovery in the 1940s, antibiotics have been among the most successful pharmaceuticals for the treatment and control of bacterial infections [1]. Today, these substances are employed extensively in human medicine, as well as in veterinary practice, livestock production, and aquaculture worldwide [2]. However, improper and non-selective use contributes the spread of antimicrobial resistance, with adverse impacts on human health and ecosystems. Gentamicin, an aminoglycoside, is used to treat severe infections, including meningitis, endocarditis, urinary tract and ocular infections, otitis, and wound and burn infections [3]. Conventional analytical methodologies, including HPLC and LC–MS, are precise but costly, time-consuming, and unsuitable for on-site testing. Given this, there is a strong need for rapid, simple, and sensitive strategies for antibiotic determination. Electrochemical sensing offers in-situ applicability, fast response, and high selectivity, rendering it an attractive option for clinical and pharmaceutical monitoring [4].

Experimental

A chromium–based metal–organic framework (MIL-101(Cr)) was combined with multi-walled carbon nanotubes (MWCNTs) to prepare a composite suspension for electrode modification. Specifically, 5 mg of MWCNTs and 3 mg of MIL-101(Cr) were dispersed in 1.25 mL of a Nafion–ethanol solution and homogenised by ultrasonication for 45 min. Subsequently, 0.75 µL of the suspension was drop-cast onto the working surface of a screen-printed carbon electrode (SPCE) and dried under ambient conditions. Several electrode configurations were compared, including MIL-101(Cr)/Nafion/SPCE, MIL-101(Cr)/MWCNTs/Nafion:ethanol (1:4)/SPCE, and MIL-101(Cr)/MWCNTs/Nafion:ethanol (1:6)/SPCE, alongside the bare SPCE. Electrochemical measurements were performed in phosphate-buffered saline (PBS, pH 7.4) with successive additions of gentamicin, using cyclic voltammetry (CV) as the detection technique.

Results and discussion

The electrochemical behaviour of bare and modified SPCEs was examined by cyclic voltammetry (CV). The bare SPCE displayed the lowest current response, while modification with MIL-101(Cr) and Nafion led to a moderate improvement. A more pronounced enhancement was observed for electrodes incorporating both materials, confirming the synergistic effect of MIL-101(Cr) and MWCNTs. Among the tested modifications, the MIL-101(Cr)/MWCNTs/Nafion:ethanol (1:4)/SPCE exhibited the highest current response, identifying it as the most effective configuration (*Figure 1*).

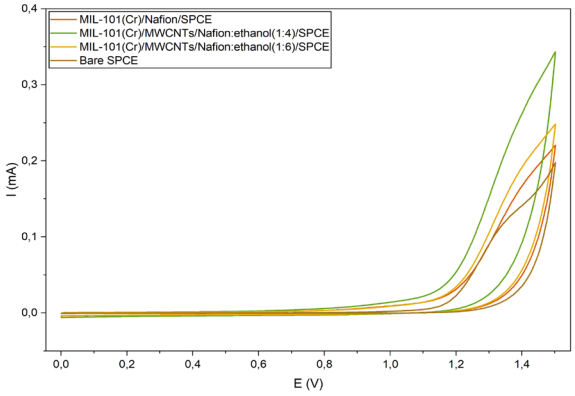

Figure 4 Cyclic voltammograms for various modifications of SPCE in the solution of 900 µM gentamicin in PBS.

The sensing performance of the optimised electrode was subsequently evaluated for gentamicin detection in PBS (pH 7.4). As illustrated in *Figure 2*, successive additions of gentamicin resulted in a gradual increase in the oxidation current, demonstrating a clear concentration-dependent response. The calibration plot showed good linearity within the tested concentration range (200–1000 µM), with a limit of detection (LOD) of 195 µM and a sensitivity of 137 nA·µM^{-1}, confirming the applicability of the developed sensor for quantitative gentamicin determination.

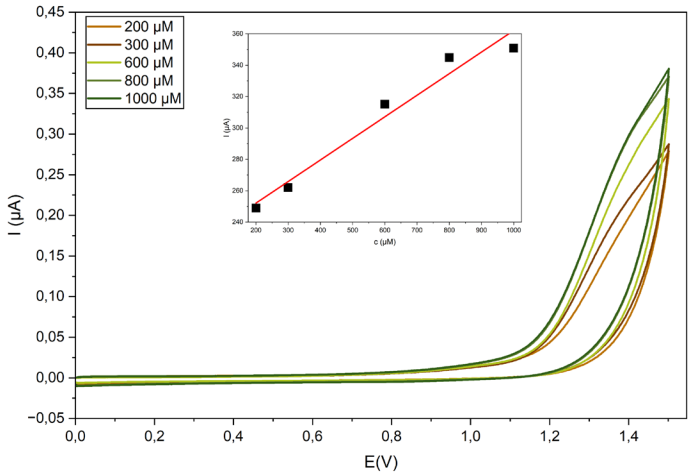

Figure 5 Cyclic voltammograms for different concentrations of gentamicin in PBS solution (200, 300, 600, 800, and 1000 µM) recorded on MIL-101(Cr)/MWCNTs/Nafion/SPCE. The inset shows the corresponding calibration plot.

These findings emphasise the combined contribution of MIL-101(Cr) and MWCNTs to the overall electrochemical performance, offering a rapid and reliable alternative for gentamicin detection, with potential applicability in biological matrices.

Acknowledgements
Funded by the EU NextGenerationEU through the Recovery and Resilience Plan for Slovakia under the project No. 09I03-03-V05-00008.

References
[1] B. Chen *et al.*, "Complex pollution of antibiotic resistance genes due to beta-lactam and aminoglycoside use in aquaculture farming," *Water Res*, vol. 134, 2018, doi: 10.1016/j.watres.2018.02.003.
[2] K. K. Brandt *et al.*, "Ecotoxicological assessment of antibiotics: A call for improved consideration of microorganisms," 2015. doi: 10.1016/j.envint.2015.09.013.
[3] E. Khaled, M. M. Khalil, and G. M. Abed el Aziz, "Calixarene/carbon nanotubes based screen printed sensors for potentiometric determination of gentamicin sulphate in pharmaceutical preparations and spiked surface water samples," *Sens Actuators B Chem*, vol. 244, 2017, doi: 10.1016/j.snb.2017.01.033.
[4] N. S. Alsaiari, K. M. M. Katubi, F. M. Alzahrani, S. M. Siddeeg, and M. A. Tahoon, "The application of nanomaterials for the electrochemical detection of antibiotics: A review," 2021. doi: 10.3390/mi12030308.

Efficient Capture of Volatile Organic Vapors by Metal-Organic Frameworks: Toward Gas Mask Filter Applications

M. Zelinska[a], K. Andrejev[a], T. Zelenka[b], M. Almasi[a,*]
[a] Department of Inorganic Chemistry, Institute of Chemistry, Faculty of Science, Pavol Jozef Šafárik University in Košice, Moyzesova 11, 040 01 Košice, Slovak Republic
[b] Department of Chemistry, Faculty of Science, University of Ostrava, 30. Dubna 22, 702 00 Ostrava, Czech Republic
* miroslav.almasi@upjs.sk

Volatile organic vapors (VOCs) represent a broad and chemically diverse class of carbon-based compounds that readily evaporate at ambient temperatures. They are released into the atmosphere through a variety of anthropogenic activities, including large-scale industrial manufacturing, chemical processing, transportation-related fuel combustion, and the use of solvents and coatings. Even routine household activities, such as painting, cleaning, or the use of adhesives, can emit measurable amounts of VOCs. Because of their abundance and mobility, VOCs are now recognized as ubiquitous indoor and outdoor air pollutants. Their impact is multifaceted: beyond their role as precursors of tropospheric ozone and secondary organic aerosols, VOCs are strongly associated with adverse human health outcomes ranging from short-term respiratory irritation to long-term carcinogenic effects. The World Health Organization and numerous regulatory bodies worldwide have therefore identified VOC abatement as a major environmental and occupational safety priority.

Historically, the mitigation of VOC emissions has relied on conventional adsorbents such as activated carbons, zeolites, or porous polymers. While effective in many cases, these materials often exhibit inherent limitations, including low selectivity, reduced uptake of highly volatile small molecules, or difficulties with regeneration and reusability. In recent decades, the advent of crystalline porous materials, particularly metal-organic frameworks (MOFs), has opened a new frontier in adsorption science. MOFs combine ultra-high surface areas with tailorable pore sizes and functionalities, offering unique opportunities for tuning host–guest interactions at the molecular scale. These advantages have established MOFs as one of the most promising classes of sorbents for selective VOC capture and filtration applications.

Within this context, HKUST-1 (Cu-BTC, MOF-199) stands out as one of the most widely studied and industrially relevant frameworks. Its crystalline architecture, based on copper paddle-wheel units and benzene-1,3,5-tricarboxylate linkers, gives rise to large, well-defined pore systems with apertures around 6–9 Å. The framework combines high porosity (surface area typically 600–1600 m^2/g) and pore volume with considerable thermal and chemical stability up to 350 °C. These attributes, together with the simplicity of its synthesis from inexpensive reagents, render HKUST-1 not only a benchmark MOF in academic research but also a realistic candidate for scale-up and implementation in applied technologies [1,2].

In this study, the adsorption behavior of HKUST-1 toward a representative set of VOCs was systematically evaluated, with the specific aim of assessing its suitability for gas mask filter applications. The target compounds included small polar solvents (methanol, formaldehyde), common aromatic pollutants (benzene, toluene, pyridine, aniline), and bulkier functionalized aromatics (benzaldehyde, benzyl bromide, salicylaldehyde). Activated HKUST-1 samples (150 °C, vacuum treatment) were exposed to saturated vapors under static conditions, and adsorption capacities were quantified thermogravimetrically after 3, 24, and 48 hours. This experimental design enabled evaluation of both rapid uptake dynamics and longer-term equilibrium behavior.

The results demonstrate pronounced differences in uptake depending on molecular size, polarity, and volatility. Rapid adsorption was observed within the first three hours for most compounds, followed by stabilization and, in some cases, slight desorption at extended times. The framework showed remarkable affinity for small, highly volatile polar molecules: methanol uptake reached as high as 1897 mg/g at 25 °C, corresponding to nearly twice the adsorbent's own weight. Formaldehyde exhibited similarly strong sorption, underscoring the importance of polarity and molecular mobility. In contrast, larger and sterically hindered molecules such as benzyl bromide and salicylaldehyde exhibited limited penetration into the porous lattice, resulting in much lower adsorption capacities (see *Figure 1*).

The effect of temperature on VOC uptake was also systematically investigated. As expected for exothermic adsorption processes, higher temperatures led to diminished sorption performance. However, even at elevated temperatures (35–45 °C), HKUST-1 retained a considerable fraction of its uptake capacity, suggesting that it could operate effectively under realistic conditions encountered in protective filtration. Importantly, adsorption data expressed in mmol/g

provided direct insight into molecular loading within the framework, allowing comparison across VOCs of widely varying molar masses.

Overall, our findings highlight HKUST-1 as a high-capacity, structurally robust, and partially selective VOC adsorbent. While the limited accessibility of bulkier VOCs indicates a size-exclusion effect inherent to its pore structure, the outstanding performance for low-molecular-weight polar vapors places HKUST-1 among the most promising candidates for practical protective devices. Compared to traditional carbonaceous adsorbents, HKUST-1 offers the advantages of crystallinity, tunability, and well-defined adsorption pathways, which could be further optimized through post-synthetic modification or composite formation with other porous phases.

The implications of this work extend beyond the laboratory scale. The demonstrated ability of HKUST-1 to capture toxic and carcinogenic VOCs suggests its direct applicability in personal protective equipment, particularly gas masks and respirator filters designed for occupational or emergency response use. Moreover, the principles uncovered here can guide the rational design of MOF-based composites for indoor air purification, vehicle cabin filters, and stationary industrial scrubbers. By clarifying the role of polarity, molecular size, and temperature on adsorption behavior, this study provides valuable insights for tailoring MOFs toward specific target pollutants.

In summary, this work not only advances the fundamental understanding of VOC adsorption in HKUST-1 but also underscores the real-world relevance of MOFs as next-generation sorbents for environmental protection and human health. Future research should explore the regeneration stability of HKUST-1 under cyclic conditions, the influence of humidity and mixed-gas environments, and the scalability of composite filters integrating MOFs with conventional adsorbents. Taken together, these directions point toward a new generation of filtration technologies that combine high efficiency with tunability, offering practical solutions to the global challenge of VOC pollution.

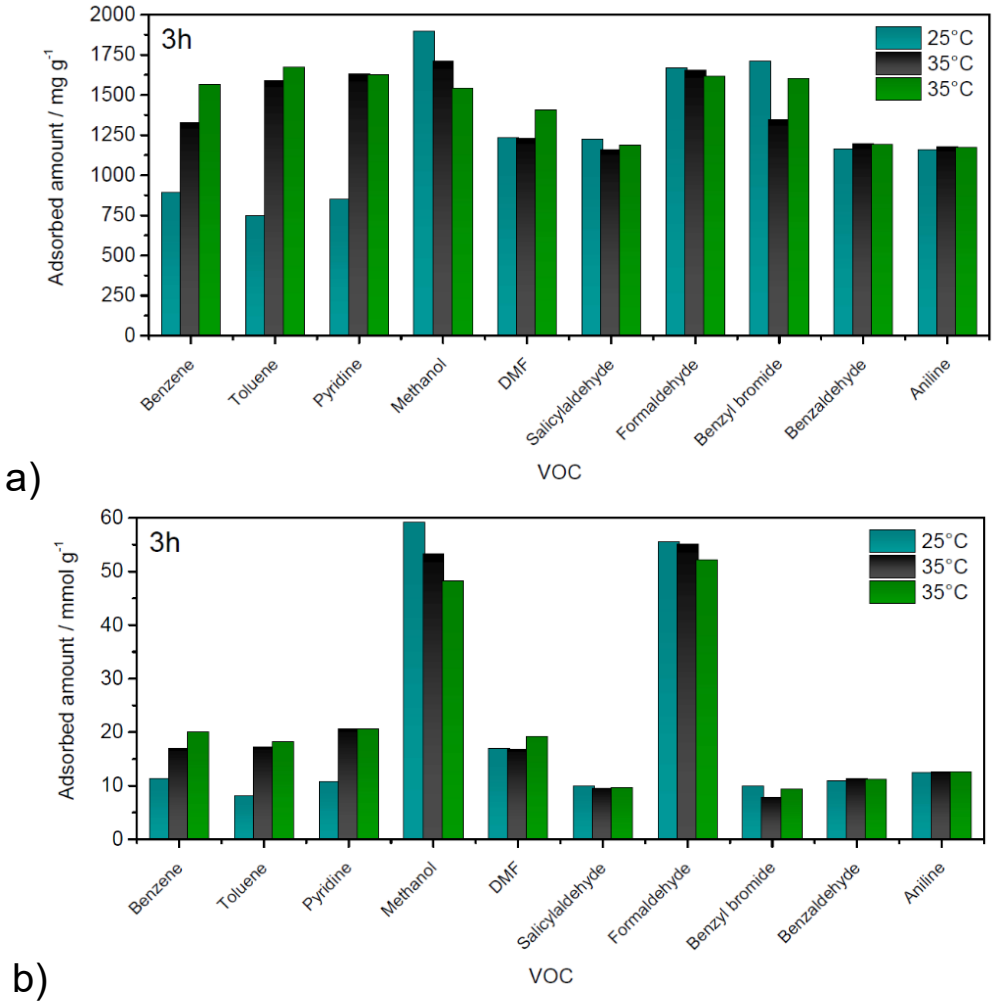

Figure 1 Dependence of the adsorbed VOC mass *a)* in mg and *b)* in mmol per one gram of activated HKUST-1 after 3 hours of exposure at 25, 35, and 45 °C.

Acknowledgements
This work was supported by VEGA project no. 1/0058/25.

References
[1] S.S. Chui, S.M. Lo, J.P.H. Charmant, A.G. Orpen, A. G., I.D. Williams, *Science* **283** (1999) 1148–1150.
[2] T. Zelenka, K. Simanova, R. Saini, G. Zelenkova, S.P. Nehra, A. Sharma, M. Almasi, *Sci. Rep.* **12** (2022) 17366.

The 9th International Conference on Novel Materials Fundamentals and Applications
Book of Abstracts

Edited by: Mgr. Soňa Király

Publisher: Pavol Jozef Šafárik University in Košice
ŠafárikPress Publishing

Year: 2025
Pages: 112
Author's sheets: 11,63
Edition: first

ISBN 978-80-574-0444-6 (e-publication)